Different effects of sonoporation on cell morphology and viability

Ji-Zhen Zhang[1], Jasdeep K. Saggar[2], Zhao-Li Zhou[3], Bing-Hu[1]*

[1] Department of Ultrasound In Medicine, Shanghai Jiao Tong University Affiliated 6th People's Hospital, Shanghai Institute of Ultrasound in Medicine, 600 Yi Shan Road, Shanghai 200233, China. [2] Department of Medical Biophysics, University of Toronto, 610 University Avenue (Room 10-610), Toronto, Ontario, Canada M5S 3E2. [3] Central Research Institute, Shanghai, Pharmaceuticals Holding Co., Ltd. Division of Antitumor Pharmacology, State Key Laboratory of Drug Research, Shanghai Institute of Materia Medica, Chinese Academy of Sciences, Shanghai 201203, China

Abstract

The objective of our study was to investigate changes in cell morphology and viability after sonoporation. Sonoportion was achieved by ultrasound (21 kHz) exposure on adherent human prostate cancer DU145 cells in the cell culture dishes with the presence of microbubble contrast agents and calcein (a cell impermeant dye). We investigated changes in cell morphology immediately after sonoporation under scanning electron microscope (SEM) and changes in cell viability immediately and 6 h after sonoporation under fluorescence microscope. It was shown that various levels of intracellular calcein uptake and changes in cell morphology can be caused immediately after sonoporation: smooth cell surface, pores in the membrane and irregular cell surface. Immediately after sonoporation, both groups of cells with high levels of calcein uptake and low levels of calcein uptake were viable; 6 h after sonoporation, group of cells with low levels of calcein uptake still remained viable, while group of cells with high levels of calcein uptake died. Sonoporation induces different effects on cell morphology, intracellular calcein uptake and cell viability.

KEY WORDS: sonoporation, molecular delivery, drug delivery, ultrasound, low frequency ultrasound, microbubble contrast agents, cell morphology

INTRODUCTION

Conventional drug delivery systems, such as systemic administration via intravenous injection or oral administration, are often not sufficient for delivery of therapeutic compounds such as proteins and genes [1, 2]. A recent development in delivery systems for therapeutic compounds is ultrasound (US)-aided intracellular delivery [3-5]. It has been demonstrated that US can achieve efficient intracellular delivery of a variety of drugs and/or genes [6-8]. Sonoporation is defined as the formation of transient, non-specific pores or openings in the cellular membranes upon US exposure was commonly considered as the main mechanism of action for efficient drug delivery [9-11]. However, several studies have recently reported heterogeneity in the levels of both small- and macro- molecular uptake by sonoporation [12-14]. Cells with various levels of molecular uptake can be generally divided into two groups: cells with high levels of molecular uptake and those with low levels of molecular uptake. The exact mechanism is still not fully understood. Zarnitsyn et al. [15] presented a theoretical model that determined membrane pore size as a function of calcein (a cell impermeant dye) uptake where calcein uptake is directly related to pore size (i.e. greatest calcein uptake in cells with the largest pores). In the current study, US was applied to adherent cells in the cell culture dishes in order to establish a model of heterogeneity in sonoporation. The possible mechanism of action was studied by observing changes in cell morphology immediately after sonoporation using scanning electron microscope (SEM) and cell viability immediately and 6 h after sonoporation using fluorescence microscope.

* Corresponding author: Bing-Hu,
Department of Ultrasound In Medicine, Shanghai Jiao Tong University Affiliated 6th People's Hospital, Shanghai Institute of Ultrasound in Medicine, 600 Yi Shan Road, Shanghai 200233, China.
Tel: 086-21-64369181; Fax: 086-21-54488254
e-mail: binghuzz@sina.cn

Submitted: 15 September 2011 / Accepted: 19 April 2012

MATERIALS AND METHODS

Cell lines

Human prostate cancer DU145 cell lines were purchased from the American Type Culture Collection (ATCC, Manassas, VA, USA). Cells were cultured as monolayers and grown to 80% confluence on cell culture dishes (35 mm in diameter) in RPMI-1640 media (GIBCO, USA) supplemented with 10% (v/v) heat-inactivated fetal bovine serum (FBS; GIBCO, USA), 2 mmol/L glutamine, 100 IU/

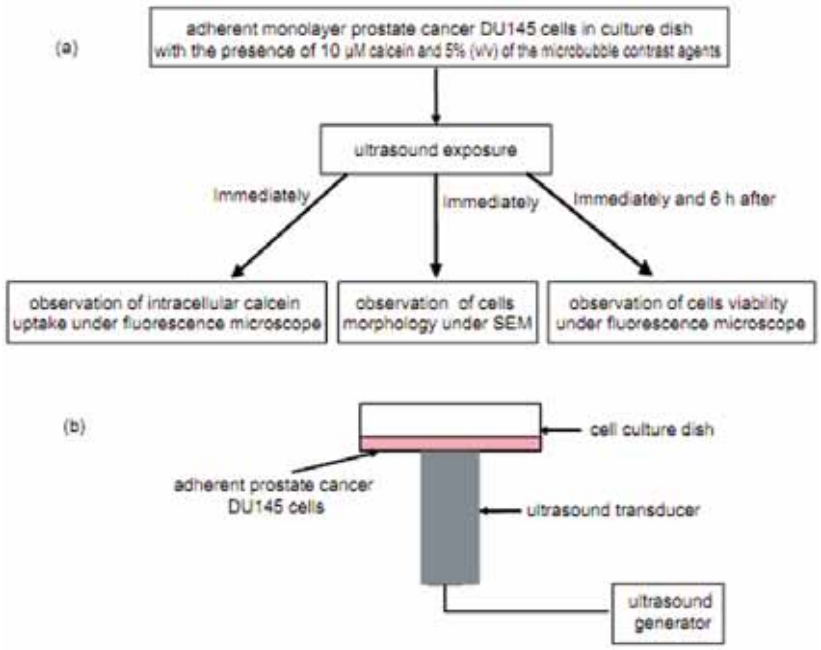

FIGURE 1. Experimental flow and ultrasound exposure setup. (a) Experimental flow (see details in *Materials and Methods*); (b) Ultrasound exposure setup. A cell culture dish (35 mm in diameter) containing adherent monolayer prostate cancer DU 145 cells was placed just above a flat 21 kHz ultrasound transducer (13 mm in diameter) with a thin layer of gel between them.

mL penicillin, 100 μg/mL streptomycin, and 10 mmol/L HEPS (pH 7.4) at 37oC, 5% CO2, and 90% relative humidity.

Cell pre-treatment

Three ml cell culture media (fresh RPMI-1640 with 10% FBS) containing 5% (v/v) of the microbubble contrast agent-Sonovue (Bracco International B.V., Italy) and 10 μM calcein (623 Da, radius=0.6 nm; A green fluorescent and cell membrane impermeant stain, Sigma, USA) was added into the cell culture dishes containing adherent human prostate cancer DU145 cells before sonication.

Ultrasound apparatus and exposure

Ultrasound was generated at 21 kHz by a function generator and amplifier (Shanghai Institute of Ultrasound in Medicine, Shanghai, China) that controlled the transducer via matching transformer (Shanghai Institute of Ultrasound in Medicine, Shanghai, China). The transducer was calibrated using laser interferometry as described by Wu et al. [16]. Acoustic power of 10 mW, 100% duty cycle and 1 s exposure time were chosen for sonication treatment. Transducer tip (flat and round with a diameter of 13 mm) was fixed by a holder and faced vertically upwards. A cell culture dish was placed just above the transducer surface with a thin layer of gel between them (Figure1).

Cell morphology observation

To view cell morphology, we imaged adherent cells using scanning electron microscope (SEM) (Quanta 200, Philips, Netherlands). Briefly, before sonication 3 ml of fresh cell media (RPMI-1640 with 10% FBS) containing 5% (v/v) of the microbubble contrast agent-Sonovue and 10 μM calcein, was added into the cell culture dish containing adherent human prostate cancer DU145 cells. Immediately (5 sec after sonication) cell culture media was discarded and 3 ml of 2% EM-grade glutaraldehyde (Sigma, USA) was added. Preparations for SEM were performed using established techniques.

Cellular viability assessment

To identify cellular viability, propidium iodide (PI) (Sigma, USA), which is able to stain the nuclei of nonviable, membrane-compromised cells with red fluorescence, was added to the cell culture dishes containing adherent human prostate cancer DU145 cells 5 min after sonication producing a final concentration of 1 μM. Propidium iodide (PI) was left on cells for a total of 10 min at room temperature, thereafter the cell culture media containing PI and calcein was removed and cells were washed twice with phosphate buffer solution (PBS; GIBCO, USA) and 1 ml of fresh RPMI-1640 cell culture media (with 10% FBS) was added prior to being assayed by fluorescence microscope (ZX70, OLYMPUS, Japan). Merged image was used to show PI staining (red) of cell with calcein uptake (green).

RESULTS

Levels of intracellular calcein uptake immediately after sonoporation

Several studies have reported that US exposure on adherent cells in the presence of microbubble contrast agents can induce cell detachment and sonoporation [17, 18]. Consistent with these studies, the substrate was partially cleared of cells following US exposure in the presence of the microbubble contrast agent-Sonovue (Figure 2A). Adherent cells, which have not been washed away but line the border between occupied and empty region, emitted green fluorescence under fluorescence microscope duo to the uptake of calcein (Figure 2B). No green fluorescence was detected for cells far way from the sonciation-induced detachment (Figure 2B). It was also shown that cells with calcein uptake can be roughly divided into two subgroups: cells with high levels of calcein uptake (strong green fluorescence, Figure 2B) and cells with low

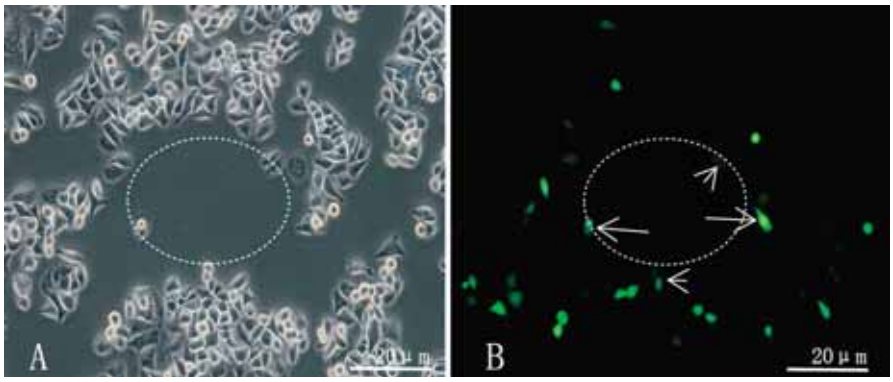

FIGURE 2. Different levels of intracellular calcein uptake immediately after sonoporation imaged by fluorescence microscope. (A, bright field) The substrate is partially cleared of cells by sonication(as indicated by the circle). (B) Cells lining at the border between occupied and empty region showed roughly two different levels of calcein uptake: low levels of calcein uptake (weak green fluorescence as indicated by short arrow) or high levels of uptake (strong green fluorescence as indicated by long arrow). Cells far away from the vacant region showed no calcein uptake.

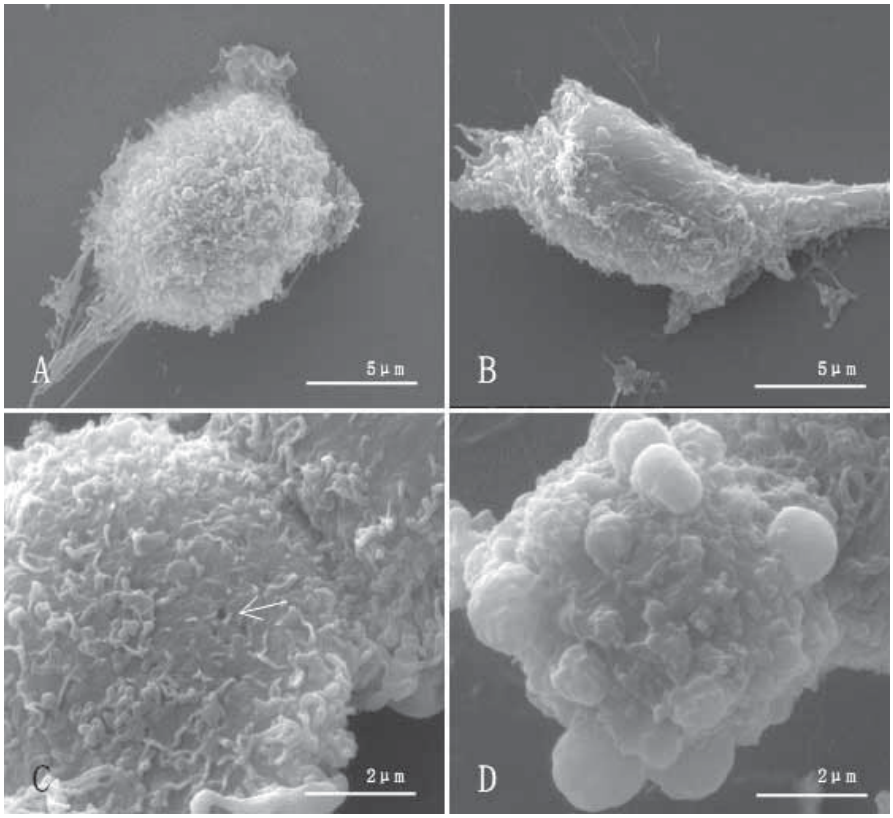

FIGURE 3. Various changes in cell morphology immediately after sonoporation. (A) SEM of adherent cells far away from vacant regions, showing abundant and homogeneous microvilli on the cellular surface; SEM of cells lining the border between occupied and vacant regions, show partly smooth surface (B), pores in the membrane (arrow) (C)and irregular cell surface (D).

levels of calcein uptake (weak green fluorescence, Figure 2B).

Changes in cell morphology immediately after sonoporation

By using scanning electron microscope (SEM), it was shown that cells far away from the vacanted regions displayed rich and homogeneous distribution of microvilli on the cellular surfaces (Figure 3A). While, various changes in cell surface morphology for those cells surrounding the vacanted regions could be detected: smooth surface (Figure 3B), pores in membrane (Figure 3C) and irregular cell surface (Figure 3D).

Changes in cell viability after sonoporation

Under fluorescence microscope, it was shown that immediately after sonoporation, both groups of cells with high levels of calcein uptake and low levels of calcein uptake were viable as evidenced by no staining with PI (Figure 4A); 6 h after sonoporation, group of cells with low levels of calcein uptake still remained viable (Figure 4A-B, negative PI staining as indicated by the long arrow), while group of cells with high levels of calcein uptake died (Figure 4A-B, PI staining changed from negative into positive as indicated by the short arrow).

DISCUSSION

This study showed different intracellular calcein uptake and changes in cell morphology and viability after sonoporation. Furthermore, group of cells with low levels of calcein uptake remained viable 6 h after sonoporation, while group of cells with high levels of calcein uptake died. Sonoporation is defined as formation of transient, nonspecific pores or openings in the cellular membranes upon US exposure [19]. Acoustic cavitation produced by US exposure is believed to be the main physical mechanism caused by US exposure [20, 21]. Acoustic cavitation is the process entailing bubbles formation, growth, vibration or even collapse in the medium under US activation [22]. Microbubble contrast agents could act as the acoustic cavitation nuclei and produce acoustic cavitation under ultrasound exposure [23]. It is currently believed that mechanical wounding on cells due to acoustic cavitation is the predominant mechanism of action of sonoporation [10]. Several studies have investigated the changes in cell morphology immediately after sonication

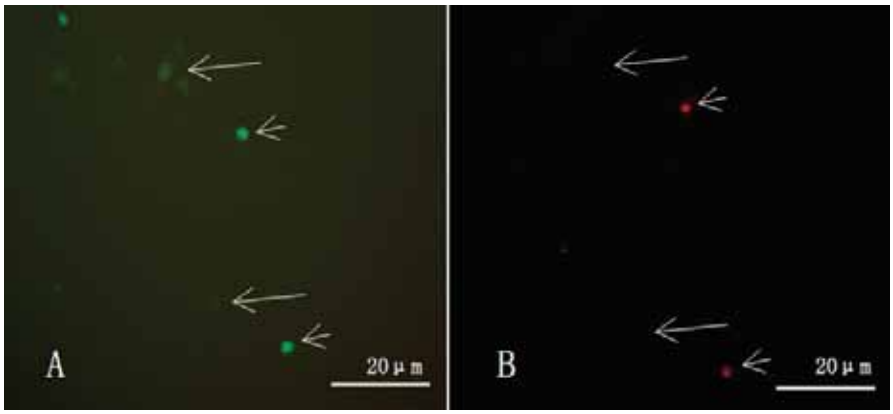

FIGURE 4. Different changes in cell viability after sonoporation imaged by fluorescence microscope. (A, merged image) Immediately after sonoporation, both groups of cells with low levels of calcein uptake (weak green fluorescence as indicated by the long arrow) and high levels of calcein uptake (strong green fluorescence as indicated by the short arrow) were viable evidenced by negative PI staining; (B, merged image 6 h after sonoporation, group of cells with low levels of calcein uptake remained viable (A-B, negative PI staining as indicated by the long arrow), while group of cells with high levels of calcein uptake died (A-B, PI staining changed from negative into positive as indicated by the short arrow).

[10, 19, 24]. However, results vary and most are focused on observing the pores in the membrane. In our study, we observed different changes in cell morphology immediately after sonoporation; these included: smooth surface, pores in the membrane and irregular cell surface . It is noteworthy that in our study smooth surface was the most common change while pores were rarely seen. One possible explanation is that the pores may have been resealed before cell fixation [25]. Our study further showed that some cells containing high levels of calcein uptake died 6 h after sonoporation; while those with low levels of calcein uptake survived. It has been reported that fractions of cells with various levels of molecular uptake of calcein can be affected by changing the US exposure intensity [12]. Therefore, combined with the study by Zarnitsyn et al. [15], it is suggested that levels of molecular uptake of calcein may be consistent with the levels of cell membrane wounds . The exact mechanism regarding how cellular membrane wounding results in delayed cellular death is still unknown. Several studies have reported that there is an immediate calcium ion influx following mechanical wounding (including sonication) [26, 27]. Hutcheson et al. [13] successfully rescued up to 44% of cells with high levels of calcein uptake from apoptosis by the addition of a calcium ionic chelator. However, several studies also show that immediate calcium ion influx after sonication is vital to the wound repairing [26-28]. Therefore, calcium ion influx after sonication may play a complex role in sonoporation [29]. However, there is still one main limitation in our study since we did not measure the accurate distribution of the acoustic field in our experimental setup. Nonetheless, the aim of our study is not to optimize the exposure parameters, but to observe the changes in cell morphology of cells with molecular uptake under this simple experimental model [30, 31].

CONCLUSION

Our study showed different effects of sonoporation on intracellular calcein uptake, cell morphology and viability. It was suggested that various changes in cell morphology may be responsible for different levels of intracellular calcein uptake and changes in cell viability after sonoporation.

ACKNOWLEDGEMENTS

The authors would like to thank the following Professors: Qian Cheng (Institute of Acoustics, Tongji University, Shanghai, China) for ultrasound parameters calibration and Wen-de Shou (Shanghai Institute of Ultrasound in Medicine, Shanghai, China) for acoustic theory consultation.

DECLARATION OF INTEREST

This work was supported in part by the National Natural Science Foundation of China (grant # 30770562) and Shanghai Science and the Technology Committee Basic Research Program (grant #10JC1412600). All authors have read and approved this manuscript. Neither the submitted paper nor any similar paper, in whole or in part has been or will be published in any other primary scientific journal. No conflict of interest exists in the submission of this manuscript.

REFERENCES

[1] Langer R. Drug delivery and targeting. Nature 1998; 392(6679 Suppl):5-10.
[2] Feril LB, Jr. Ultrasound-mediated gene transfection. Methods Mol Biol 2009;542:179-194.
[3] Mitragotri S. Healing sound: the use of ultrasound in drug delivery and other therapeutic applications. Nat Rev Drug Discov 2005;4(3):255-260.
[4] Pua EC, Zhong P. Ultrasound-mediated drug delivery. IEEE Eng Med Biol Mag 2009; 28(1):64-75.
[5] Zderic V. Ultrasound-enhanced drug and gene delivery: a review. Conf Proc IEEE Eng Med Biol Soc 2008; 2008:4472.
[6] Li W, Liu S, Ren J, Xiong H, Yan X, Wang Z. Gene transfection to retinal ganglion cells mediated by ultrasound microbubbles in vitro.

Acad Radiol 2009;16(9):1086-1094.
[7] Negishi Y, Matsuo K, Endo-Takahashi Y, Suzuki K, Matsuki Y, Takagi N, et al. Delivery of an angiogenic gene into ischemic muscle by novel bubble liposomes followed by ultrasound exposure. Pharm Res 2010; 28(4):712-719.
[8] Mohan P, Rapoport N. Doxorubicin as a molecular nanotheranostic agent: effect of doxorubicin encapsulation in micelles or nanoemulsions on the ultrasound-mediated intracellular delivery and nuclear trafficking. Mol Pharm 2010;7(6):1959-1973.
[9] Kudo N, Okada K, Yamamoto K. Sonoporation by single-shot pulsed ultrasound with microbubbles adjacent to cells. Biophys J 2009; 96(12):4866-4876.
[10] Schlicher RK, Radhakrishna H, Tolentino TP, Apkarian RP, Zarnitsyn V, Prausnitz MR. Mechanism of intracellular delivery by acoustic cavitation. Ultrasound Med Biol 2006; 32(6): 915-924.
[11] Fan Z, Kumon RE, Park J, Deng CX. Intracellular delivery and calcium transients generated in sonoporation facilitated by microbubbles. J Control Release 2009;142(1):31-39.
[12] Guzman HR, Nguyen DX, McNamara AJ, Prausnitz MR. Equilibrium loading of cells with macromolecules by ultrasound: effects of molecular size and acoustic energy. J Pharm Sci 2002; 91(7):1693-1701.
[13] Hutcheson JD, Schlicher RK, Hicks HK, Prausnitz MR. Saving cells from ultrasound-induced apoptosis: quantification of cell death and uptake following sonication and effects of targeted calcium chelation. Ultrasound Med Biol 2010; 36(6):1008-1021.
[14] Mehier-Humbert S, Bettinger T, Yan F, Guy RH. Plasma membrane poration induced by ultrasound exposure: implication for drug delivery. J Control Release 2005;104(1):213-222.
[15] Zarnitsyn V, Rostad CA, Prausnitz MR. Modeling transmembrane transport through cell membrane wounds created by acoustic cavitation. Biophys J 2008;95(9):4124-4138.
[16] Wu Xian-mei Qian Meng-lu. Vibration measuring technique using laser interferometer for calibration of transducers. TECHNICAL ACOUSTICS 2000;19(2):83-85.
[17] Ohl CD, Wolfrum B. Detachment and sonoporation of adherent HeLa-cells by shock wave-induced cavitation. Biochim Biophys Acta 2003;1624(1-3):131-138.
[18] Zarnitsyn VG, Prausnitz MR. Physical parameters influencing optimization of ultrasound-mediated DNA transfection. Ultrasound Med Biol 2004;30(4):527-538.
[19] Tachibana K, Uchida T, Ogawa K, Yamashita N, Tamura K. Induction of cell-membrane porosity by ultrasound. Lancet 1999;353(9162):1409.
[20] Forbes MM, Steinberg RL, O'Brien WD, Jr. Examination of inertial cavitation of Optison in producing sonoporation of chinese hamster ovary cells. Ultrasound Med Biol 2008; 34(12): 2009-2018
[21] Lai CY, Wu CH, Chen CC, Li PC. Quantitative relations of acoustic inertial cavitation with sonoporation and cell viability. Ultrasound Med Biol 2006; 32(12):1931-1941.
[22] Apfel RE. Acoustic cavitation: a possible consequence of biomedical uses of ultrasound. Br J Cancer Suppl 1982; 5:140-146.
[23] Karshafian R, Bevan PD, Williams R, Samac S, Burns PN. Sonoporation by ultrasound-activated microbubble contrast agents: effect of acoustic exposure parameters on cell membrane permeability and cell viability. Ultrasound Med Biol 2009;35(5):847-860.
[24] Schlicher RK, Hutcheson JD, Radhakrishna H, Apkarian RP, Prausnitz MR. Changes in cell morphology due to plasma membrane wounding by acoustic cavitation. Ultrasound Med Biol 2010; 36(4):677-692.
[25] Zhou Y, Kumon RE, Cui J, Deng CX. The size of sonoporation pores on the cell membrane. Ultrasound Med Biol 2009; 35(10):1756-1760.
[26] Deng CX, Sieling F, Pan H, Cui J. Ultrasound-induced cell membrane porosity. Ultrasound Med Biol 2004;30(4):519-526.
[27] Kumon RE, Aehle M, Sabens D, Parikh P, Han YW, Kourennyi D, et al. Spatiotemporal effects of sonoporation measured by real-time calcium imaging. Ultrasound Med Biol 2009; 35(3):494-506.
[28] Kumon RE, Aehle M, Sabens D, Parikh P, Kourennyi D, Deng CX. Ultrasound-induced calcium oscillations and waves in Chinese hamster ovary cells in the presence of microbubbles. Biophys J 2007; 93(6): L29-31.
[29] Hassan MA, Campbell P, Kondo T. The role of Ca(2+) in ultrasound-elicited bioeffects: progress, perspectives and prospects. Drug Discov Today 2010;15(21-22):892-906.
[30] Kodama T, Tomita Y, Koshiyama K, Blomley MJ. Transfection effect of microbubbles on cells in superposed ultrasound waves and behavior of cavitation bubble. Ultrasound Med Biol 2006; 32(6):905-914.
[31] Rahim A, Taylor SL, Bush NL, ter Haar GR, Bamber JC, Porter CD. Physical parameters affecting ultrasound/microbubble-mediated gene delivery efficiency in vitro. Ultrasound Med Biol 2006;32(8):1269-1279.

Anti-fibrotic effect of Aliskiren in rats with deoxycorticosterone induced myocardial fibrosis and its potential mechanism

Likun Ma[1*], Jinsheng Hua[1], Lifeng He[1], Qian Li[1], Junling Zhou[1], Jiangtao Yu[2]

[1] Department of Cardiology, Anhui Provincial Hospital, No 17 Lujiang Road, Hefei 230001, China. [2] Department of Cardiology, Zentralklinik Bad Berka GmbH, Robert-Koch-Allee 9, Bad Berka, DE- 99437, Germany.

Abstract

The objective of our study was to investigate the effect of Aliskiren, a renin inhibitor, on the deoxycorticosterone (DOCA) induced myocardial fibrosis in a rat model and its underlying mechanism. A total of 45 Sprague-Dawley (SD) rats underwent right nephrectomy and were randomly assigned into 3 groups: control group (CON group: silicone tube was embedded subcutaneously); DOCA treated group (DOC group: 200 mg of DOCA was subcutaneously administered); DOCA and Aliskiren (ALI) treated group (ALI group: 200 mg of DOCA and 50 mg/kg/d ALI were subcutaneously and intragastrically given, respectively). Treatment was done for 4 weeks. Sirius red staining was employed to detect the expression of myocardial collagen, and the myocardial collagen volume fraction (CVF) and perivascular collagen volume area (PVCA) were calculated. Radioimmunoassay was carried out to measure the renin activity (RA) and content of angiotensin II (Ang II) in the plasma and ventricle. Western blot assay was done to detect the expressions of extracellular signal-regulated kinase 1/2 (ERK1/2), phosphorylated ERK1/2 (PERK1/2) and matrix metalloproteinase 9 (MMP-9). In the DOC group and ALI group, the CVF and PVCA were significantly increased; the RA and Ang II levels in the plasma and ventricle were remarkably lowered when compared with the CON group. The RA and Ang II levels in the ventricle of the ALI group were significantly lower than those in the DOC group. Moreover, the expressions of ERK1/2, PERK1/2 and MMP9 were the lowest in the CON group, but those in the ALI group were significantly reduced as compared to the DOC group. ALI can inhibit the DOCA induced myocardial fibrosis independent of its pressure-lowing effect, which may be related to the suppression of RA and Ang II production, inhibition of ERK1/2 phosphorylation and MMP9 expression in the heart.

KEY WORDS: Aliskiren, deoxycorticosterone, myocardial fibrosis, renin- angiotensin - aldosterone system

INTRODUCTION

Myocardial fibrosis is a common pathological feature shared by several heart diseases at the end stage. To prevent or even reverse myocardial fibrosis has been a key goal in the prevention and treatment of severe cardiovascular events including heart failure, arrhythmia and sudden cardiac death. Studies have demonstrated that renin - angiotensin - aldosterone system (RAAS) plays important roles in the regulation of myocardial collagen metabolism and the occurrence of myocardial fibrosis [1, 2]. Evidence shows Aliskiren (ALI), a new rennin inhibitor, can not only lower the blood pressure, but improve the myocardial fibrosis and subsequent remodeling via its anti-inflammatory and anti-oxidative effects [3, 4]. Currently, the anti-fibrotic effect of ALI and its potential mechanism are less studied. The present study aimed to investigate the cardioprotective effect of ALI on the deoxycorticosterone (DOCA) induced myocardial fibrosis and its potential mechanism in a rat model.

* Corresponding author: Likun Ma,
Department of Cardiology of Anhui Provincial Hospital,
No 17 Lujiang Road, Hefei 230001, China
Tel:+86551-2283339; Fax : +86551-2282121
e-mail: docma96@sina.com

Submitted: 14 October 2011 / Accepted: 16 April 2012

MATERIALS AND METHODS

Reagents

ALI (Novartis, Switzerland), DOCA (Sigma, USA), primary antibodies against β-actin, extracellular signal kinase 1/2 (ERK1/2), phosphorylated ERK1/2 (PERK1/2) and metalloproteinase-9 (MMP-9) (Santa Cruz, USA), secondary antibodies, two - quinolinecarboxylic acid (BCA) (Beijing Zhongshan Golden-Bridge Biotech, China), electrochemiluminescence (ECL) kit (Pierce), Sirius red (Beijing Haide Biotech, China) and radioimmunoassay kit (Beijing Yuanzi Biotech, China) were used in the present study.

Grouping and modelling

A total of 45 Sprague-Dawley (SD) male rats weighing 187~245 g were purchased from the Animal Center of Anhui Medical University. The investigation conforms with the Guide for Care and Use of Laboratory Animals published by

the US National Institutes of Health (NIH Publication, 8th edition). Animals were randomly assigned into 3 groups (n=15 per group): control (CON) group, DOCA (DOC) group and ALI (ALI) group. Following anesthesia with intraperitoneal 10% chloral hydrate (300 mg/kg), right nephrectomy was done in these animals. One week after surgery, animals were given access to 1% NaCl and received following treatments. In the CON group, silicone tube was embedded subcutaneously in the left lower abdomen. In the DOC group, 200 mg of DOCA were embedded in the left lower abdomen. In the ALI group, 200 mg of DOCA were embedded in the left lower abdomen and animals were intragastrically treated with ALI at 50 mg/kg/d for 4 weeks. In addition, animals in the CON group and DOC group were also intragastrically treated with normal saline for consecutive 4 weeks.

Measurement of blood pressure and sample collection

At the end of treatment, rats were intraperitoneally anesthetized with 10% chloral hydrate followed by cannulation of right carotid artery for the measurement of mean arterial blood pressure (MABP) using a multi-channel physiological recorder. Then, 3 ml of blood were collected into the anti-coagulated tube and rats were sacrificed by exsanguinations. Thoracotomy was performed and the heart collected. The atrium, major vessels and connective tissues were removed and the left ventricle was divided into two: one was fixed in 4% paraformaldehyde followed by processing for histological staining for collagen; the other was stored at -80°C for the detection of protein expression by western blot assay. Blood was centrifuged at 1000 rpm/min for 5 min and the plasma was collected and stored at -20°C for use.

Detection of myocardial fibrosis

The heart tissues were embedded in the paraffin and cut into sections followed by Sirius red staining for collagen. A total of 8 fields without blood vessels were randomly selected from each section and representative photographs were captured with Nikon camera followed by analysis using Image-Pro plus 6.0 image analysis system. The collagen area and total area of each field were measured, and myocardial collagen volume fraction (CVF) was calculated as collagen area / total area. The CVFs from 8 fields were averaged and used as the final CVF of this sample. In addition, 4 fields with small blood vessels at cross section were randomly collected, and the perivascular collagen volume area (PVCA) and lumen area (LA) determined. The PVCA was normalized by the LA (PVCA/LA). The PVCAs from 4 fields were averaged and used as the final PVCA of this sample.

Detection of renin and angiotensin II by radioimmunoassay

Briefly, in each group, 100 mg of ventricle were homogenized, and then the homogenate and plasma were independently divided into two: one was kept at 37°C for 1 h which may facilitate the binding of renin (RA) to angiotensinogen producing angiotensin I (Ang I) (experiment group); the other was stored at 4°C serving as controls. The Ang I level in the experiment group and control group was measured by radioimmunoassay according to the manufacturer's instructions. The difference in Ang I between experiment group and control group was normalized by the time of incubation as the production rate of Ang I. The production rate of Ang I in unit time was defined as the renin activity of this sample and the unit was ng /ml/h. According to the manufacturer's instructions, the Ang II level in the plasma and ventricle was also measured and its unit was pg/ml.

Detection of ERK1/2, PERK1/2 and MMP9 expressions in the ventricle by Western blot assay

The ventricle was homogenized and total protein extracted followed by detection of protein concentration. Then, the protein concentration of different sample was adjusted to the same level and 75 μg of proteins were subjected to polyacrylamide gel electrophoresis. The protein was transferred onto nitrocellulose membrane. Following washing and blocking overnight, the membrane was treated with primary antibody (1:1000) at room temperature for 2 h under continuous shaking. After washing, the membrane was incubated with secondary antibody (1:40000) at room temperature for 1 h under continuous shaking. Visualization was done using ECL kit and X-ray film was obtained. The bands were scanned using Bio-Rad image system and the optical density (OD) was determined followed by analysis with Quantity-one. The OD of target genes was normalized by that of β-actin as the relative expression of target genes.

Statistical analysis

Statistical analysis was performed using SPSS version 15.0. Qualitative data were expressed as mean ± standard deviation (X±s). Means among groups were compared with one way analysis of variance, and comparisons of rate were done with chi square test. A value of $p<0.05$ was considered statistically significant.

RESULTS

MABP in different groups

The MABP in the DOC group and ALI group was 23.73±1.50 kPa and 22.85±1.21 kPa, respectively, which were markedly higher than that in the CON group (15.87±0.67 kPa) ($p<0.05$). However, there was no significantly difference between DOC group and ALI group ($p>0.05$).

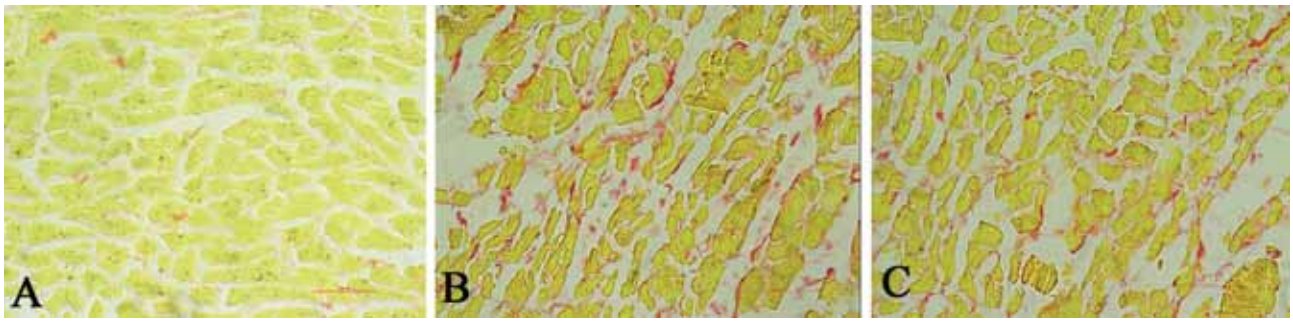

FIGURE 1. Staining of collagen in the ventricle (×400; A: control; B: DOCA; C: ALI)

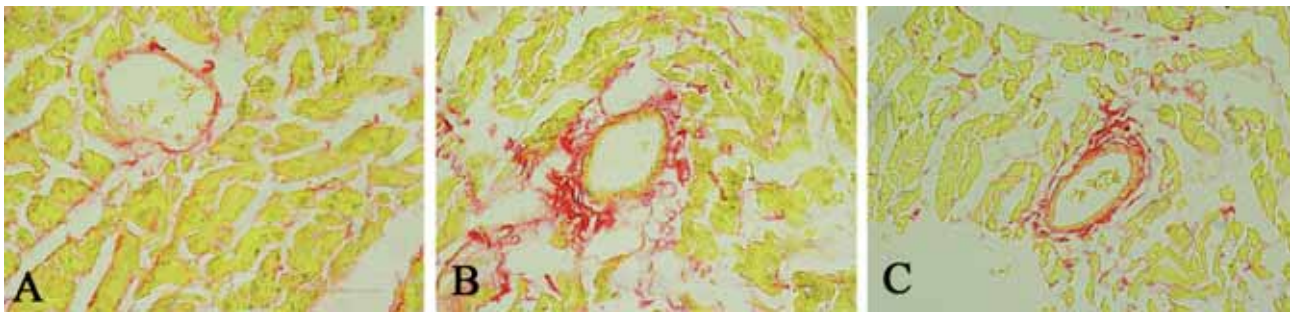

FIGURE 2. Staining of blood vessels in the ventricle (×400; A: control; B: DOCA; C: ALI)

TABLE 1. CVF and PVCA in different groups (X±s)

	CON group (n=13)	DOC group (n=11)	ALI group (n=12)
CVF	4.71±0.60	14.35±1.41*	8.11±1.13**#
PVCA	16.94±1.02	26.17±1.95**	21.22±1.31**##

Note: * p <0.05 and ** p<0.01 vs CON group;
# p <0.05 and ## p<0.01 vs DOC group.

TABLE 2. RA and Ang II levels in the plasma and ventricle of different groups (X±s)

	CON group (n=13)	DOC group (n=11)	ALI group (n=12)
Plasma RA	47.10±4.00	2.40±0.46**	2.22±0.21**
Ventricle RA	6.13±0.20	3.17±0.30*	2.17±0.20*#
Plasma Ang II	17.98±4.70	10.13±3.10*	8.05±2.60*
Ventricle Ang II	4.11±0.87	1.80±0.34*	1.12±0.22*#

Note: * p <0.05 and ** p <0.01 vs CON; # p <0.05 vs ALI group.

Collagen content in the ventricle of different groups

Following Sirius red staining, the collagens were scarlet and non-collagen tissues yellow (Figure 1. and 2.). The CVF and PVCA in different groups are shown in Table 1. When compared with the control group, the CVF and PVCA in the DOC group and ALI group were markedly increased (p<0.05 and p<0.01, respectively). However, the CVF and PVCA in the ALI group was dramatically lower than those in the DOC group (p<0.05 and p<0.01, respectively). This finding implies ALI improves the DOC induced myocardial fibrosis.

RA and Ang II levels in the plasma and ventricle

The RA level of the plasma and ventricle of DOC group and ALI group was significantly lower than those in the CON group (p<0.05 or p<0.01). Significant difference in the RA level was found in the ventricle between DOC group and ALI group (p<0.05), but marked difference was absent in the RA level of the plasma (p>0.05). The Ang II level of the plasma and ventricle of the DOC group and ALI group was also significantly decreased when compared with CON group (p<0.05). Significant difference in the Ang II level was observed between ALI group and DOC in the ventricle (p<0.05) but not in the plasma (p>0.05)(Table 2).

Protein expressions of ERK1/2, PERK1/2 and MMP-9 in the ventricle

The protein expressions of ERK1/2, PERK1/2 and MMP-9 are shown in Figure 3. Analysis showed the expressions of ERK1/2, PERK1/2 and MMP-9 in the CON group were the lowest, followed by ALI group, and those in the DOC group the highest. Significant difference in the expressions of ERK1/2, PERK1/2 and MMP-9 was found between any two groups (p<0.01). Moreover, the expressions of ERK1/2, PERK1/2 and MMP-9 in the ALI group were significantly higher than those in the CON (p<0.05) but lower than those in the DOC group (p<0.05 or p<0.01).

DISCUSSION

In the present study, the DOCA induced myocardial fibrosis rat model was employed and the anti-fibrotic ef-

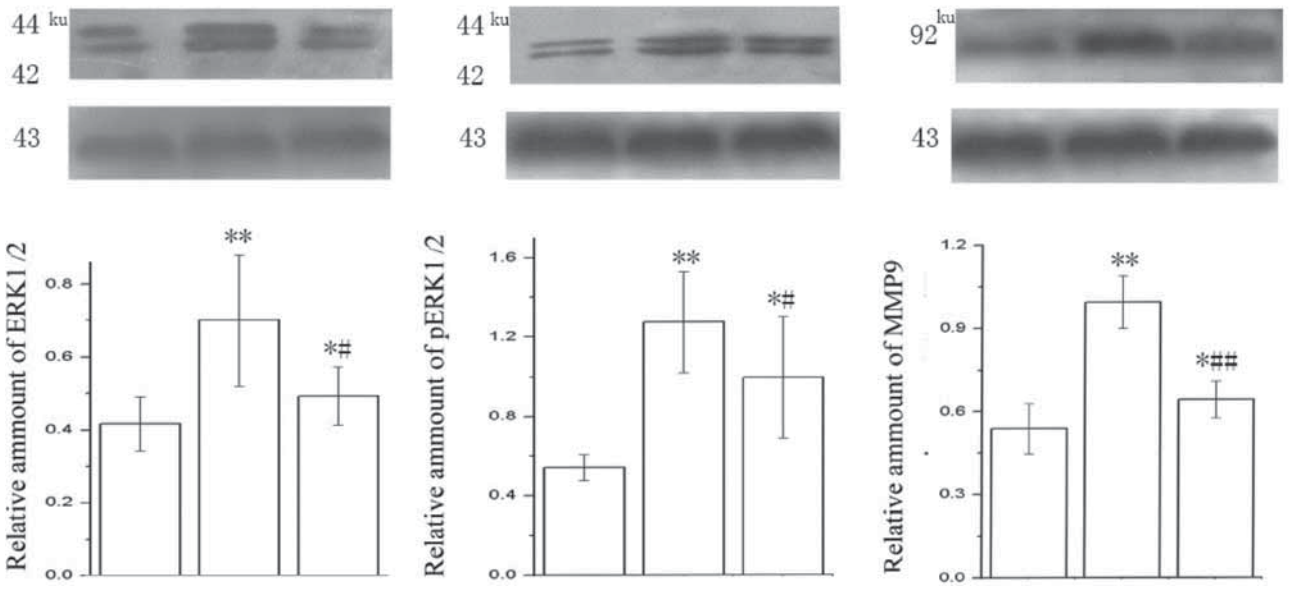

FIGURE 3. Protein expressions of ERK1/2, PERK1/2 and MMP-9 in Western blot assay (CON: control group; DOC: DOCA group; ALI: ALI group. *p<0.05 and **p<0.01 vs control group; #p<0.05 and # #p<0.01 vs DOCA group).

fect of ALI was investigated. Our findings revealed ALI could improve the myocardial fibrosis demonstrated by Sirius red staining, reduce the RA and Ang II levels in the ventricle and the expressions of ERK1/2, PERK1/2 and MMP9 as compared to the DOCA treated animals. Myocardial fibrosis refers to the aberrant deposition of extracellular matrix (ECM) in the heart, and characterized by increase of collagen in the interstitium, imbalance and irregular arrangement of different types of collagen. The imbalance between the synthesis and degradation of collagen is a major cause of myocardial fibrosis. Under the pathological conditions, the proliferation and phenotype of cardiac fibroblasts change and these cells produce a large amount of collagens resulting in imbalance between type I and type II collagens and subsequent deposition of collagens between myocardial cells. MMPs play critical role in the myocardial fibrosis through affecting the degradation of ECM. MMP9 can degrade normal collagens such as gelatin, elastin, collagen type IV collagen, type V collagen and mucin but has no influence on abnormal collagens [5]. In the myocardial fibrosis, the myocardial interstitium is occupied by abnormal collagens (mainly type I and III collagens). Under pathological conditions, the MMP-9 expression is increased and then degrades the normal collagens. Thus, the myocardial interstitium between myocardial cells loses and a large amount of abnormal collagens generated. Westermann et al. [4] investigated the effect of ALI on the rat myocardial infarction. Their results showed ALI could reduce the deposition of collagen in the infarction region and subsequent myocardial fibrosis via reducing the MMP-9 activity. Our results also revealed the MMP-9 expression was markedly elevated in rats with DOCA induced myocardial fibrosis accompanied by increased extracellular deposition of collagen. However, following ALI treatment, the MMP-9 expression and deposition of collagen were markedly decreased and myocardial fibrosis improved. In addition, studies have shown that RAAS plays an important role in the regulation of collagen metabolism in the heart and blood vessels, and Ang II and aldosterone are two major effector proteins [6, 7]. There is evidence that angiotensin-converting enzyme inhibitors (ACEI), angiotensin receptor blockers (ARB) and aldosterone receptor antagonists can significantly improve the fibrosis [2]. However, long-term application of ACEI and ARB may lead to the Ang II escape [8]. It has been confirmed that Ang II can be synthesized via both ACE-dependent and ACE-independent pathways. Continuous use of ACEI and ARB may cause accumulation of Ang I and activate ACE-independent pathways resulting in increase in Ang II. Of note, 60-70% of Ang II in the tissues is synthesized via ACE-independent pathways [9]. ALI, a renin inhibitor, acts on the first rate-limiting step of RAAS chain and blocks the activation of RAAS leading to the decrease in Ang II and aldosterone production [10]. Thus, theoretically, ALI has potent anti-fibroric effect on myocardial fibrosis. Singh et al. [11] showed, in streptomycin induced hyperglycemia rats, the ALI was superior to benazepril and losartan in improving myocardial fibrosis and apoptosis of myocardial cells. In the present study, the blood pressure was not dramatically lowered following administration of ALI, but the DOCA induced myocardial fibrosis was obviously improved. Studies showed the ventricular RAAS plays a more critical role in the myocardial fibrosis than circulation RAAS does [9, 12]. Our study further confirmed the RA and

Ang II in the circulation were largely unchanged followed ALI treatment, but those in the heart were dramatically decreased. These findings suggest the anti-fibrotic effect of ALI is related to the suppression of local Ang II production. Currently, the mechanisms underlying the anti-fibrotic effect of ALI are not completely clear. Our results showed the anti-fibrotic effect of ALI may be attributed to the suppression of phosphorylation of ERK1/2 signaling pathway. In recent years, studies show the Ang II/angiotensin receptor 1 (AT1R) mediated myocardial fibrosis is related to the ERK1/2 signaling pathway [13]. The binding of Ang II to AT1R can activate the phospholipase C on the cell membrane resulting in the hydrolysis of phosphatidylinositol phosphate and production of diacylglycerol. The later promotes the release of Ca^{2+} in the sarcoplasmic reticulum and endoplasmic reticulum. Ca^{2+} can act as a second messenger to activate ERK1/2 signaling pathway. The activation of ERK1/2 signaling pathway may facilitate the transcription of early response genes (such as c-fos) in the cardiac fibroblasts, skeletal muscle α-actin gene, β-myosin heavy chain gene and embryonic contractile protein gene and promote the expression of growth factors in fibroblasts. In addition, a large amount of ECM and collagen are produced, the proliferation of fibroblasts promoted and expressions of Iα1 and IIIα1 increased resulting in myocardial fibrosis [14, 15]. Our results showed the expressions of ERK1/2 and PERK1/2 in the ALI group were markedly decreased when compared with the DOC group. We speculate that ALI can decrease the production of AngII and local RA to reduce the Ang II/AT1R induced activation of ERK1/2, which finally exerts the anti-fibrotic effects.

CONCLUSION

Evidence shows that RAAS plays important roles in the occurrence of myocardial fibrosis and ALI has anti-fibrotic effect via its anti-inflammatory and anti-oxidative effects. The present study demonstrates that ALI as an inhibitor of renin can improve the DOCA induced myocardial fibrosis, which may be attributed to the suppression of myocardial RAAS, decrease in Ang II level and inhibition of phosphorylation of ERK1/2 signaling pathway and MMP-9 expression. However, more studies are required to confirm our results.

ACKNOWLEDGEMENTS

This study was supported by the International Cooperation Projects of Department of Science & Technology of Anhui Province (2009) (No: 0908070342)

DECLARATION OF INTEREST

We declare no conflict of interest

REFERENCES

[1] Ma TK, Kam KK, Yan BP, Yam YY. Renin-angiotensin-aldosterone system blockade for cardiovascular diseases: current status. Br J Pharmacol 2010; 160(6):1273-1292.
[2] Susic D, Varagic J, Frohlich ED. Cardiovascular effects of inhibition of renin- angiotensin-aldosterone system components in hypertensive rats given salt excess. Am J Physiol Heart Circ Physiol 2010; 298(4): H1177-1181.
[3] Gradman AH, Schmieder RE, Robert L, Nussberger J, Chiang Y, Bedigian MP. Aliskiren, a novel orally effective renin Inhibitor, provides dose-dependent antihypertensive efficacy and placebo-like tolerability in hypertensive patients. Circulation 2005; 111(8): 1012-1018.
[4] Westermann D, Riad A, Lettau O, Roks A, Savvatis K, Becher PM, et al. Renin inhibition improves cardiac function and remodeling after myocardial infarction independent of blood pressure. Hypertension 2008; 52(6):1068-1075.
[5] Li J, Schwimmbeck PL, Tschope C, Leschka S, Husmann L, Rutschow S, et al. Collagen degradation in a murine myocarditis model: relevance of matrix metalloproteinase in association with inflammatory induction. Cardiovasc Res. 2002;56(2):235-247.
[6] Johar S, Cave AC, Narayanapanicker A, Grieve DJ, Shah AM. Aldosterone mediats angiotensin II-induced interstitial cardiac fibrosis via a Nox2-containing NADPH oxidase. The FASEB Journal 2006; 20(9):1546-1548.
[7] Brilla CG. Aldosterone and myocardial fibrosis in heart failure. Herz 2000; 25(3): 299- 306.
[8] Athyros VG, Mikhailidis DP, Kakafika AI, Tziomalos K, Karagiannis A. Angiotensin II reactivation and aldosterone escape phenomena in renin-angiotensin-aldosterone system blockade: is oral renin inhibition the solution? Expert Opin Pharmacother. 2007; 8(5): 529-535.
[9] Xu J, Oscar A, Carretero B, Peng H, Shesely EG, Xu J, et al. Local angiotensin II aggravates cardiac remodeling in hypertension. Am J Physiol Heart Circ Physiol 2010; 299(5): H1328-1338.
[10] Nussberger J, Wuerzner G, Jensen C, Brunner HR. Angiotensin II suppression in humans by the orally active renin inhibitor aliskiren (SPP100): comparison with enalapril. Hypertension 2002; 39(1): E1-8.
[11] Singh VP, Le B, Khode R, Baker KM, Kumar R. Intracellular angiotensin II production in diabetic rats is correlated with cardiomyocyte apoptosis, oxidative stress, and cardiac fibrosis. Diabetes 2008; 57(12): 3297-3306.
[12] Zhong JC, Basu R, Guo D, Chow FL, Byrns S, Schuster M, et al. Angiotensin-converting-enzyme 2 suppresses pathological hypertrophy, myocardial fibrosis, and cardiac dysfunction. Circulation 2010; 122(7): 717-728.
[13] Olson ER, Shamhart PE, Naugle JE, Meszaros JG. Angiotensin II-induced extracellular signal-regulated kinase 1/2 activation is mediated by protein kinase Cdelta and intracellular calcium in adult rat cardiac fibroblasts. Hypertension 2008; 51(3):704-711.
[14] Tang W, Wei Y, Le K, Li Z, Bao Y, Gao J, et al. Mitogen-activated protein kinases ERK 1/2- and p38-GATA4 pathways mediate the Ang II-induced activation of FGF2 gene in neonatal rat cardiomyocytes. Biochem Pharmacol 2011; 81(4):518-525.
[15] Mehta PK, Griendling KK. Angiotensin II cell signaling: physiological and pathological effects in the cardiovascular system. Am J Physiol Cell Physiol 2007; 292(1):C82-97.

TFF1 inhibits proliferation and induces apoptosis of gastric cancer cells *in vitro*

Yanli Ge[#], Junjie Zhang[#], Jianchun Cao[#], Qiong Wu, Longe Sun, Likun Guo, Zhirong Wang[*]

Department of Gastroenterology, Tongji Hospital, Tongji University, Shanghai200065, China

Abstract

Trefoil Factor Family (TFF) plays an essential role in the intestinal epithelial restitution, but the relationship between TFF1 and gastric cancer (GC) is still unclear. The present study aimed to determine the role of TFF1 in repairing gastric mucosa and in the pathogenesis of GC.

The TFF1 expression in different gastric mucosas was measured with immunohistochemistry. Then, siRNA targeting TFF1 or plasmids expressing TFF1 gene were transfected into BGC823 cells, SGC7901 cells and GES-1 cells. The cell proliferation was detected with MTT assay and apoptosis and cell cycle measured by flow cytometry.

From normal gastric mucosa to mucosa with dysplasia and to gastric cancer, the TFF1 expression had a decreasing trend. Down-regulation of TFF1 expression significantly reduced the apoptosis of three cell lines and markedly facilitated their proliferation but had no significant effect on cell cycle. Over-expression of TFF1 could promote apoptosis of three cell lines and inhibit proliferation but had no pronounced effect on cell cycle. TFF1 can inhibit proliferation and induce apoptosis of GC cells *in vitro.*

KEY WORDS: Trefoil Factor Family 1, gastric cancer, apoptosis, *in vitro*

INTRODUCTION

Although the incidence of gastric cancer (GC) has declined over the past 30 years worldwide, especially in western countries, it remains the second leading cause of cancer-related death and accounts for 10.4% of cancer deaths globally [1]. About 1150000 GC cases and 738000 cancer deaths are estimated to have occurred in 2008 worldwide [2]. More than one-half of GC patients have lymph node metastases when they are initially diagnosed or operated, which usually results in poor prognosis [3-5]. Therefore, it is important to investigate the pathogenesis of GC, find effective measures to prevent and treat GC. The trefoil factor family (TFF), which comprises gastric peptides pS2/TFF1 and spasmolytic peptide (SP)/TFF2 and intestinal trefoil factor (ITF)/TFF3, plays an essential role in the intestinal epithelial restitution [6]. They are small (7~12 kDa) protease-resistant proteins and are abundantly secreted onto the mucosal surface by mucus-secreting cells in the gastrointestinal tract. The TFFs share an absolutely conserved distinct motif of six cysteine residues that define a so-called "trefoil" domain, which is also known as a "P" domain [7]. At certain physiological conditions, in the presence of a tissue-specific distribution, TFF plays an important role in mucosal protection and wound healing. But in malignant tissues, TFF is highly expressed and correlated strongly with the genesis, metastasis and invasion of tumor cells. These indicate that TFF may be a common mediator of oncogenic responses to different stimuli. The biological functions of TFF involve complex regulatory processes. TFF1 was first discovered in breast cancer cell line MCF-7 in 1982 [8-9]. In normal tissues, the main site of expression of TFF1 is the mucosal epithelial cells of gastric body and antrum in a site-specific fashion. However, under pathological conditions, such as ulceration, the TFF1-expression of site-specific fashion is absent, TFF1 can be identified in any damaged mucosas, and its expression is up-regulated to participate in gastrointestinal epithelial reconstruction and repair process [10]. However, there is lack of TFF1 expression in human GC. To determine the function of TFF1, the mouse TFF1 gene was inactivated. The antral and pyloric gastric mucosa of mpS2-null mice was dysfunctional and exhibited severe hyperplasia and dysplasia. All homozygous mutant mice developed antropyloric adenoma, and 30% developed multifocal intraepithelial or intramucosal carcinomas. These results indicate that TFF1 is essential for the nor-

# These authors contributed equally to this work.
* Corresponding author: Zhirong Wang,
Department of Gastroenterology, Tongji Hospital,
Tongji University, Shanghai 200065, China
Tel: +8621-66111329; Fax: +8621-56050502
E-mail: docwangwang@yeah.net

Submitted: 8. December 2011 / Accepted: 27. February 2012

mal differentiation of antral and pyloric gastric mucosa and may function as a gastric-specific tumor suppressor gene [11]. The aim of our study is to determine the role of TFF1 in repairing gastric mucosa and in the pathogenesis of GC. To this end, the TFF1 expression was detected in different gastric mucosas. Then, siRNA targeting TFF1 and plasmids expressing TFF1 were transfected into normal gastric mucosal epithelial cells (GES-1 cells [12]), highly malignant GC cell line (BGC823 cells) and moderately malignant GC cell line (SGC7901 cells), respectively, to investigate the effect of TFF1 on the biological behaviors of gastric mucosal epithelial cells, which provides evidence for further investigation and application of TFF1 target therapy.

MATERIALS AND METHODS

Sample collection and immunohistochemistry

GC tissues and adjacent normal and atypical hyperplasia gastric mucosas were obtained from 45 patients undergoing gastroscopy at Tongji Hospital of Tongji University. The characteristics of these patients are shown in Table 1. All antibodies used for immunohistochemistry were purchased from Zhongshan Goldenbridge Biotechnology CO., LTD (Beijing, China). All other chemicals and reagents were commercially available and had the highest purity. Tissues were fixed in 10% formaldehyde in phosphate buffered saline (PBS), embedded in paraffin, and cut into 5-μm sections. Sections were heated at 50°C overnight, deparaffinzed with xylene twice, and rinsed in a decreasing ethanol series (100-70%) for 5 min/solution. Samples were treated with 3% H_2O_2 for 30 min to inactivate endogenous peroxidase. Antigen retrieval was done with 0.01 M Na-citrate buffer (pH 6.0) in a microwave oven for 30 min. Sections were incubated at 4 °C overnight in moist chambers with primary antibody (1:100) and then with biotinylated secondary antibody (Zhongshan Goldenbridge Biotechnology CO., LTD., Beijing, China, SP-Kit) for 30 min at room temperature, followed by incubation with streptavidin peroxidase. Visualization was done with diaminobenziding tetrachloride and counterstaining was performed with haematoxylin. In negative controls, the primary antibody was replaced with PBS. Sections were observed under a light microscope and positive cells had brown granules in cytoplasm. Five fields were randomly selected from each section at high magnification, and 100 cells were counted in each field, followed by calculation of percentage of positive cells. Sections with positive cells of >15% was regarded as positive.

Cell culture

Two gastric adenocarcinoma cell lines (BGC823 cells and SGC7901 cells) (Cell bank of Chinese Academic of Sciences), as well as normal gastric epithelial cell line (GES-1 cells) (Tumor Institute of Beijing Medical University, China) were maintained in RPMI 1640 medium (Gibco BRL, USA) supplemented with 10% fetal bovine serum (FBS; Hangzhou Sijiqing, China) and 100 μg/ml streptomycin and penicillin G (Amresco, USA) at 37 °C under 5% humidified CO_2. Passaging was performed every 3 days by trypsinization (Sigma, USA).

Synthesis of TFF1-siRNA and Cell Transfection

mRNA sequence of TFF1 was obtained from GeneBank. With Invitrogen's online design software BLOCK-iTTM RNAi Designer, three sites (stealth 115, stealth 144, stealth 268), and they were selected and designed to be three sets of targeting stealth siRNA sequence. The selection and design were based on three principles: avoiding the 5' and 3' end non-coding region, selecting the sequences with G/C ratio between 35% and 55% and using BLAST to exclude other coding sequences. Stealth siRNA sequences are shown in Table 2. When the cell confluence reached about 40%~60%, transfection of Stealth siRNAs and stealth RNA negative control was performed with LipofectamineTM2000 according to manufacturer's instructions (Invitrogen, USA). Cells transfected with Stealth siRNAs was defined as Stealthgroup, those transfect with Stealth negative control as negative control group, and those without transfection as blank control group.

Detection of TFF1 mRNA expression by RT-PCR

Total RNA was extracted with Trizol reagent (Invitrogen, USA). About 5 μg of RNA were used for reverse transcription with random primers to synthesize first strand cDNA, followed by conventional PCR amplification with 1 μl of cDNA as template. The forward primers, reverse primers and anticipated size of products and GAPDH are shown in Table 3. The volume of reaction system was 25 μl, and reaction conditions were as follows: denaturation at 94 °C for 1 min; an-

TABLE 1. Characteristics of 45 patients

	n	Age (yr) (mean ± SD)	Sex	
			Male	Female
Normal gastric mucosa	15	56±13	7	8
Atypical hyperplasia gastric mucosa	15	55±8	9	11
GC mucosa	15	56±11	12	8

TABLE 2. Sequences of stealth siRNAs

siRNA target point	Sequences of stealth siRNAs
stealth_115	5'-CACUGUACACGUCUCUGUCUGGGCC-3'
stealth_144	5'-AAACCACAAUUCUGUCUUUCACGGG-3'
stealth_268	5'-AAAUUCACACUCCUCUUCUGGAGGG-3'

TABLE 3. Primers for RT-PCR

gene	Primers (5'-3')	Size (bp)
TFF1	Forward: ATGGCCACCATGGAGAACAA	159
	Reverse: ATTTGCACACTGGGAGGGCG	
GAPDH	Forward: ACCACAGTCCATGCCATCAC	452
	Reverse: TCCACCACCCTGTTGCTGTA	

nealing at 59 °C for 1 min; extension at 72 °C for 1 min. The products were then subjected to agarose gel electrophoresis, and images were captured to analyze the quality of RNA.

Determination of cell proliferation with MTT assay

Cell viability was determined by MTT assay. Different cell lines were seeded at 10^5/ml into 96-well plates, and then divided into blank control group, blank transfection group, stealth_115 group, stealth_144 group and stealth_268 group. At 24 h after transfection, the cell proliferation was determined by MTT assay every other 24 h for 5 days. In brief, at designed time points, MTT was added into each well at a final concentration of 0.5 mg/ml followed by incubation for 4 h at 37 °C. The formazan was dissolved by addition of dimethylsulfoxide (DMSO) and absorbance (A) was measured with microplate reader (Bio-Rad, USA) at 570 nm. The inhibition rate (IR) was calculated formulas follow: $IR\% = (1-A_{experiment}/A_{control})\times 100\%$.

Detection of cell cycle by flow cytometry

At 72 h after transfection, cells (1×10^6 cells) were harvested and washed twice in cold PBS. Cells were fixed in 70% ethanol and washed in cold PBS. Then, the cells were suspended in 1 ml of propidium iodide (PI, Sigma, USA) solution containing 40 μg/ml PI, 100 μg/ml RNAase (Sigma, USA), 0.1% (w/v) sodium citrate and 0.1% (v/v) Triton X. Cells were incubated at room temperature in dark for at least 30 min, and analyzed by flow cytometry (Beckman, USA).

Detection of cell apoptosis by flow cytometry

At 72 h after transfection, 5×10^5 cells were harvested. According to the instructions in Annexin V-FITC kit (Nanjing Keygen Biotech. Co. Ltd., China), cells were suspended in 500 μl of binding buffer and 5 μl of Annexin V-FITC followed by addition of 5 μl of PI and subsequent incubation for 15 min at room temperature in dark. Apoptosis was detected by flow cytometry.

Construction of plasmid TFF1-pcDNA3.1 and cell transfection

Human plasmid TFF1-pcDNA3.1 was constructed and identified by Shanghai Shuiyuan Biotechnology Company. Cells were divided into TFF1-pcDNA3.1 transfection group, pcDNA3.1 negative control group and blank control group. Cells were seeded into 24-well plates. When cell confluence reached about 50%, transfection was performed with LipofectamineTM2000 according to manufacturer's instructions (Invitrogen, USA).

Detection of TFF1 protein expression by western blot

Total protein was extracted and 30 μg of proteins were subjected to polyacrylamide gel electrophoresis. Then, the proteins were transferred onto PVDF membrane, which were blocked for 2 h at 4 °C in 5% non-fat milk and then incubated with mouse anti-human TFF1 or GAPDH monoclonal antibody (Santa Cruz, USA; 1:2000) for 1.5 h at room temperature. After washing in PBST thrice (10 min for each), the membrane was incubated with HRP-conjugated goat anti-mouse secondary antibody (Santa Cruz, USA; 1:2000) at room temperature for 1.5 h. Following rinsing in PBS, visualization was done and images were captured with a Touching gel imaging system. In negative control group, primary antibody was replaced with PBS.

Determination of cell proliferation with MTT assay

Different cell lines were inoculated at 10^5/ml into 96-well plates, and then divided into blank control group, TFF1-pcDNA3.1-transfection group and pcDNA3.1 transfection group. At 24 h after transfection, cell proliferation was measured with MTT assay every other 24 h for 5 days. The procedures of MTT assay were abovementioned.

Detection of cell cycle by flow cytometry

At 48 h after transfection, cells (1×10^6 cells) were harvested and processed with above procedures. Cell cycle was measured by flow cytometry.

Detection of cell apoptosis by flow cytometry

At 48 h after transfection, 5×10^5 cells were harvested and processed with above procedures. Cell apoptosis was detected by flow cytometry.

Statistical analysis

SPSS version 12.0.1 statistical software was employed for statistical analysis and data were expressed as means ± standard deviation ($\overline{X} \pm s$). Independent sample t-test was used to compare data between two groups and one-way ANOVA to compare date among multiple groups. If there were significant differences, a further least significant difference method would be used for pairwise comparison. A value of $p < 0.05$ was considered statistically significant.

RESULTS

TFF1 Expressionin different mucosal tissues

TFF1 were mainly expressed in the cytoplasm of gastric mucosal cells. Perinuclear accumulation was the most obvious and positive cells were stained brown. The closer to the cell membrane is, the deeper the color is. The positive expression rate of TFF1 in normal gastric mucosa was 100% (15/15). In mucosas with dysplasia, the TFF1 expression was slightly reduced and the positive expression rate was 80.0% (16/20). From normal gastric mucosa, dysplasic mucosa to

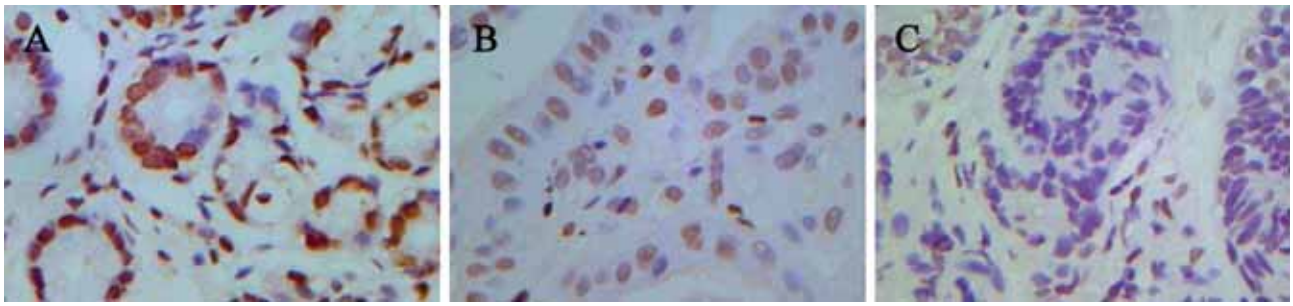

FIGURE 1. Immunohistochemistry for TFF1 in different gastric mucosas. A: normal gastric mucosa. B: dysplasic gastric mucosa. C: GC.

TABLE 4. TFF1 protein expression in different patients

Group	Total	Positive (N)	Negative (N)	Positive rate (%)
gender				
male	28	23	5	82.1
female	27	21	6	77.8
age				
≥60 yr	31	24	7	77.4
<60 yr	24	20	4	83.3
gastric mucosas				
normal gastric mucosa	15	15	0	100
dysplasic gastric mucosa	20	16	4	85.0*
GC	20	13	7	65.0*

*$p < 0.05$ vs normal gastric mucosa

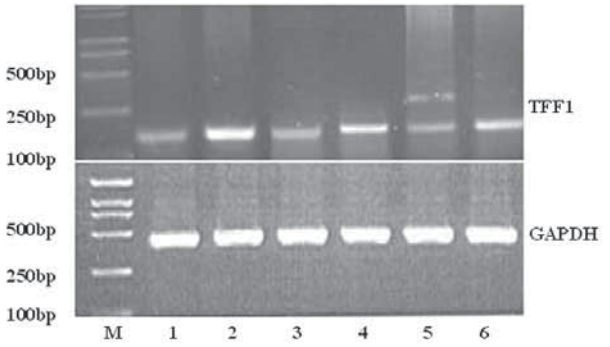

FIGURE 2. TFF1 mRNA expression in stealth_144 group at 48 h after transfection. M: DNA Marker; 1: GES-1 cells with transfection; 2: control GES-1 cells; 3: BGC-823 cells with transfection; 4: control BGC-823 cells; 5: SGC7901 cells with transfection; 6: control SGC7901 cells

GC, the TFF1 expression had a gradually decreasing trend, and significant difference in TFF1 expression was noted among groups (Table 4, Figure 1). The positive expression rate of TFF1 was 82.1% in males (23/28) and 77.8% in females (21/27) showing no significant difference. The positive expression rate of TFF1 was 77.4% in patients aged ≥ 60 years (24/31) and 83.3% in those aged <60 years (20/24) showing no marked difference. These results suggest that TFF1 expression was independent of both age and gender (Table 4).

Stealth siRNA inhibited mRNA expression of TFF1

Results from RT-PCT showed stealth siRNA significantly inhibited TFF1 expression in a time dependent manner. At 24 h after transfection, the inhibition of TFF1 expression was present, and then reached a maximal level at 48 h after transfection but became to reduce at 72 h after transfection. Different stealth siRNAs inhibited the TFF1 expression when compared with control group and blank transfection group. The inhibitory effect of stealth_144 was the most obvious and, at 48 h after transfection, the inhibition rate of TFF1 expression in GES-1 cells, BGC823 cells and SGC7901 cells was 69.0%, 55.6% and 70.5%, respectively. The inhibitory effect was comparable among 3 different cell lines. Although TFF1 expression in negative control group was slightly lower than that in control group, there was no significant difference ($p>0.05$) (Figure 2).

Down-regulation of TFF1 reduced apoptosis rate and promoted cell proliferation but had no effect on cell cycle

MTT assay showed that the proliferation of three cell lines undergoing transfection with stealth siRNAs increased significantly at 48 h and 72 h after transfection ($p<0.05$), and the increase in steath_144 group was the most obvious and reached a peak level at 72 h after transfection. The proliferation remained comparable among cells at 24 h, 96 h and 120 h after transfection ($p>0.05$) (Table 5, Figure 3). The apoptosis rate of three cell lines was significantly reduced at 72 h after TFF1 stealth siRNA transfection when compared with control group ($p<0.05$). The reduction of apoptosis rate in stealth_144 group was most obvious and the apoptosis rate in BGC823 cells, SGC7901 cells and GES-1 cells was reduced by 41.4%, 45.4% and 45.3%, respectively. However, there was no

TABLE 5. Proliferation of BGC823 cells, SGC7901 cells and GES-1 cells at 72 h after stealth siRNA transfection

group	BGC823		SGC7901		GES-1	
	A value	IR%	A value	IR%	A value	IR%
control	1.107±0.02		1.122±0.04		0.931±0.05	
blank transfection	1.113±0.10	-0.5	1.098±0.23	2.1	0.902±0.12	1.2
stealth_115	1.121±0.05*	-12.6	1.30±0.11*	-15.9	1.004±0.08*	-7.8
stealth_144	1.129±0.12*	-19.8	1.331±0.21*	-18.6	1.117±0.25*	-20.0
stealth_268	1.119±0.08*	-10.8	1.283±0.15*	-14.3	1.103±0.17*	-18.5

*$p < 0.05$ vs control group

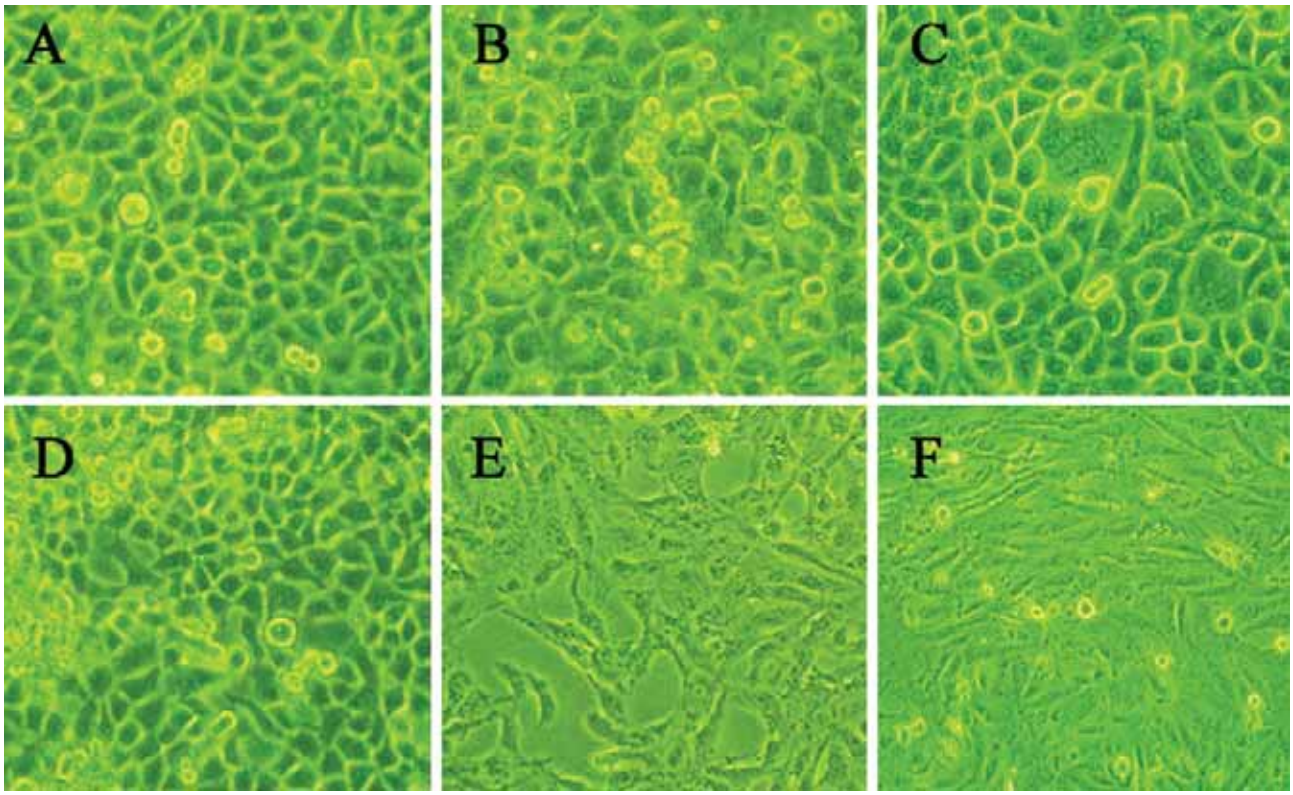

FIGURE 3. Stealth siRNA promotes cell proliferation at 72 h after transfection (×200) A: control SGC7901 cells. B: SGC7901 transfected with stealth_144. C: control BGC823 cells. D: BGC823 transfected with stealth_144. E: control GES-1 cells. F: GES-1 transfected with stealth_144.

TABLE 6. Cell cycle and apoptosis rate of BGC823 cells at 72 h after stealth siRNA transfection

Group	Cell cycle			Apoptosis rate
	G_0/G_1	S	G_2/M	
Black Control	56.72±2.11	36.78±1.10	6.5±0.89	4.83±0.56
Stealth negative control	57.07±1.68	35.43±1.21	7.2±0.26	5.03±0.38
Stealth_115	57.27±1.32	35.86±1.38	6.87±0.35	2.96±0.51*
Stealth_144	55.98±1.43	36.42±1.31	7.6±0.28	2.83±0.25*
Stealth_268	56.43±1.69	37.21±1.38	6.36±0.36	3.02±0.14*

*$p < 0.05$ vs control group

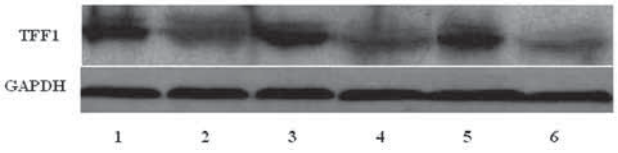

FIGURE 4. TFF1 protein expression at 48 h after transfection with TFF1-pcDNA3.1. 1: GES-1 cells with transfection; 2: control GES-1 cells; 3: BGC-823 cells with transfection; 4: control BGC-823 cells; 5: SGC7901 cells with transfection; 6: control SGC7901 cells

marked difference in apoptosis among cells transfected with different stealth siRNAs .There was no significant alteration in cell cycle among stealth_115 group, stealth_144 group and stealth_268 group at 72 h after transfection (p>0.05) (Table 6).

TFF1 protein expression after transfection with TFF1-pcDNA3.1

When compared with TFF1 expression before transfection, the TFF1 protein expression in GES-1 cells, BGC823 cells and SGC7901 cells was markedly increases (p<0.05) in a time dependent manner. Increase of TFF1 expression was noted as early as 24 h after transfection, but the TFF1 expression was similar to that in control group (p>0.05). TFF1 expression reached a peak level at 48 h after transfection but began to reduce at 72 h after transfection (Figure 4)

Over-expression of TFF1 promoted apoptosis, inhibited cell proliferation but had no effect on cell cycle

MTT assay showed that cell proliferation reduced after TFF1-pcDNA3.1 transfection,. The IR was the most obvious at 48 h after transfection (p<0.05). The IRs of GES-1 cells, BGC823

TABLE 7. Effect of pcDNA3.1 transfection on proliferation of BGC823 cells, SGC7901 cells and GES-1 cells

Groups	BGC823		SGC7901		GES-1	
	A	IR%	A	IR%	A	IR%
Control	0.960±0.13		1.074±0.08		0.876±0.05	
pcDNA3.1 blank	0.942±0.08	1.8	1.027±0.14	2.1	0.868±0.21	1.2
TFF1-pcDNA3.1	0.648±0.07*	32.5	0.754±0.11*	29.8	0.667±0.08*	23.8

*$p < 0.05$ vs control group

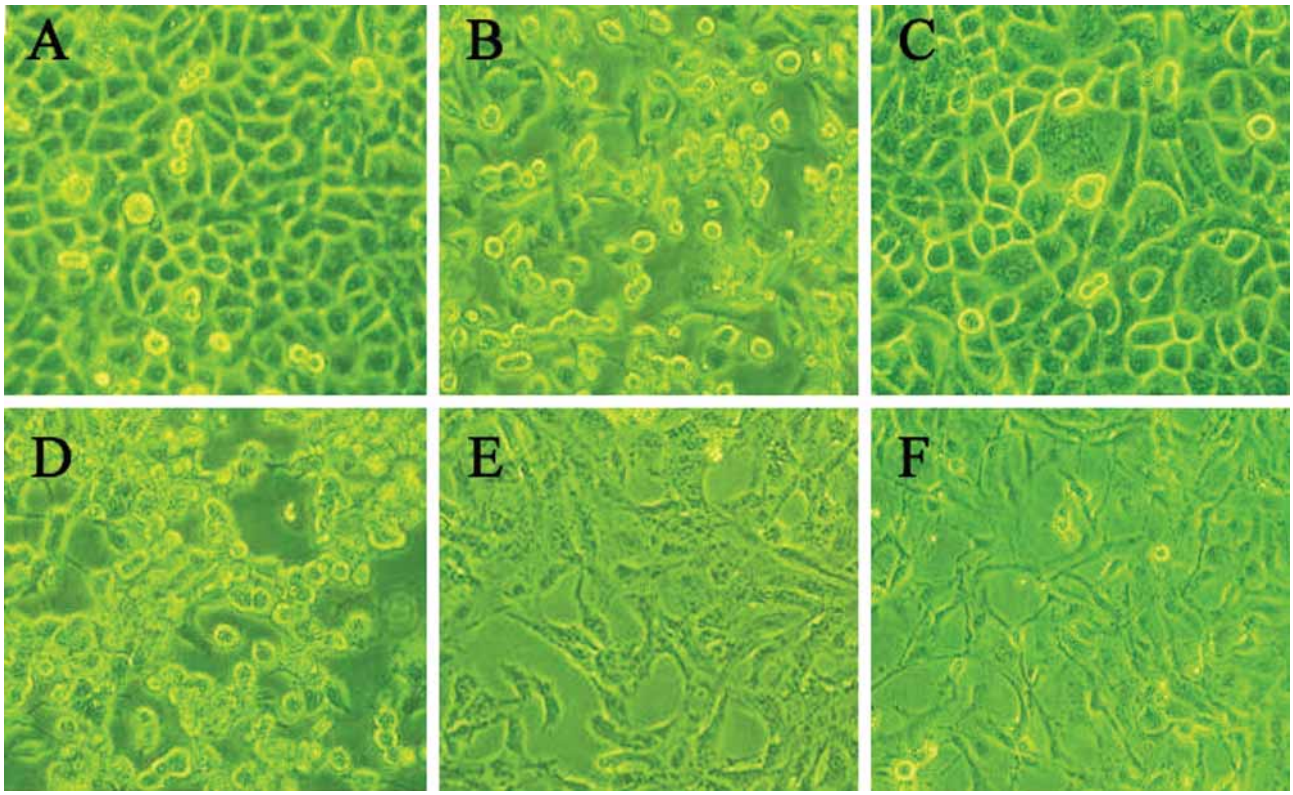

FIGURE 5. TFF1-pcDNA3.1 transfection inhibited cell proliferation (48 h; ×200) A:control SGC7901 cells; SGC7901 cells with TFF1-pcDNA3.1 transfection; C: control BGC823 cells; D: BGC823 cells with TFF1-pcDNA3.1 transfection; E:control GES-1 cells; F: GES-1 cells with TFF1-pcDNA3.1 transfection

TABLE 8. Changes in cell cycle and apoptosis rate of BGC823 cells at 48 h after TFF1-pcDNA3.1 transfection (%)

Group	Cell Cycle			Apoptosis Rate
	G_0/G_1	S	G_2/M	
Black Control	56.72±2.11	36.78±1.10	6.5±0.89	4.83±0.56
pcDNA3.1 control	55.23±1.72	37.29±3.11	7.48±0.45	4.57±0.23
TFF1-pcDNA3.1	46.67±2.89*	47.23±2.65*	6.10±0.54	14.38±0.89*

*$p < 0.05$ vs control group

cells and SGC7901 cells were 23.8%, 32.5% and 29.8%, respectively. At 72 h and 96 h after transfection, the IR was also dramatically reduced when compared with control group ($p<0.05$). At 24 h and 120 h after transfection, there was no significant alteration in the IR ($p>0.05$) (Table 7, Figure 5). The apoptosis rate of TFF1-pcDNA3.1 transfected cells markedly increased at 48 h after transfection when compared with control group ($p<0.05$). The apoptosis rate increased from 6.28 ± 0.33 to 18.46 ± 1.23 in GES-1 cells, from 4.83 ± 0.56 to 14.38 ± 0.89 in BGC823 cells, and from 7.23 ± 0.48 to 19.85 ± 0.74 in SGC7901 cells (Table 8). After TFF1-pcDNA3.1 transfection, the proportion of cells in G1 and G2/M phase markedly decreased, while that in S-phase significantly increased, indicating that cells were arrested in S phase. The cell cycle distribution was markedly different from that in control group ($p<0.05$) (Table 8).

DISCUSSION

Under physioligical conditions, human TFF1 is mainly expressed in epithelial cells of gastrointestinal tract. TFF1 expression has regional and cellular selectivity, and, in normal tissues, TFF1 is expressed in the gastric antrum, the crypt of gastric body and mucosa. Low TFF1 expression is also noted in the small intestine, colon and breast epiderm. However, under pathological conditions, the specificity in TFF1 expression is absent. When the gastrointestinal mucosa is injured, TFF1 may be expressed in the injured mucosa of gastrointestinal tract, and its expression is rapidly up-regulated to participate in the reconstruction and repair process of epithelial cells in gastrointestinal tract. Our study found that, in normal gastric mucosa, the TFF1 expression was mainly found in gastric epithelial cells, gastric pits and glands, which was consistent with previous study. In addition, TFF1 is now considered as a tumor suppressor, and may be a stomach-specific suppressor factor. In humans, about 50% of GC patients show loss of human pS2 expression. It is generally believed that GC is preceded by a precancerous progress with the following well-recognized steps: normal gastric mucosa, chronic active inflammation, multifocal atrophy (gland loss), intestinal metaplasia, complete type-intestinal metaplasia, incomplete type-dysplasia [13, 14]. The accumulation of many genetic and molecular changes is closely

related to the evolution [15]. Taupin et al. [16] investigated the expressions of pS2 and ITF in different gastric mucosal injury models. Results showed that, in the gastric mucosa metaplasia-dysplasia-gastric cancer process, the TFF1 expression was gradually reduced, and TFF1 expression was lost earlier than the differentiation of gastric epithelial metaplasia, suggesting that loss of TFF1 expression is an early event in the occurrence of GC. Our results confirmed that TFF1 expression had a decreasing trend from normal gastric mucosa, gastric dysplasia to GC, consistent with previous findings. In recent years, studies have shown that TFF1 is relevant with cell proliferation and apoptosis to some extents. Rodrigues et al. [17] found that, in colon cancer cells undergoing transfection of TFF1, cell dispersion was promoted possibly through cyclooxygenase (COX) and thromboxane A2 (TXA-2) receptor dependent mechanism, enhancing the ability of cell infiltration. Another study [18] indicated that TFF1 played a dual role on the gastrointestinal cells: on one hand, TFF1 can block the transition from G1 phase to S phase, which interrupts the gastrointestinal cell differentiation and reduces cell proliferation; on the other hand, TFF1 prevents chemical factor-induced apoptosis. These reveal TFF1 is a regulatory factor of gastrointestinal cell differentiation. To reduce cell proliferation and induce differentiation are functional characteristics of tumor suppressors. Apoptosis refers to the programmed cell death in the growth, development and differentiation of cells and pathological environments. It is a type of cell death different from necrosis. Recent studies have found that apoptosis plays a unique role in the renewing of gastrointestinal mucosa and in the pathological processes of some digestive diseases. TFF1 exerts its anti-tumor effect through regulating the balance between cell proliferation and apoptosis. Taupin et al. [19] investigated the influence of TFF3 and its mutants on apoptosis and results showed that TFF3 trefoil domain mutant and alteration could promote cell migration, and increase the resistance to death during the process of migration. The mutations of trefoil domain were also detectable in TFF1, a protein with similar structure to TFF3, and this region is critical for the anti-tumor effect of TFF1 [20]. In our study, the TFF1 mRNA expression was inhibited by Stealth siRNA transfection, and the TFF1 was over-expressed followed transfection of plasmids expressing TFF1 gene. After inhibition of TFF1 expression by siRNA targeting TFF1, the proliferation rate of human GC cells and normal human gastric epithelial cells significantly increased and apoptosis decreased, but cell cycle was not significantly altered. After transfection with plasmids expressing TFF1, results revealed the proliferation rate of human GC cells and normal human gastric epithelial cells significantly decreased, apoptosis increased, and cells in G1 and G2/M phase decreased, while cells in S-phase increased and cells were arrested in S phase, which suggest that TFF1 can exert important effects on cell proliferation and apoptosis. It is speculated that the inhibition of GC by TFF1 may be attributed to that it can regulate the balance between cell proliferation and apoptosis. Cell proliferation is promoted and apoptosis rate reduced after silencing TFF1 expression which breaks the balance of TFF1 expression. The biological characteristics of a tumor are infinite proliferation and de-differentiation. The reduced TFF1 expression may promote the GC development. This speculation is needed to be further confirmed. As a whole, despite a growing number of studies have confirmed TFF1 plays a crucial role in the occurrence and development of GC, the exact mechanism of anti-tumor effect of TFF1 is still poorly understood and more studies are required.

CONCLUSION

In our study, we find that TFF1 can inhibit proliferation and induce apoptosis of GC cells *in vitro*.

DECLARATION OF INTEREST

The authors report no conflicts of interest.

REFERENCES

[1] Jemal A, Siegel R, Ward E, Hao Y, Xu J, Murray T, et al. Cancer statistics, 2008. CA Cancer J Clin 2008, 58: 71-96.

[2] Jemal A, Bray F, Center MM, Ferlay J, Ward E, Forman D. Global Cancer Statistics. CA Cancer J Clin 2011;61(2):69-90.

[3] Abe N, Watanabe T, Suzuki K, Machida H, Toda H, Nakaya Y, et al. Risk factors predictive of lymph node metastasis in depressed early gastric cancer. Am J Surg 2002; 183:168-72.

[4] Yamaguchi T, Sano T, Katai H, Sasako M, Maruyama K. Node-positive mucosal gastric cancer: a follow-up study. Jpn J Clin Oncol 2001; 31:153-6.

[5] Chen CY, Wu CW, Lo SS, Hsieh MC, Lui WY, Shen KH. Peritoneal carcinomatosis and lymph node metastasis are prognostic indicators in patients with Borrmann type IV gastriccarcinoma. Hepatogastroenterology 2002; 49:874-7.

[6] Kjellev S. The trefoil factor family - small peptides with multiple functionalities. Cell Mol Life Sci. 2009 ;66(8):1350-69.

[7] Wong WM, Poulsom R, Wright NA. Trefoil peptides . Gut 1999; 44(6): 890-895.

[8] Masiakowski P, Breathnach R, Bloch J, Gannon F, Krust A, Chambon P. Cloning of cDNA sequences of hormone-regulated genes from the MCF-7 human breast cancer cell line. Nucleic Acids Res. 1982;10(24):7895-903.

[9] Prud'homme JF, Fridlansky F, Le Cunff M, Atger M, Mercier-Bodart C, Pichon MF, et al. Cloning of a gene expressed in human breast cancer and regulated by estrogen in MCF-7 cells. DNA 1985; 4: 11-21.

[10] Pera M, Heppell J, Poulsom R, Teixeira FV, Williams J. Ulcer associated cell lineage glands expressing trefoil peptide genes are induced by chronic ulceration in ileal pouch mucosa. Gut 2001;48:792-796.

[11] Lefebvre O, Chenard MP, Masson R, Linares J, Dierich A, LeMeur M, et al. Gastric mucosa abnormalities and tumorigenesis in mice lacking the pS2 trefoil protein. Science 1996;274(5285): 259-62.

[12] Ke Y, Ning T, Wang B. Establishment and characterization of a SV40 transformed human fetal gastric epithelial cell line-GES-1.

Zhonghua Zhong Liu Za Zhi 1994;1:7-10.
[13] Correa P, Haenszel W, Cuello C, Tannenbaum S, Archer M. A model for gastric cancer epidemiology. Lancet 1975; 2: 58-60.
[14] Correa P. Human gastric carcinogenesis: a multistep and multifactorial process-First American Cancer Society Award Lecture on Cancer Epidemiology and Prevention. Cancer Res 1992; 52:6735-6740.
[15] Tahara E. Genetic pathways of two types of gastric cancer. IARC Sci Publ, 2004; (157): 327 -349.
[16] Taupin D, Pedersen J, Familari M, Cook G, Yeomans N, Giraud AS. Augmented Intestinal Trefoil Factor (TFF3) and Loss of pS2 (TFF1) Expression Precedes Metaplastic Differentiation of Gastric Epithelium. Lab Invest 2001; 81(3): 397-408.
[17] Rodrigues S, Van Aken E, Van Bocxlaer S, Attoub S, Nguyen QD, Bruyneel E, et al. refoil peptide as proangiogenic factor in vivo and in vitro: implication of cyclooxygenase-2 and EGF receptor signaling. FASEB J 2003; 17(1): 7-16.
[18] Bossenmeyer-Pourié C, Kannan R, Ribieras S, Wendling C, Stoll I, Thim L, et al. The trefoil factor 1 participates in gastrointestinal cell differentiation by delaying G1-S phase transition and reducing apoptosis. J Cell Biol 2002; 157(5): 761-770.
[19] Taupin DR, Kinoshita K, Podolsky DK. Intestinal Trefoil factor confers colonic epithelial resistance to apoptosis. Proc Natl Acad Sci USA, 2000; 97(2): 799-804.
[20] Yio X, Diamond M, Zhang JY, Weinstein H, Wang LH, Werther L, et al. Trefoil factor family 1 mutations enhance gastric cancer cell invasion through distinct signaling pathways. Gastroenterology 2006; 130(6): 1696-706.

Prevalence of 1691G>A *FV* mutation in Poland compared with that in other Central, Eastern and South-Eastern European countries

Grażyna Adler[1#*], Jeremy S C Clark[2#], Beata Łoniewska[3], Ewa Czerska[4], Nermin N Salkic[5], Andrzej Ciechanowicz[2]

[1] Department of Medical Biology, Pomeranian Medical University, Powst.Wlkp. 72, 70-111 Szczecin, Poland. [2] Department of Clinical and Molecular Biochemistry,, Pomeranian Medical University , Powst. Wlkp. 72, 70-111Szczecin, Poland. [3] Department of Neonatal Diseases, Pomeranian Medical University, Powst. Wlkp. 72, 70-111 Szczecin, Poland. [4] Central Laboratory, Regional Hospital, Arkońska 4, 71-455 Szczecin, Poland. [5] Department of Gastroenterology and Hepatology, University Clinical Center Tuzla, , Trnovac bb, 75 000 Tuzla, Bosnia and Herzegovina

Abstract

The 1691G>A *FV* variant has been described as a common genetic risk factor in venous thromboembolism. The purpose of this study was to provide a further frequency value for 1691G>A *FV* in Poland and to collate summary data from Central (Poland, Czech, Slovakia), Eastern (Russia, Belarus, Ukraine) and South-Eastern (Slovenia, Croatia, Bosnia and Herzegovina, Serbia, Montenegro, Macedonia, Bulgaria) European countries. For this purpose in 2007 the 1691G>A *FV* variant was analyzed by polymerase chain reaction-restriction fragment length polymorphism from DNA collected in 2005-2006. We studied 650 subjects: 400 newborns and 250 older individuals (mean age 46.1 y) from Poland and compared results with reports from other countries, as well as with the frequency trend of 845G>A *HFE* across South-Eastern European countries using centroid cities. From our 1691G>A *FV* study we identified 626 GG homozygotes, 23 GA heterozygotes, and 1 AA homozygote (n = 650), giving an A allele frequency of 1.9%, and a summed frequency value for Poland of 2.0% (n = 1588); the frequency in Central European countries was 3.9% (n = 4559), mostly due to the high value in the Czech Republic: 5.1% (n = 2819); the South-Eastern European countries had 2.5% (n = 2410). Among the Eastern European countries the 1691G>A *FV* allele frequency was 1.9% (n=791), between the South-Eastern and Eastern European countries there was no significant difference (p=0.17). We confirm that the 1691G>A *FV* allele frequency in Poland, as well as other countries compared, is significantly lower than that in Czech.

KEY WORDS: Factor V, FV Leiden, centroids

INTRODUCTION

Synthesized in the liver, blood coagulation Factor V (FV) is a multidomain glycoprotein encoded by a gene consisting of 25 exons, located on chromosome 1q23. The 1691G>A *FV* transition in exon 10 of factor 5 causes an arginine to glutamine substitution (R506Q) known as Factor V Leiden. This genetic disorder is characterized by poor anticoagulant response to activated protein C and is the most common risk factor for thromboembolic disease [1]. Major clinical observations are that the presence of 1691G>A *FV* increases risk of deep vein thrombosis [2-4] and is also associated with a increased relative risk for pregnancy loss and possibly other obstetric complications [5,6].

The frequency of the 1691G>A *FV* allele varies worldwide and differences are observed between geographic locations and ethnic populations: The 1691G>A *FV* allele is very rare or non-existent in Asia (0.6%) and some regions of Africa (0.0%) [7-9]. On the other hand, Settin et al. [10] has described the prevalence of the mutant allele at the level of 10.2% in Egypt. In Poland, the prevalence of the variant 1691G>A *FV* has been previously given by several researchers [11-15]. One objective of this research was to give a larger sample size with a 650 subjects from the West Pomeranian province of Poland. This value is then compared to previous groups of Poles and values from other countries. Note that the population now inhabiting the region of West Pomerania resulted from extensive mixing of Polish peoples from all regions of Poland after the Second World War and therefore can provide a representative sample for the whole of Poland [16, 17]. A second objective was to present summary data: to our knowledge summary data for 1691G>A *FV* from Central (Poland, Czech, Slovakia), Eastern (Russia, Belarus, Ukraine) and South-Eastern (Slovenia, Croatia, Bosnia and Herze-

# Both authors equally contributed to this work.
* Corresponding author: Grażyna Adler,
Department of Medical Biology, Pomeranian Medical University, Powst. Wlkp.72, PL 70-111 Szczecin, Poland
Tel:+48914661490, Fax: +48914661492
e-mail: gra2@pum.edu.pl

Submitted: 25 January 2012 / Accepted: 20 March 2012

govina, Serbia, Montenegro, Macedonia, Bulgaria) European countries has not been presented before. The third aim of this study was to provide summed frequency values for 1691G>A *FV* in these countries, gathered from studies using similar methods ie. by polymerase chain reaction-restriction fragment length polymorphism (PCR-RFLP).

MATERIAL AND METHODS

Samples

The experimental study was performed (in 2007) on a group of 650 Polish individuals, divided into two subgroups: 400 newborns (187 female and 213 male) - and 250 older subjects (mean age 46.1 y, range: 2-87 y, 169 female and 81 male) - all inhabitants of the West Pomeranian province of Poland. The older subjects, of Polish origin, were consecutive healthy visitors to the analytical laboratory VITA at Darlowo, Poland, and no exclusion criteria were used. The sub-group of newborns has been described previously [14]. All neonates were of Polish origin, with Polish grandparents, and informed consent was obtained from all parents. The Ethical Committee of the Pomeranian Medical University approved the protocol of the study (BN- 001/57/05).

Procedure

For identification of the NM_000130.4:c.1691G>A *F5* alteration (here designated as 1691G>A *FV*) we used PCR-RFLP. Genomic DNA was extracted from 100 µL of umbilical blood (for newborns) or full blood (for older subjects), using the QIAamp DNA Blood Mini Kit (QIAGEN, Hilden, Germany). For a 10 µl-PCR, ~20 ng of genomic DNA was used. The PCR mixture contained 10x buffer (pH 8.3, 1.5 mM $MgCl_2$), 0.2 mM each of the deoxynucleoide triphosphates, 0.5 U Polymerase *Taq* (MBI Fermentas, Lithuania) and 4 pmol each of the forward and reverse primers as designed by Gandrille et al. [18]. Primers were synthesized by TIB MOLBIOL, Poznan, Poland. PCRs were performed in a Mastercycler Gradient device (Eppendorf, Hamburg, Germany) with the following temperature profile: initial denaturation at 94˚C for 5 min; 35 cycles of 20 s at 94˚C, 40 s at 56˚C and 40 s at 72˚C; and final extension step at 72˚C for 7 min. Amplification was followed by digestion of a 241 bp product with Hind III restriction enzyme (5'-A↓AGCTT-3') (MBI Fermentas, Lithuania) for 16 hours at 37˚C. The PCR digestion products were separated in 3 % agarose gels, stained with ethidinum bromide and recorded with a DS-34 Polaroid Instant Camera (Polaroid, Germany) using UV light (Transilluminator 4000, Stratagene, La Jolla, CA, USA). Hind III digestion yields fragments: 241 bp. (homozygote GG); 241, 209 and 32 bp. (heterozygote GA); 209 and 32 bp. (homozygote AA). Genotypes of GA and AA subjects were also confirmed by DNA sequencing (3100-Avant Genetic Analyzer, Applied Biosystems Hitachi, Foster City, CA, USA). For summary trend data of 1691G>A *FV* in South-Eastern European countries including Turkey the values are plotted against latitude of centroid cities (from BRRG - Buero fuer Raumforschung, Raumplanung und Geoinformation, Oldenburg, Germany: http://www.brrg.de/database.php?language= en&cId=0&dId=47) with latitude derived from Google maps (Google Inc, USA; http://www.mapcrow.info): Centroid cities "represent the political, administrative and cultural centre of the region". Graphical materials were developed using Designworks software (GSP Ltd, London, UK) and Microsoft Office (Microsoft, Redmond, WA, USA).

Statistical analysis

Fifty-five statistical comparisons (using z-tests) were made between all pairs of summary prevalence values for all countries studied. With Bonferroni correction a critical *p*-value of (0.05/55 = 0.0009) was used to define statistical significance. Z-tests and correlation coefficients (tested by linear regression) were calculated using Statistica (data analysis software system, version 8.0, StatSoft, Inc. 2007, www.statsoft.com).

RESULTS

The frequency of the 1691G>A *FV* allele in the study group (n = 650) proved to be 1.9%. We identified 626 GG homozygotes, 23 GA heterozygotes, and 1 AA homozygote, conforming to the expected Hardy-Weinberg equilibrium. This gives a summed frequency value for Poland of 2.0% (n = 1588). The average frequency of the 1691G>A *FV* allele in Central, Eastern and South-Eastern European countries was 3.2 % and varied from 0.6% (Belarus) to 5.1% (Czech Republic). The frequency of 1691G>A *FV* from our results (Table 1) and summary data from other countries (Table 2) are shown, and a map showing the summed frequencies for 1691G>A *FV* is shown in Figure 1. In Central European countries the frequency of 1691G>A *FV* was 3.9% (n = 4559) and varied from 5.1% in the Czech Republic through 2.1% in Poland (including our study) to 1.3% in Slovakia [11-13, 15, 19, 20]. The Czech Republic value was found to be significantly different from that in Poland, Russia, Ukraine, Slovenia, Croatia and Serbia/Montenegro, us-

TABLE 1. Allele frequencies for 1691G>A *FV* in present study.

Population	Group	Number of individuals	Frequency of 1691A *FV* allele (%)
Poland	Present study - newborns	400	2.3
	Present study - older individuals (mean age 46 y.o)	250	1.4
	Present study - whole group	650	1.9

TABLE 2. Allele frequencies for 1691G>A *FV* in Central, Eastern and South-Eastern European countries.

Country	Reference	Number of individuals		Frequency of 1691A *FV* allele (%)	
		per study	sum per country	per study	per country (weighted mean)
Poland	*Our study*	*650*	1588	*1.9*	2.0
	Herrmann FH et al, 1997 [11]	200		2.5	
	Łopaciuk S et al., 2001 [12]	238		2.1	
	Seremak-Mrozikiewicz A et al, 2010 [15]	400		1.8	
	Nizankowska-Mogilnicka E et al, 2003 [13]	100		1.5	
Czech Republic	Procházka M et al, 2003 [19]	2371	2819	5.4	5.1
	Paseka J et al, 2000 [20]	448		3.3	
Slovakia	Hudecek J et al, 2003 [21]	152	152	1.3	1.3
Slovenia	Meglic L et al, 2003 [22]	56	526	2.9	2.5
	Petrovic D et al, 2003 [23]	115		2.2	
	Petrovic D et al, 2001 [24]	132		2.3	
	Bedencic M et al, 2008 [25]	223		3.2	
Croatia	Coen D et al, 2001 [26]	155	749	2.0	1.6
	Jukic I et al, 2009 [27]	200		1.8	
	Cikes V et al, 2004 [28]	168		1.2	
	Alfirevic Z et al, 2010 [29]	106		1.4	
	Eterović D et al, 2007 [30]	120		1.3	
Bosnia and Herzegovina	No data found	No data		No data	
Serbia/*Serbia and Montenegro	Kovac M et al, 2010 [31]	128	499	0.8	2.2
	Mikovic D et al, 2000 [32]	50		2.0	
	* Djordjevic V, et al, 2004 [33]	120		2.9	
	Salatić I et al, 2011 [34]	71		2.8	
	Djordjevic V et al, 2003 [35]	130		2.7	
Macedonia	Arsov T et al, 2006 [36]	130	130	3.5	3.5
Bulgaria	Boyanovsky B et al, 2001 [37]	100	506	4.5	3.6
	Kovacheva K et al, 2007 [38]	80		3.1	
	Ivanov P et al, 2007 [39]	49		3.1	
	Ivanov P et al, 2008 [40]	98		3.6	
	Ivanov P et al, 2009 [41]	79		3.2	
	Ivanov PD et al, 2009 [42]	100		3.5	
Russia	Baranovskaya S et al, 1998 [43]	483	539	1.4	2.4
	Avdonin PV et al, 2006 [44]	56		1.8	
Ukraine	Tatarsky P et al, 2010 [45]	172	172	0.9	0.9
Belarus	Lipay NV et al, 2007 [46]	80	80	0.6	0.6

*Weighted average

ing two-proportion z-tests for comparisons between all countries studied except Turkey (with Bonferroni correction, $p < 0.001$, Table 3). In Eastern European countries the frequency of this mutant allele was 1.9% (n = 791) and varied from 2.4% in Russia through 0.9% in Ukraine to 0.6% in Belarus [43, 45, 46]. The prevalence of the 1691G>A *FV* allele in South-Eastern European countries was 2.5% (n=2410) varying from 3.6% in Bulgaria to 1.6% in Croatia. Unfortunately no data were found for Bosnia and Herzegovina, despite an extensive search. The 1691G>A *FV* variant follows a roughly increasing trend from West to East (Figure 2).

DISCUSSION

In the countries examined, which are predominantly inhabited by Slavic peoples, the allele frequencies for 1691G>A *FV* provide a mosaic (Figure 1). In our study group the frequency of the 1691G>A *FV* allele was consistent with the previous summed frequency value for Poland (2.0%) [11-13,15] and is similar to that in France (2.2%) [47], Switzerland [48] and the Netherlands [49-50] (each 2.2%) as well as to that in Serbia (2.2%) [31-35] and Russia (2.4%) [43, 44]. This value is, however, significantly different from that in the adjacent Czech Republic. To our knowledge we give the first summary study of the frequency distribution of the 1691G>A *FV* allele in Central, Eastern and South-Eastern European countries. A total of 7760 control individuals originating from 11 countries in provide the value for the frequency (3.2%) of this mutated al-

TABLE 3. *p*-values from two-proportion z-tests between 1691A *FV* frequency values of Central, Eastern and South-Eastern European countries. Significant differences, after Bonferroni correction (critical $p = 0.05/55 = 0.0009$), are shown in bold.

Country	*p*-value									
	Macedonia	Bulgaria	Russia	Poland	Belarus	Ukraine	Slovakia	Slovenia	Croatia	Serbia/ Montenegro
Czech Republic	0.2162	0.0413	0.0001	<0.0001	0.0098	0.0004	0.0028	0.0003	<0.0001	0.0001
Macedonia	-	0.9347	0.2932	0.0854	0.0573	0.0221	0.0769	0.3478	0.0285	0.2060
Bulgaria	-	-	0.1069	0.0037	0.0448	0.0101	0.0414	0.1456	0.0013	0.0617
Russia	-	-	-	0.4288	0.1445	0.0864	0.2437	0.8813	0.1459	0.7615
Poland	-	-	-	-	0.2095	0.1608	0.3978	0.3297	0.3464	0.6972
Belarus	-	-	-	-	-	0.7257	0.4837	0.1310	0.3231	0.1773
Ukraine	-	-	-	-	-	-	0.6242	0.0728	0.3305	0.1245
Slovakia	-	-	-	-	-	-	-	0.2121	0.6994	0.3252
Slovenia	-	-	-	-	-	-	-	-	0.1075	0.6543
Croatia	-	-	-	-	-	-	-	-	-	0.2745
Serbia/Montenegro	-	-	-	-	-	-	-	-	-	-

FIGURE 1. Allele frequencies (bold), number of subjects (not bold) for 1691G>A *FV* in Central, Eastern and South-Eastern countries (summed frequencies from references in Table 2).

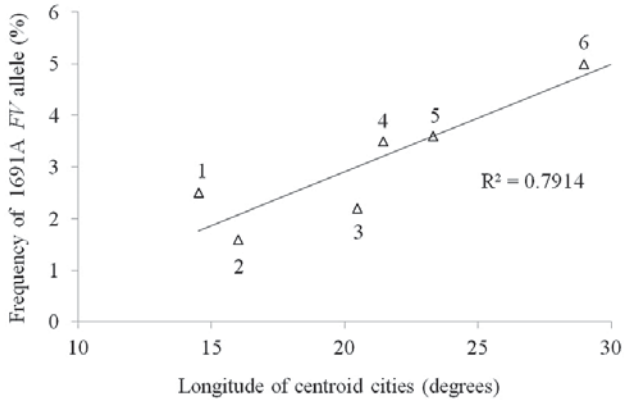

FIGURE 2. Trend in frequency of 1691G>A *FV* in South-Eastern Europe. Centroid cities: 1, Ljubljana (Slovenia); 2, Zagreb (Croatia); 3, Belgrade (Serbia and Montenegro); 4, Skopje (Macedonia); 5, Sofia (Bulgaria); 6, Istanbul (Turkey)

lele in these countries. However, if the Czech value is removed the summed frequency for the 10 remaining countries is 2.2%. These percentages indicate that future genetic counseling will be of some benefit in this region. The reasons for this mosaic in 1691G>A *FV* frequencies is not known. However, population movements have contributed to ethnic groups, cultures and consequently inheritance mixing, both throughout thousands of years of prehistory as well as in recent documented history. In the Southern Slavs there is a rough upward trend for 1691G>A *FV* in a southeasterly direction from Croatia (1.6%) and Serbia (2.2%) to Macedonia (3.5%) and Bulgaria (3.6%) (Figure 2). In neighboring Turkey this trend continues in a southeasterly direction as the frequency is even higher, at 5.0% [51-57]. This trend opposes that for 845G>A *HFE* [58]. It would be interesting to fill the gaps in the data for 1691G>A *FV* in Bosnia and Herzegovina, and it would be interesting to examine the prevalence of 1691G>A *FV* in the Western Slavic group in Germany (the Sorbs).

CONCLUSIONS

The frequency of the 1691G>A *FV* allele in Poland, summed from our study and previous studies, 2.0%, was similar to that in most countries studied, and similar to the summed frequency value for all Central, Eastern and South-Eastern countries (with the value for the Czech Republic removed), ie. 2.2%. The values for Poland, Russia, Ukraine, Slovenia, Croatia and Serbia/Montenegro were significantly different from that in the adjacent Czech Republic. In the South-Eastern European countries there is a rough upward trend for 1691G>A *FV* in a southeasterly direction, which opposes that for 845G>A *HFE* (Figure 2 [58]).

ACKNOWLEDGEMENT

Funding: This study was funded entirely by the Pomeranian Medical University, Szczecin, Poland. We would like to thank César de Diego Díez, at GISCO, Luxembourg, for providing NUTS population centroid data.

DECLARATION OF INTEREST

The authors state there is no conflict of interest.

REFERENCES

[1] Kujovich JL. Factor V Leiden thrombophilia. Genet Med 2011;13(1):1-16.
[2] Koster T, Rosendaal FR, de Ronde H, Briët E, Vandenbroucke JP, Bertina RM. Venous thrombosis due to poor anticoagulant response to activated protein C: Leiden Thrombophilia Study. Lancet 1993;342(8886-8887):1503-1506.
[3] Ridker PM, Miletich JP, Stampfer MJ, Goldhaber SZ, Lindpaintner K, Hennekens CH. Factor V Leiden and risks of recurrent idiopathic venous thromboembolism. Circulation 1995;92(10):2800-2802.
[4] Rosendorff A, Dorfman DM. Activated protein C resistance and factor V Leiden: a review. Arch Pathol Lab Med 2007;131(6):866-871.
[5] Ridker PM, Miletich JP, Buring JE, Ariyo AA, Price DT, Manson JE, et al. Factor V Leiden variant as a risk factor for recurrent pregnancy loss. Ann Intern Med 1998;128(12 Pt 1):1000-1003.
[6] Foka ZJ, Lambropoulos AF, Saravelos H, Karas GB, Karavida A, Agorastos T, et al. Factor V leiden and prothrombin G20210A variants, but not methylentetrahydrofolate reductase C677T, are associated with recurrent miscarriages. Hum Reprod 2000;15(2):458-462.
[7] Hira B, Pegoraro RJ, Rom L, Govender T, Moodley J. Polymorphisms in various coagulation genes in black South African women with placental abruption. BJOG 2002;109(5):574-575.
[8] Ahmad F, Kannan M, Yadav V, Biswas A, Saxena R. Impact of

thrombogenic mutations on clinical phenotypes of von Willebrand disease. Clin Appl Thromb Hemost 2010;16(3):281-287.
[9] They-They TP, Hamzi K, Moutawafik MT, Bellayou H, El Messal M, Nadifi S. Prevalence of angiotensin-converting enzyme, methylenetetrahydrofolate reductase, Factor V Leiden, prothrombin and apolipoprotein E gene polymorphisms in Morocco. Ann Hum Biol 2010;37(6):767-777.
[10] Settin A, Dowaidar M, El-Baz R, Abd-Al-Samad A, El-Sayed I, Nasr M. Frequency of factor V Leiden variant in Egyptian cases with myocardial infarction. Hematology 2008;13(3):170-174.
[11] Herrmann FH, Koesling M, Schoeder W, Latman R, Jimenez-Bonilla R, Lopaciuk S, et al. Prevalence of factor V Leiden variant in various populations. Genet Epidemiol 1997;14(4):403-411.
[12] Lopaciuk S, Bykowska K, Kwiecinski H, Mickielewicz A, Czlonkowska A, Mendel T, et al. Factor V Leiden, prothrombin gene G20210A variant, and methylenetetrahydrofolate reductase C677T genotype in young adults with ischemic stroke. Clin Appl Thromb Hemost 2001;7(4):346-350.
[13] Nizankowska-Mogilnicka E, Adamek L, Grzanka P, Domagala TB, Sanak M, Krzanowski M, et al. Genetic polymorphisms associated with acute pulmonary embolism and deep venous thrombosis. Eur Respir J 2003;21(1):25-30.
[14] Adler G, Parczewski M, Czerska E, Loniewska B, Kaczmarczyk M, Gumprecht J, et al. An age-related decrease in factor V Leiden frequency among Polish subjects. J Appl Genet 2010;51(3):337-341.
[15] Seremak-Mrozikiewicz A, Drews K, Wender-Ozegowska E, Mrozikiewicz PM. The significance of genetic polymorphisms of factor V Leiden and prothrombin in the preeclamptic Polish women. J Thromb Thrombolysis 2010;30(1):97-104.
[16] Ploski R, Wozniak M, Pawlowski R, Monies DM, Branicki W, Kupiec T et al. Homogeneity and distinctiveness of Polish paternal lineages revealed by Y chromosome haplogroup analysis. Human Genetics 2002; 110(6): 592-600.
[17] Kayser M, Lao O, Anslinger K, Augustin C, Bargel G, Edelmann J et al. Significant genetic differentiation between Poland and Germany follows present-day political borders, as revealed by Y-chromosome analysis. Human Genetics 2005; 117(5):428-443.
[18] Gandrille S, Alhenc-Gelas M, Aiach M. A rapid screening method for the factor V Arg506-->Gln variant. Blood Coagul Fibrynolysis 1995;6(3):245-248.
[19] Procházka M, Happach C, Marsál K, Dahlbäck B, Lindqvist PG. Factor V Leiden in pregnancies complicated by placental abruption. BJOG 2003;110(5): 462-466.
[20] Paseka J, Unzeitig V, Cibula D, Buliková A, Matýsková M, Chroust K. The factor V Leiden variant in users of hormonal contraceptives. Ceska Gynekol 2000;65(3):156-59.
[21] Hudecek J, Dobrotová M, Hybenová J, Ivanková J, Melus V, Pullmann R, et al. Factor V Leiden and the Slovak population [in Czech]. Vnitr Lek 2003;49(11):845-850.
[22] Meglic L, Stegnar M, Milanez T, Bozic M, Peterlin B, Peternel P, et al. Factor V Leiden, prothrombin 20210G > A, methylenetetrahydrofolate reductase 677C > T and plasminogen activator inhibitor 4G/5G polymorphism in women with pregnancy-related venous thromboembolism. Eur J Obstet Gynecol Reprod Biol 2003;111(2):157-163.
[23] Petrovic D, Milanez T, Kobal J, Bregar D, Potisk KP, Peterlin B. Prothrombotic gene polymorphisms and atherothrombotic cerebral infarction. Acta Neurol Scand 2003;108(2):109-113.
[24] Petrovic D, Zorc M, Keber I, Peterlin B. Joint effect of Gc.1691G>A factor V point variant and factor 5II Arg/Gln(353) gene polymorphism on the risk of premature coronary artery disease. Ann Genet 2001;44(1):33-36.
[25] Bedencic M, Bozic M, Peternel P, Stegnar M. Major and potential prothrombotic genotypes in patients with venous thrombosis and in healthy subjects from Slovenia. *Pathophysiol* Haemost Thromb 2008;36(2):58-63.
[26] Coen D, Zadro R, Honović L, Banfić L, Stavljenić Rukavina A. Prevalence and association of the factor V Leiden and prothrombin G20210A in healthy subjects and patients with venous thromboembolism. Croat Med J 2001;42(4):488-492.
[27] Jukic I, Bingulac-Popovic J, Dogic V, Babic I, Culej J, Tomicic M, et al. ABO blood groups and genetic risk factors for thrombosis in Croatian population. Croat Med J 2009;50(6):550-558.
[28] Cikes V, Abaza I, Krzelj V, Terzić IM, Tafra R, Trlaja A, et al. Prevalence of factor V Leiden and G6PD 1311 silent variants in Dalmatian population. Arch Med Res 2004;35(6): 546-548.
[29] Alfirevic Z, Simundic AM, Nikolac N, Sobocan N, Alfirevic I, Stefanovic M, et al. Frequency of factor II G20210A, factor V Leiden, MTHFR C677T and PAI-1 5G/4G polymorphism in patients with venous thromboembolism: Croatian case-control study. Bioch Med 2010;20(2):229-235.
[30] Eterović D, Titlić M, Culić V, Zadro R, Primorac D. Lower contribution of factor V Leiden or G202104 variants to ischemic stroke in patients with clinical risk factors: pair-matched case-control study. Clin Appl Thromb Hemost 2007;13(2):188-193.
[31] Kovac M, Mitic G, Mikovic Z, Djordjevic V, Savic O, Mandic V, et al. Thrombophilia in women with pregnancy-associated complications: fetal loss and pregnancy-related venous thromboembolism. Gynecol Obstet Invest 2010;69(4):233-238.
[32] Mikovic D, Rakicevic L, Kovac M, Radojkovic D. Prevalence of factor V Leiden variant in Yugoslav thrombophilic patients and its relationship to the laboratory diagnosis of APC resistance. Thromb Haemost 2000;84(4):723-724.
[33] Djordjevic V, Rakicevic LJ, Mikovic D, Kovac M, Miljic P, Radojkovic D, et al. Prevalence of factor V leiden, factor V cambridge, factor II G20210A and methylenetetrahydrofolate reductase C677T variants in healthy and thrombophilic Serbian populations. Acta Haematol 2004;112(4):227-229.
[34] Salatić I, Kiralj K, Mitić G, Veselinović I, Vapa D. *FV* Leiden variant and deep venous thrombosis in Vojvodina: a case-control study. J Med Biochem 2011;30(1):51-54.
[35] Djordjevic V, Rakicevic LJ, Mikovic D, Kovac M, Radojkovic D, Savic A. The *FV* Leiden, FII G20210A and MTHFR C677T variants in healthy and thrombophilic Yugoslav population. J Thromb Haemost 2003; 1(Suppl 1): Abstr: P0338.
[36] Arsov T, Miladinova D, Spiroski M. Factor V Leiden is associated with higher risk of deep venous thrombosis of large blood vessels. Croat Med J 2006;47(3):433-439.
[37] Boyanovsky B, Russeva M, Ganev V, Penev M, Baleva M. Prevalence of factor V Leiden and prothrombin 20210 A variant in Bulgarian patients with pulmonary thromboembolism and deep venous thrombosis. Blood Coagul Fibrinolysis 2001;12(8):639-642.
[38] Kovacheva K, Ivanov P, Konova E, Simeonova M, Komsa-Penkova R. Genetic thrombophilic defects (Factor V Leiden, prothrombin G20210A, MTHFR C677T) in women with recurrent fetal loss [in Bulgarian]. Akush Ginekol (Sofia) 2007;46(7):10-16.
[39] Ivanov P, Komsa-Penkova R, Ivanov I, Bozhinova S, Stoianova A. Carriers of thrombophilic factor among women with preeclampsia (preliminary report) [in Bulgarian]. Akush Ginekol (Sofia) 2007;46(8):3-8.
[40] Ivanov P, Komsa-Penkova R, Kovacheva K, Ivanov Y, Stoyanova A, Ivanov I, et al. Impact of thrombophilic genetic factors on pulmonary embolism: early onset and recurrent incidences. Lung 2008;186(1): 27-36.
[41] Ivanov P, Komsa-Penkova R, Konova E, Kovacheva K, Ivanov I, Ivanov M, et al. Inherited thrombophilic factors in women with unexplained intrauterine fetal deaths [in Bulgarian]. Akush Ginekol (Sofia) 2009;48(4):3-7.
[42] Ivanov PD, Komsa-Penkova RS, Konova EI, Kovacheva KS, Simeonova MN, Popov JD. Association of inherited thrombophilia with embryonic and postembryonic recurrent pregnancy loss. Blood Coagul Fibrinolysis 2009;20(2):134-140.
[43] Baranovskaya S, Kudinov S, Fomicheva E, Vasina V, Solovieva D, Khavinson V, et al. Age as a risk factor for myocardial infarction in Leiden variant carriers. Mol Genet Metab 1998;64(2):155-157.
[44] Avdonin PV, Kirienko AI, Kozhevnikova LM, Shostak NA, Babadaeva NM, Leont'ev SG, et al. C677T variant in methylentetrahydrofolatereductase gene in patients with venous thromboses from the central region of Russia correlates with a high risk of pulmonary artery thromboembolism [in Russian]. Ter Arkh 2006;78(6):70-76.

[45] Tatarsky P, Kucherenko A, Livshits L. Allelic polymorphism of FII, *FV* and MTHFR genes in population of Ukraine. Tsitol Genet 2010;44(3):3-8.
[46] Lipay NV, Dmitriev VV, Borisenok MB. Thrombotic complications during cancer treatment in children. Exp Oncol 2007;29(3):231-235.
[47] Delluc A, Le Moigne E, Tromeur C, Noel-Savina E, Couturaud F, Mottier D et al. Site of venous thromboembolism and prothrombotic mutations according to body mass index. Results from the EDITH study. Br J Haematol 2011;154(4):486-491.
[48] Redondo M, Watzke HH, Stucki B, Sulzer I, Biasiutti FD, Binder BR, et al. Coagulation factors II, V, VII, and X, prothrombin gene 20210G-->A transition, and factor V Leiden in coronary artery disease: high factor V clotting activity is an independent risk factor for myocardial infarction. Arterioscler Thromb Vasc Biol 1999;19(4):1020-1025.
[49] Slooter AJC, Rosendaal FR, Tanis BC, Kemmeren JM, van der Graaf Y, Algra A. Prothrombotic conditions, oral contraceptives, and the risk of ischemic stroke. J Thromb Haemost 2005;3(6):1213-1217.
[50] van Dunné FM, de Craen AJM, Heijmans BT, Helmerhorst FM, Westendorp RGJ. Gender-specific association of the factor V Leiden variant with fertility and fecundity in a historic cohort. The Leiden 85-Plus Study. Hum Reprod 2006;21(4):967-971.
[51] Ozbek U, Tangun Y. Frequency of factor V Leiden in Turkey. Int J Hematol 1996;64(3-4):291-292.
[52] Akar N, Akar E, Dalgin G, Sözüöz A, Omürlü K, Cin S. Frequency of Factor V (1691 G> A) variant in Turkish population. Thromb Haemost 1997;78(6):1527-1528.
[53] Gürgey A, Mesci L. The prevalence of factor V Leiden (1691 G->A) variant in Turkey. Turk J Pediatr 1997;39(3):313-315.
[54] Atasay B, Arsan S, Günlemez A, Kemahli S, Akar N. Factor V Leiden and Prothrombin gene 20210A variant in neonatal thromboembolism and in healthy newborns and adults: a study in a single center. Pediatr Hematol Oncol 2003;20(8):627-634.
[55] Agaoglu N, Turkyilmaz S, Ovali E, Ucar F, Agaoglu C. Prevalence of prothrombotic abnormalities in patients with acute mesenteric ischemia. World J Surg 2005;29(9):1135-1138.
[56] Eroglu Z, Biray Avci C, Kilic M, Kosova B, Ozen E, Gunduz C, et al. The prevalence of factor V Leiden gene variant analysis of donor and recipient at the organ transplantation Center of Ege University. Ege Tip Dergisi 2006;45(3):185-189.
[57] Ulukus M, Eroglu Z, Yeniel AO, Toprak E, Kosova B, Turan OD, et al. Frequency of factor V Leiden (Gc.1691G>A), prothrombin (G20210A) and methylenetetrahydrofolate reductase (C677T) genes variants in woman with adverse pregnancy outcome. J Turkish-German Gynecol Assoc 2006;7(3):195-201.
[58] Adler G, Clark JS, Łoniewska B, Ciechanowicz A. Prevalence of 845G>A HFE mutation in Slavic populations: an east-west linear gradient in South Slavs. Croat Med J 2011;52(3):351-357.

Anatomical variations and morphometric study of the optic strut and the anterior clinoid process

Eldan Kapur*, Amina Mehić

Department of Anatomy, Medical Faculty, University of Sarajevo, Čekaluša 90, 71000 Sarajevo, Bosnia and Herzegovina

Abstract

The optic strut and the anterior clinoid process represent bony structures that are closely related to anatomically and clinically significant elements such as the cavernous sinus, the internal carotid artery, the optic nerve and the pituitary gland. The objective of our study was to quantify dimensions of the optic strut and anterior clinoid process, and to determine variations in positions and forms of these structures. A descriptive anatomical study was performed on 200 dry human skulls. We analyzed dimensions and variations in position of the optic strut, dimensions of the anterior clinoid process as well as the incidence and forms of the caroticoclinoid foramen. The average thickness of the optic strut on skulls belonging to males was 3 mm and 2.8 mm on those belonging to females. The optic strut was most commonly attached to the anterior two fifths on the lower side of the anterior clinoid process. On the male skulls the average width of the anterior clinoid process was 9.4 mm (right) and 9.1 mm (left). Its length was 9.9 and 9.3 mm. On female skulls the average width of the process was 8.7 mm (right) and 8.3 mm (left), while the length measured 9.3 mm on the right and 8.9 mm on the opposite side. In our sample, a complete caroticoclinoid foramen appeared in 4.25%, a contact form in 2.75%. At last, an incomplete form of the foramen was observed in 9.75%. The anatomic variations of the investigated structures must be considered during the approaches to the cavernous sinus and neurovascular elements of the sellar region.

KEY WORDS: optic strut, anterior clinoid process, caroticoclinoid foramen

INTRODUCTION

The anterior clinoid process is a part of the roof to the cavernous sinus in its frontal portion. During surgeries on tumors and aneurysms in the parasellar and suprasellar region, the anterior clinoid process and the optic strut must be moved from the lesser wing of sphenoid bone to provide a better approach to the operating field, primarily to the internal carotid artery and the optic nerve, and to minimize the need for brain retraction [1,2]. The superficial and the thin deep layer of the dura cover the upper and lower sides of the anterior clinoid process. Removal of the anterior clinoid process (anterior clinoidectomy) allows a full approach to the anterior portion of the cavernous sinus and to the vertical segment of the internal carotid artery. It's a significant problem in neurosurgical procedures to find a massive anterior clinoid process, which by removing can cause optic nerve and internal carotid artery injury [3]. The caroticoclinoid foramen was first described by Henle (1885) as a bony foramen formed by merging of the anterior and middle clinoid processes' tops. According to Williams [4] and Lang [5] this foramen is formed by the ossification of the caroticoclinoid ligament in early childhood. The existance of this foramen is of great importance to brain surgeons since it disables retraction or mobilization of the cavernous segment of the internal carotid artery, even after release of proximal and distal dural ring [1], as well as proper tumor extirpation in sellar region, especially meningeoma of the tuberculum sellae [6, 7]. A preoperative detection of caroticoclinoid foramen, particularly by CT imaging, has a huge clinical significance, for its appearance conditions an inappropriate retraction of the cavernous segment of the internal carotid artery which can lead to its rupture with fatal outcome [8].

MATERIALS AND METHODS

Samples

As material for osteological analysis we used 200 dry human skulls of the osteological collection of Department of Anatomy at Medical Faculty, University of Sarajevo, of both

* Corresponding author: Eldan Kapur,
Department of Anatomy, Medical Faculty, University of Sarajevo,
Čekaluša 90, 71000 Sarajevo, Bosnia and Herzegovina
Tel:+387 33 226 478
E-mail: eldan_kapur@hotmail.com

Submitted: 8. February 2012 / Accepted: 30. March 2012

TABLE 1. Gender and age distribution of the investigated skulls

GENDER	N	RANGE	X±SD
♂	109 (54.5%)	23-91	50.5±18.24
♀	91 (35.5%)	19-84	51.5±16.62

genders and different age. Out of 200 analyzed skulls, 109 or 54.5% belonged to males, and 91 or 35.5% originated from females (Table 1).

Procedure

On the osteological material we conducted following morphometric measurements (using manuel caliper) and analysis:

1. dimensions and variations in the position of the optic strut,
2. dimensions of the anterior clinoid process,
3. incidence and forms of the caroticoclinoid foramen.

Statistical analysis

In the study we used the method of statistical and comparative analysis and processed the acquired data using SPSS-15.0 statistical software. The statistical analysis included calculating basic parameters of descriptive statistics like mean value, standard deviation and standard error of the mean value for single analyzed group. The results are presented in tables. We tested statistical significance of mean values by crossing individual parameters of analyzed groups. The testing was performed by Stundent's t-test, and $p<0.05$ is considered statistically significant.

RESULTS

The optic strut is a bony formation located between upper side of the body and the lesser wing of sphenoid bone. This formation separates optic canal from the medial portion of superior orbital fissure. Position of the optic strut was determined based on relation between the length of anterior clinoid process and the distance measuring from the optic strut to the top of the anterior clinoid process. On examined skulls of both genders it has been found that the optic strut was attached to the anterior fifth of anterior clinoid process in 11,6% cases on the right side, and in 14.5% on the left. Its attachment to the anterior two fifths of the process was registered in 42% on the right side and the 47.8% on the left side. The least seen positions of the attachment site are entirely to the front, by the base of anterior clinoid process – in 1.4% on the right and 4.3% on the left side, as well as entirely to the back, by the top of the process - in 2.9% on the right and 0.9% on the left side (Table 2). On all the skulls we measured the width of anterior clinoid process in its base, and the length from the base's midline to the top as shown in Figure 1. The anterior clinoid process in almost every observed male skull was triangular in shape, its base oriented to the front and top to the back and medially. In eleven skulls – in 5.5% cases, we found the process to be quadrangular in shape. In the total of 109 analyzed male skulls, the mean value of PCA width on the right side measured 9.4±1.4 mm, ranging between 5.9 and 12.1 mm. On the left side the PCA width range was between 5.8 and 14.0 mm, mean value 9.1 mm and standard deviation of ±1.7mm. The length of the process in males measured 9.9±1.6 mm on the right, and 9.3±1.4 mm on the left (Table 3). On the skulls originated from females, the mean value of PCA width on the right side measured 8.7±1.5 mm, ranging from 5.7 to 11.6 mm, and 8.3±2.1 mm on the left, minimal value being 4.9, maximal value 12.7 mm. The process' mean value length in females on the right side was 9.3±1.6 mm, and 8.9±2.0 mm on the left side (Table 3). There were statistically significant differences in mean width and in mean length of the anterior clinoid process between man and woman on the both sides of the examined skulls ($p<0.05$).

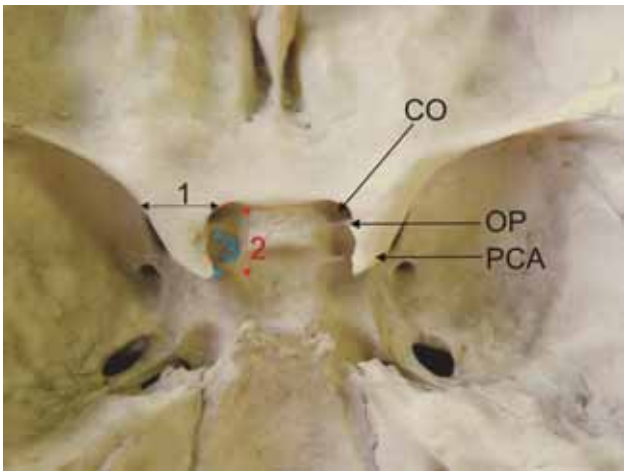

FIGURE 1. The measured parameters on the anterior clinoid process. 1-width in the base, 2-length from base to the top, 3-length from the top to the posterior margin of the optic strut (PCA-processus clinoideus anterior, OP-optic strut, CO-canalis opticus).

TABLE 2. Location of the optic strut in relation to the anterior clinoid process (PCA – *processus clinoideus anterior*)

ATTACHMENT SITE	RIGHT SIDE	LEFT SIDE
BY THE BASE OF THE PCA*	1.4%	4.3%
ANTERIOR FIFTH OF THE PCA	11.6%	14.5%
ANTERIOR TWO FIFTHS OF THE PCA	42.0%	47.8%
ANTERIOR THREE FIFTHS OF THE PCA	37.7%	27.5%
ANTERIOR FOUR FIFTHS OF THE PCA	4.4%	5.0%
POSTERIOR FIFTH OF THE PCA	2.9%	0.9%

TABLE 3. Dimensions of the anterior clinoid process (width and length in milimetars) considering gender and side of the examined skulls.

	MALE		FEMALE	
	Right	Left	Right	Left
WIDTH	9.4±1.4 (5.9-12.1)	9.1±1.7 (5.8-14.0)	8.7±1.5 (5.7-11.6)	8.3±2.1 (4.9-12.7)
LENGTH	9.9±1.6 (6.4-12.6)	9.3±1.4 (6.1-14.1)	9.3 ±1.6 (6.0-12.1)	8.9 ± 2.0 (5.6-13.1)

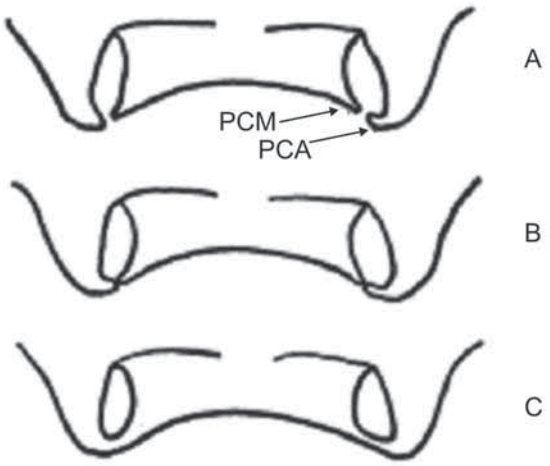

FIGURE 2. Illustration of three forms of caroticoclinoid foramen. PCA-processus clinoideus anterior, PCM-processus clinoideus medius A – incomplete form, B – contact form, C – complete form.

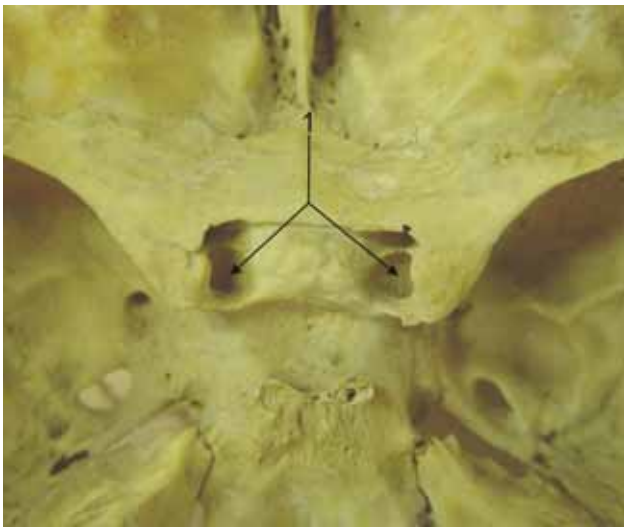

FIGURE 3. Male skull (age 58). A complete form of the caroticoclinoid foramen bilaterally (1).

The caroticoclinoid foramen (*foramen caroticoclinoideum*) is formed when tops of the anterior and middle clinoid processes merge on the upper side of sphenoid bone. The merge can appear to be complete and incomplete. Aside from these two forms of the foramen, we also analyzed the so called contact form when there's a suture between the two clinoid processes (Figure 2). The complete form of caroticoclinoid foramen on the total of 109 male skulls (218 sides) was found to be bilateral in only one case (Figure 3), or 1.83%. Unilaterally, it appeared in six skulls (2.75%), in four cases on the right side, and in remaining two cases on the left. An incomplete caroticoclinoid foramen was found in larger number of male skulls. It appeared bilaterally in five skulls – 4.58% cases, and we registered this form to appear unilaterally in eleven male skulls (5.04%), of which seven were on the right and four on the left side. In six skulls we found the complete form to be on one side, there was also an incomplete form of caroticoclinoid foramen on the opposite side. The incidence of the contact form of the foramen with presence of the interclinoid suture was higher on the left side (1.37%) than on the right (0.45%) in male skulls we observed (Figure 4). The contact form of the foramen was found bilaterally in two male skulls equaling 3.66% (Figure 5). Based on previous results, we can conclude that the caroticoclinoid foramen in all three forms appeared in 37 cases, which is 16.97%. It should be kept in mind that the entire statistics was performed on a sample of 218 sides of the investigated male skulls (Table 4). The transverse diameter of the foramen measured in average 5.32±0.52 mm on the right, and 5.21±0.73 on the left. In male skulls with the incomplete form of the foramen the distance between tops of the ante-

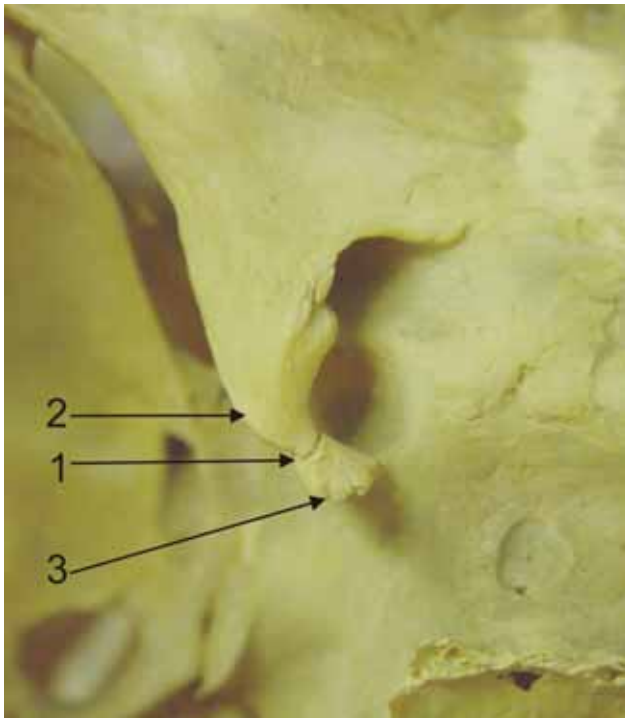

FIGURE 4. Male skull (age 45, lef side). Contact form of the caroticoclinoid foramen. 1-suture between the anterior and the middle clinoid process, 2-anterior clinoid process, 3-middle clinoid process.

TABLE 4. The incidence of complete, incomplete and contact form of the caroticoclinoid foramen in male skulls (n=218)

	SIDE	COMPLETE FORM	CONTACT FORM	INCOMPLETE FORM
Unilaterally	Right	4 (1.83%)	1 (0.45%)	7 (3.21%)
	Left	2 (0.91%)	3 (1.37%)	4 (1.83%)
Bilaterally		1 (0.91%)	2 (1.83%)	5 (2.29%)
Total		8 (3.66%)	8 (3.66%)	21 (9.63%)

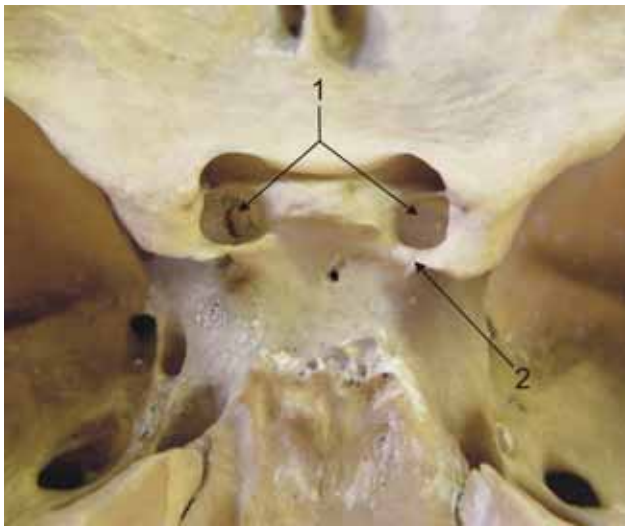

FIGURE 5. Male skull (age 64). Complete (on the left) and contact form of the caroticoclinoid foramen (on the right). 1- caroticoclinoid foramina, 2-interclinoid suture.

rior and middle clinoid processes measured 3.12±0.92 mm on the right side and 2.94±1.34 on the left. While analyzing female skulls (91 skulls - 182 sides), we found complete caroticoclinoid foramen bilaterally in two skulls (2.19%). The incomplete form on a single side was registered in five skulls - 2.74% cases. Out of those five, three were on the right and two on the left side. Similar to male skulls, incomplete caroticoclinoid foramen was found in larger number of female skulls as well: in five skulls bilaterally (5.49%) and eight skulls unilaterally (4.39%). In the group of eight skulls where incomplete foramen was found unilaterally, five were observed on the right and three on the left side. In three out of five female skulls with unilaterally presented complete foramen there was an incomplete form found on the opposite side. We haven't found the contact form of caroticoclinoid foramen bilaterally in female skulls. Incidence of this form unilaterally however was 1.09% (two skulls) on the left side and 0.54% on the right (one skull). Of the 91 analyzed female skulls we found the three forms of caroticoclinoid foramen to appear in 30 cases, which is 16.48% (Table 5). The transverse diameter of the foramen in complete and contact form measured in average 4.97±0.63 mm on the right side, and 4.99±0,54 mm on the left. In female skulls

TABLE 5. The incidence of complete, incomplete and contact form of caroticoclinoid foramen on female skulls (n=192)

	SIDE	COMPLETE FORM	CONTACT FORM	INCOMPLETE FORM
Unilaterally	Right	3 (1.64%)	1 (0.54%)	5 (2.74%)
	Left	2 (1.09%)	2 (1.09%)	3 (1.64%)
Bilaterally		2 (2.19%)	-	5 (5.49%)
Total		9 (4.94%)	3 (1.64%)	18 (9.89%)

TABLE 6. The incidence of complete, incomplete and contact form of caroticoclinoid foramen on the entire sample (n=400), considering sides of skulls.

	SIDE	COMPLETE FORM	CONTACT FORM	INCOMPLETE FORM
Unilaterally	Right	7(1.75%)	2(0.50%)	12(3.00%)
	Left	4(1.00%)	5(1.25%)	7(1.75%)
Bilaterally		3(1.50%)	2(1.00%)	10(5.00%)
Total		17(4.25%)	11(2.75%)	39(9.75%)

with incomplete form of the foramen, the distance between tops of the anterior and middle clinoid processes measured 3.02±0.76 mm on the right side, and 2.84±0.97 mm on the left. The total number of different forms of connection between the anterior and the middle clinoid process on the entire osteological sample is displayed in Table 6.

DISCUSSION

On male skulls, average width of the base of anterior clinoid process measured 9.4 mm on the right side and 9.1 mm on the left, maximum values being 12.1 and 14 mm. Its length measured from the base to the top was 9.9 mm and 9.3 mm. In female skulls the mentioned dimensions of anterior clinoid were less by 3 to 9 mm in average. The dimension of PCA given in our study are significantly larger compared to the dimension given by other authors, that are refering to skulls of the population of Central America and East Asia [9], while compared to the skulls of European origin in the study of Hauser and Di Stefano, the dimensions are similar. These differencies could be explained by racial features. Along with a strong and massive anterior clinoid process there's an additional problem of its possible pneumatization, which can be visualised by CT scanning, leading to sphenoid and ethmoid sinus opening during clinoidectomy [10, 11]. The optic strut represents a bony formation that connects the body of sphenoid bone and its lesser wing. Positioned like that, the optic strut separates optic canal from the medial portion of superior orbital fissure. Surgical procedures on cavernous sinus and suprasellar region demand a total removal of the optic strut as well as anterior clinoid process [2]. The optic strut itself or its parts that are not removed can lead to an optic nerve or internal carotid artery injury. The strut is placed laterocaudally to the optic nerve, so to remove it without damaging the nerve we recommend resection in the direction from anterior and medially to posterior and laterally. In addition, based on analysis we conducted on dry skulls we advise the optic strut to be removed before anterior clinoid process so the process could be completely released. Otherwise, we risk the anterior process' bony fragments that are left behind, may cause damage of the internal carotid and the optic nerve [12]. Optic strut's thickness on

TABLE 7. Comparison of the caroticoclinoid foramen and interclinoid bone bridges' incidence by different studies.

AUTHOR	SERIES	CAROTICOCLINOID FORAMEN			INTERCLINOID BONE BRIDGES
		unilaterally	bilaterally	total	
Keyers (1935)	2187	-	-	27.46%	8.68%
Azeredo (1988)	270	2.22%	4.05%	6.27%	3.04%
Inoue (1990)	50	22.0%	14.0%	36.0%	4.0%
Lee (1997)	73	15.7%	1.4%	17.1%	-
Erturk (2002)	507	13.02%	7.5%	20.51%	4.14%
Erturk and Kayalioglu (2004)	171	23.98%	11.69%	35.67%	8.18%
Our study (2011)	200	9.25%	7.5%	16.75%	6.75%

male skulls we investigated was 3 mm ± 1.2 mm in average, and 2.8 mm ± 0.9 mm on female skulls. We observed no statistically significant differencies regarding gender. The optic strut was most commonly attached to front two fifths on the lower side of anterior clinoid process (42% on the right side and 47.8% on the left). We noticed that, when the optic strut had been attached to the posterior fifth of anterior clinoid process (2.9% on the right and 0.9% on the left), it was the thickest, with maximal values of 4.5 mm in male skulls and 4 mm in female skulls. These data on size and dimensions of the optic strut should be kept in mind during surgical procedures on cavernous sinus and region of orbital apex. Knowing the precise location of the optic strut and its variations are very important while analyzing CT images, since it represents a valuable landmark in proper evaluation and differentiation of the optic canal, superior orbital fissure and anterior clinoid process on coronal and axial scans [13]. In our sample consisting of 109 male and 91 female skulls (400 sides) the complete form of caroticoclinoid foramen was discovered in 17 cases - 4.25%. The contact form of the foramen when tops of anterior and middle clinoid processes connect into the so called interclinoid suture [14] was detected in 11 cases, which is 2.75% in a sample of 400 sides. The incomplete form was present in 39 cases - 9.75%. An insight into the results show us that the complete, contact and incomplete forms of caroticoclinoid foramen were more often found in men, and were more often found on right side of the skulls regardless of gender. There are considerable racial differencies in the incidence of different forms of the foramen too. In the study by Lee et al. [9], the complete and incomplete forms of caroticoclinoid foramen were found in 17.1% cases, Maxi (1950 – quoted by Erturk) [14], registered them in 23.4 % (among population of Central America), while Keyers (1935 – quoted by Lee) [9] registered their appearance in 27.46% among American caucasions, predominantly on the left side. Azeredo et al. [15] registered caroticoclinoid foramen in the skulls of Portuguese population in 6.27%, and in the study by Reisch et al. we can see that the incidence among Germans was 14%. Erturk [14] describe three forms of caroticoclinoid foramen: a complete form (complete fusion of the anterior and the middle clinoid process), an incomplete form (if the processes don't fuse completely) and a contact form (when the tops of the processes fuse with a suture inbetween). This author found the three forms of the foramen in 23.68% cases. The incidence of different forms of the foramen varies within the range from 6.27% [15] to 35.67% [14] (Table 7). When it's a question of side of a skull the foramen appeares on, most studies proclaim higher incidence on the right side, with an exception of studies performed in USA [5], that indicate higher incidence of caroticoclinoid foramen on the left side, as well as more significant number of complete or incomplete foramina bilaterally.

CONCLUSION

The autors opine that anatomical knowlege of optic strut and anterior clinoid process, may be clinically important for surgeons operating in the region of cavernous sinus or the surrounding structures. Our investigations may be helpfull for pre-operative planning. Presence of any variations may result in unnecessary injury to the complicated neurovascular structures in the vicinity of cavernous sinus.

DECLARATION OF INTEREST

Authors have no conflict of interest to declare.

REFERENCES

[1] Dolenc V. Direct microsurgical repair of intracavernous vascular lesions. J Neurosurg 1983; 58: 824-831
[2] Yonekawa Y et al. Selective extradural anterior clinoidectomy for supra-and parasellar processes: Tehnical note. Journal of Neurosurgery. 1997; 87(4):636-642
[3] Hayashi N, Masouka T, Tomita T, Sato H, Ohtani O, Endo S. Surgical anatomy and efficient modifications of procedures for selective extradural anterior clinoidectomy, Minim Invasiv Neurosurg 2004; 47(6): 355-358
[4] Williams PL, Gray H. Gray's Anatomy, 37th ed./edited by Williams PL et al, Churchill Livingstone, Edinburgh-New York 1989:569-570
[5] Lang J. Structure and postnatal organization of heretofore uninvestigated and infrequent ossification of the sella turcica region, Acta Anat 1977; 99:121-139
[6] Ozdogmus O, Saka E, Tulay C, Gurdal E, Uzun I, Cavdar S. The anatomy of caroticoclinoid foramen and its relation with the internal carotid artery, Surg Radiol Anat. 2003; 25(3-4):241-246
[7] Jarrahy R, Shahinian H. Surgical managament of pituitary tumors, Skull base Instutute, Los Angeles; CA. 2004
[8] Newman SA. The cavernous sinus, Neurosurg Clin N Am 1999; 10(4):731-757
[9] Lee HY. Anterior clinoid process and optic strut in Koreans. Yon-

sei Med J. 1997; 38(3):151-154
[10] Huynh Le-P, Natori Y, Sasaki T. Surgical anatomy of the anterior clinoid process, J Clin Neurosci. 2004; 11(3):283-287
[11] Kantarci M, Karasen RM, Alper F, Onbas O, Okur A, Karaman A. Remarkable anatomic variations in paranasal sinus region and their clinical importance, Eur J Radiol 2004; 50(3): 296-302
[12] Inoue T, Rhoton AL, Theele D, Barry ME. Surgical approaches to the cavernous sinus: a microsurgical study, Neurosurgery 1990; 26:903-932
[13] Daniels DL, Shiwei Y, Pech P, Haughton VM. Computed tomography and magnetic resonanace imaging of the orbital apex. Radiol Clin North Am 1987; 25(4):803-817
[14] Erturk M, Kayalioglu M, Govsa F. Anatomy of the clionoidal region with special emphasis on the caroticoclinoid foramen and interclinoid osseous bridge in a recent Turkish population, Neurosurg Rev 2004; 27(1):22-26
[15] Azeredo RA, Libreti FA, Watanabe IS. Anatomical variations of the clinoid process of the human sphenoid bone, Arq Cent Estud Curso Odontol. 1988 -1989; 25-26(1-2):9-11

TREM-1 is a positive regulator of TNF-α and IL-8 production in U937 foam cells

Yu-Shi Wang, Xiang-Jun Li*, Wai-Ou Zhao

Department of Cardiovascular, the First Hospital of Jilin University, 71 Xinmin of Chaoyang district, Changchun 130021, China

Abstract

The purpose of our study was to investigate the expression levels of TREM-1 (triggering receptor expressed on myeloid cells-1) in U937 foam cells and determine whether TREM-1 regulates the production of tumor necrosis factor-alpha and interleukin-8 in these cells.

Human U937 cells were incubated with phorbol 12-myristate 13-acetate and then oxidized human low-density lipoprotein to induce foam cell formation. Oil red O staining was used to identify the foam cells. The production of IL-8 and TNF-α by U937 foam cells was assayed by enzyme-linked immunosorbent assay. The expression of TREM-1 mRNA in U937 foam cells was detected by reverse transcription-polymerase chain reaction. Moreover, U937 foam cells were transfected by small interfering RNA using Lipofectamine 2000 to knockdown TREM-1. Western blot was performed to assay protein expression of TREM-1 and ELISA was used to examine the effect of TREM-1 knockdown on IL-8 and TNF-α production.

PMA and ox-LDL induced U937 cells to form foam cells. The production of TNF-α and IL-8 was found to be significantly elevated in U937 foam cells, concomitant with a significant up-regulation of TREM-1 mRNA. TREM-1 siRNA was able to partially silence the expression of TREM-1 protein and remarkably inhibited TNF-α and IL-8 production in U937 foam cells, suggesting that TREM-1 is a positive regulator of TNF-α and IL-8 production in U937 foam cells.

Our finding that TREM-1 controls the production of IL-8 and TNF-α in U937 foam cells defines a potentially critical role of TREM-1 in the pathogenesis of atherosclerosis and implicates TREM-1 as a potential therapeutic target for the disease.

KEY WORDS: TREM-1, foam cell, TNF-α, IL-8, atherosclerosis.

INTRODUCTION

Atherosclerosis is a complex, progressive disease that is newly recognized to have a strong inflammatory component [1, 2]. In the early stage of atherosclerosis, monocytes migrate into the arterial intima and differentiate into macrophages that can take up oxidized low-density lipoprotein (ox-LDL) to stimulate differentiation into foam cells [3, 4]. The accumulation of foam cells in the artery wall causes the formation of fatty streak(s), the earliest visible lesion of atherosclerosis [5]. The uptake of ox-LDL by macrophages results in the production of numerous proinflammatory cytokines that can amplify the inflammatory response and promote the evolution of atheroma [6]. Interleukin-8 (IL-8) and tumor necrosis factor-alpha (TNF-α) are two important proatherosclerotic cytokines secreted by ox-LDL-activated macrophages [7-10]. Both of these molecules have been found to be up-regulated at the sites of formation of atherosclerotic plaques [11, 12]. IL-8 may induce the firm adhesion of monocytes to endothelial cells and mediate the intimal accumulation of macrophages in atherosclerotic lesions [13, 14], while TNF-α can enhance macrophage foam cell formation by inhibition of intracellular lipid catabolism and, therefore, contribute to atherosclerotic development and progression [15]. Accumulating evidence indicates that infectious processes may contribute to atherosclerosis [16]. Infectious agents, such as cytomegalovirus [17], *Chlamydop hila pneumoniae* [18], *Helicobacter pylori* [19], and parvovirus [20], have been shown to augment the production of cytokines in macrophages and provide inflammatory stimuli that can accelerate atherogenesis. TREM-1 (triggering receptor expressed on myeloid cells-1) is an activating receptor that is selectively expressed on neutrophils and monocytes/macrophages and can be up-regulated by bacterial and fungal stimuli [21]. Engagement of TREM-1 on monocytes can trigger the release of large amounts of proinflammatory cytokines, including IL-8 and TNF-α, and amplify inflammatory responses [21, 22]. At present, it remains unclear whether TREM-1 is upregulated during foam cell formation and, if it is, whether TREM-1 regulates the production of proin-

* Corresponding author: Xiang-Jun Li,
School of Pharmaceutical Sciences, Jilin University, 71 Xinmin of Chaoyang district, Changchun 130021, China
Tel: +8618643199605; Fax: 0431-88786259
E-mail: wys720528@yahoo.com.cn

Submitted: 18. April 2011 / Accepted: 9. January 2012

flammatory cytokines by macrophage-derived foam cells. In the present study, we established an *in vitro* foam cell formation model by stimulating human myelomonocytic U937 cells with phorbol 12-myristate 13-acetate (PMA) and ox-LDL to investigate the expression of TREM-1 in macrophage-derived foam cells and its relationship with the secretion of TNF-α and IL-8. Furthermore, small interfering RNA (siRNA) was employed to knockdown TREM-1 in order to examine TREM-1 effects on the production of TNF-α and IL-8 in U937 foam cells.

MATERIALS AND METHODS

Cell culture and induction of foam cell formation

Human myelomonocytic cell line U937 was purchased from KeyGen Biotech (Nanjing, China) and was maintained in RPMI-1640 medium (Gibco, USA) containing 10% fetal bovine serum (FBS) in a 5% CO_2 incubator at 37°C. U937 cells during the logarithmic growth phase (at a density of 1.0×10^9 cells/L) were stimulated with 100 nmol/L of PMA (Sigma, USA) for 72 h to induce the formation of macrophage-like U937 cells. After 12 hours of culture in serum-free medium, PMA-induced U937 cells were divided into three groups and incubated with RPMI-1640 medium containing 10% FBS (PMA group), 100 mg/L of LDL (PMA+LDL group) or 100 mg/L of ox-LDL (PMA + ox-LDL group; Yuanyuan Biotechnology, Guangzhou, China). Experiments were performed in quintuplicate. After 24 h of culture, supernatants were collected to measure the contents of TNF-α and IL-8, and the cells were harvested for detection of TREM-1 mRNA expression by reverse transcription-polymerase chain reaction (RT-PCR).

Identification of U937 foam cells

U937 foam cells were identified by oil red O staining. Briefly, adherent U937 foam cells were stained with freshly prepared 0.3% oil red O solution for 20 min. Cell nuclei were then counterstained with hematoxylin solution for 5 min. After rinsing with 70% ethanol, cells were mounted onto glass slides with an aqueous mounting reagent. Stained cells were observed under an inverted light microscope (TE2000; Nikon, Japan).

RT-PCR

Total RNA was isolated from cells using the TRIzol Reagent (Gibco) according to the manufacturer's protocol. Reverse transcription was performed using M-MLV reverse transcriptase and oligo-dT primers (Fermentas, USA) following the manufacturer's instructions. PCR was then carried out to determine the expression levels of TREM-1 and glyceraldehyde-3-phosphate dehydrogenase (GAPDH, control) mRNAs using the following parameters: pre-denaturation at 94°C for 5 min; 30 cycles of denaturation at 94 °C for 30 s, annealing at 55 °C for 30 s, and extension at 72 °C for 30 s; and, a final extension at 72 °C for 10 min. The sequences of the TREM-1 and GAPDH primers were as follows: TREM-1 forward, 5'-TGCTGTGGATGCTCTTTGTC-3' and reverse, 5'-CACAGTTCTGGGGCTGGTAT-3'; GAPDH forward, 5'-ACCACAGTCCATGCCATCAC-3' and reverse, 5'-TCCACCACCCTGTTGCTGTA-3'. The PCR products were resolved by electrophoresis on a 2% agarose gel containing ethidium bromide (0.5 μg/ml). The expression level of TREM-1 mRNA relative to GAPDH transcripts was determined by densitometric scanning (Gel Image system-1600; Tanon, Shanghai, China).

Cytokine measurement

TNF-α and IL-8 in culture supernatants were assayed by enzyme-linked immunosorbent assay (ELISA) using commercial kits (Westang, Shanghai, China), according to the manufacturer's instructions. Briefly, 100 μl culture supernatants were added into the 96-well plate. After incubation for 2 h at 37 °C, the plate was washed three times with cleaning solution [TBST: 20 mmol/L Tris-HCl, 150 mmol/L NaCl , 0.05% (V/V) Tween 20]. With the exception of the negative control, all the wells were supplemented with 100 μl of horseradish peroxidase (HRP)-antibody working solution and incubated at 37 °C for 1 h. After washing as above, a drop of substrate A and B were added sequentially. After incubation at 37 °C for 15 min, a drop of end solution was added into each well, and the absorbed density (OD) was detected at 450 nm.

siRNA transfection

The following two oligonucleotides encoding a TREM-1 siRNA were obtained from Dharmacon (Lafayette, USA): sense, 5'-CCGGAAGTGTATGTGATCAGAGTAAT TCAAGAGATTACTCTGATCACATACACTTTTTTTG-3'; antisense, 5'-AATTCAAAAAAAGTGTATGTGATCAGAGTAATCTCTTGAATTACTCTGATCACATACACTT-3'. Macrophage-like U937 cells induced with PMA as described above were used for siRNA transfection. In addition to the TREM-1 siRNA group (TREM-1 siRNA), an empty liposome group (empty liposome) and a random siRNA group (negative siRNA) were used as negative controls. Transfection was performed using Lipofectamine 2000 according to the manufacturer's protocol. After 48 h of transfection, cells were treated with 100 mg/L of ox-LDL as described above and subjected to detection of TREM-1 protein expression by Western blot, and TNF-α and IL-8 production by ELISA.

Western blot

Western blot was performed using routine procedures. Briefly, total protein was harvested by cell lysis solution

(20 mmol/L Tris, 150 mmol/L NaCl, 1 mM EDTA, 1% Triton X-100, 2.5 mmol/L sodium pyrophosphate, 1 mmol/L β-Glycerolphosphate, 1 μg/ml Leupetin, 1 mmol/L phenylmethylsulfonyl fluoride, pH 7.5) and the quantity was estimated by Lowry analysis [23]. Cellular proteins (50 μg) were resolved by SDS-PAGE using 15% polyacrylamide gels and transferred to polyvinylidene fluoride membranes. After incubation with rabbit anti-TREM-1 polyclonal antibody (1:100; sc-48762; Santa Cruz Biotechnology, Santa Cruz, CA, USA), rabbit anti-PKC polyclonal antibody (1:200; sc-10800; Santa Cruz Biotechnology, Santa Cruz, CA, USA) or rabbit anti-GAPDH polyclonal antibody (1:100; sc-25778; Santa Cruz Biotechnology, Santa Cruz, CA, USA), the bands were detected by using an HRP-conjugated secondary antibody (1:100; Santa Cruz Biotechnology, Santa Cruz, CA, USA). The immunoblot signals were visualized using the Immobilon Western Chemilum HRP Substrate (WBKLS0100; Millipore Corporation, Billerica, MA, USA). The protein expression level of TREM-1 relative to GAPDH was determined by densitometric scanning.

Statistical analysis

Numerical data have been expressed as mean ± standard deviation (SD). Statistical analysis was performed using the SSPS 11.0 software package. Intergroup differences were compared using one-way analysis of variance (ANOVA) and $p<0.05$ was considered to be significantly different.

RESULTS

PMA and ox-LDL induced the differentiation of U937 cells into foam cells

As shown in Figure 1A, the untreated U937 cells exhibited the characteristic round shape. After incubation with PMA for 72 h, the majority of U937 cells shifted to an ameboid shape and began to aggregate and adhere, indicating the differentiation from monocytes into macrophage-like cells (Figure 1B). In the presence of ox-LDL, PMA-induced macrophage-like cells showed obvious foamy changes as many oil red O-positive lipid droplets were observed in the cytoplasm. Some cells showed an enlarged size due to uptake and accumulation of an excessive amount of ox-LDL (Figure 1C). In contrast, no obvious lipid droplets were observed in PMA-induced macrophage-like cells with (data not shown) or without (Figure 1B) LDL treatment.

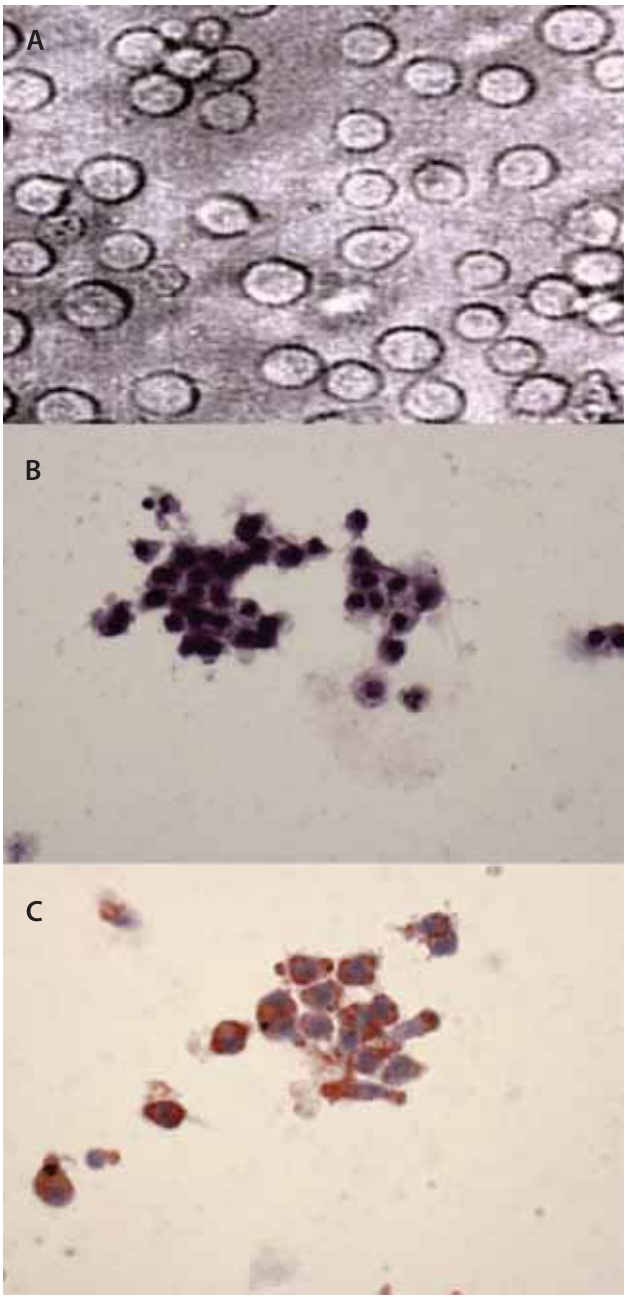

FIGURE 1. PMA and ox-LDL induced the differentiation of U937 cells into foam cells. (A). Inverted microscopy showed the characteristically round U937 cells prior to treatment. (B). After incubation with PMA for 72 h, the U937 cells shifted to an ameboid shape, and aggregated and adhered, indicating their differentiation from monocytes into macrophage-like cells. (C). In the presence of ox-LDL, PMA-induced macrophage-like cells showed obvious foamy changes: many oil red O-positive lipid droplets were observed in the cytoplasm; some cells showed an enlarged size due to uptake and accumulation of excessive ox-LDL (magnification ×200).

TNF-α and IL-8 levels were elevated in U937 foam cells

To determine the effects of ox-LDL treatment on the levels of TNF-α and IL-8 in PMA-induced U937 cells, ELISA was performed (Figure 2). The levels of both TNF-α and IL-8 in PMA+ox-LDL U937 cells were found to be significantly higher than those in PMA and PMA+LDL groups (all $p<0.05$): TNF-α, 100.38 ± 10.24 (PMA+ox-LDL) *vs.* 13.68±1.56 (PMA) and 15.87 ± 1.63 (PMA+LDL); IL-8, 97.88 ± 9.37 (PMA+ox-LDL) *vs.* 20.39 ± 2.40 (PMA) and 23.43 ± 3.59 (PMA+LDL). The levels of both TNF-α and IL-8 in PMA+LDL group were slightly higher than those in

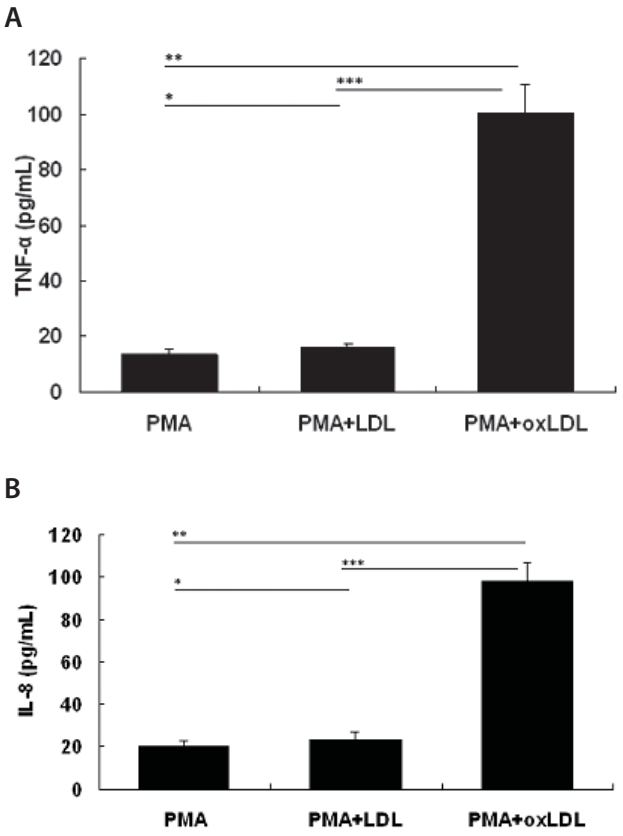

FIGURE 2. TNF-α and IL-8 levels were elevated in U937 foam cells. The levels of TNF-α (A) and IL-8 (B) secreted by PMA-induced U937 cells in the presence of ox-LDL were determined by ELISA. Data have been shown as mean ± SD (n = 5). *p > 0.05 *vs.* PMA; **p < 0.05 *vs.* PMA; *** p < 0.05 *vs.* PMA+LDL.

the PMA group, but there were no significant differences observed (p>0.05). These results indicated that the levels of both TNF-α and IL-8 were elevated in U937 foam cells.

TREM-1 mRNA expression was up-regulated in U937 foam cells

To examine the impact of ox-LDL treatment on the expression of TREM-1 mRNA in PMA-induced U937 cells, the level of TREM-1 mRNA relative to GAPDH was determined by RT-PCR (Figure 3). The relative level of TREM-1 mRNA in PMA+ ox-LDL U937 cells was significantly higher than those in PMA and PMA+LDL groups: 0.73 ± 0.06 (PMA+ox-LDL) *vs.* 0.42 ± 0.05 (PMA) and 0.51 ± 0.06 (PMA+LDL) (both p<0.05; Figure3 A and B). However, there was no significant difference observed in the relative level of TREM-1 mRNA between PMA and PMA+LDL groups (p>0.05). These data clearly indicated that TREM-1 mRNA expression was up-regulated in U937 foam cells.

TREM-1 siRNA partially silenced the expression of TREM-1 protein in PMA-induced U937 cells

To examine whether TREM-1 is involved in the regulation of TNF-α and IL-8 production in U937 foam cells, siRNA-mediated silencing of the TREM-1 gene was performed. Western blot analysis indicated that the expression of TREM-1 protein was significantly down-regulated in PMA-induced U937 cells transfected with TREM-1 siRNA, as compared to untransfected cells or cells transfected with empty liposome or negative siRNA (p<0.05, Figure 4 and Table 1).

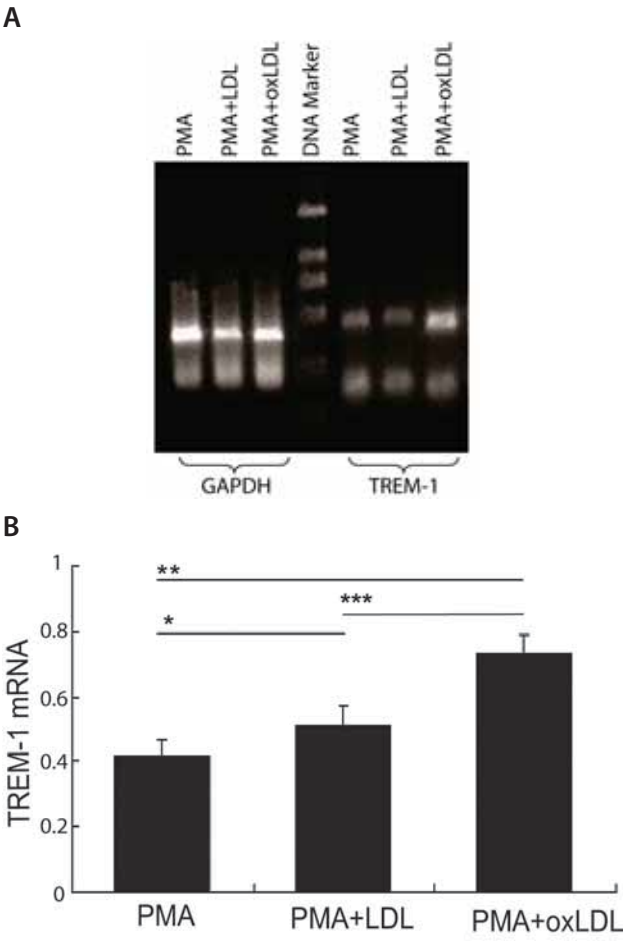

FIGURE 3. . TREM-1 mRNA expression was up-regulated in U937 foam cells. The expression levels of TREM-1 mRNA in U937 foam cells were determined by RT-PCR. Data have been shown as mean ± SD (n = 5). (A). Representative image showing the expression of TREM-1 and GAPDH mRNAs in U937 foam cells; (B). Quantitative analysis of the expression level of TREM-1 mRNA relative to GAPDH mRNA. *p > 0.05 *vs.* PMA; **p < 0.05 *vs.* PMA; ***p < 0.05 *vs.* PMA+LDL.

TABLE 1. siRNA inhibited ox-LDL-induced TREM-1 expression and TNF-α and IL-8 secretion in U937 foam cells

Group	TREM-1 (relative expression)	TNF-α content (pg/mL)	IL-8 content (pg/mL)
PMA	0.29 ± 0.03	23.54 ± 2.46	22.39 ± 2.25
PMA+ox-LDL	0.48 ± 0.05*	83.68 ± 8.24*	84.65 ± 8.25*
TREM-1 siRNA	0.32 ± 0.04#	25.35 ± 2.36#	24.43 ± 2.59#
Negative siRNA	0.58 ± 0.06*	86.28 ± 8.53*	86.58 ± 8.46*
Empty liposome	0.54 ± 0.05*	79.94 ± 8.15*	82.73 ± 8.29*

Data shown are mean ± SD (n = 5). *p < 0.05 *vs.* the PMA group; # p < 0.05 *vs.* the PMA+ox-LDL group, Negative siRNA group or Empty liposome group, respectively.

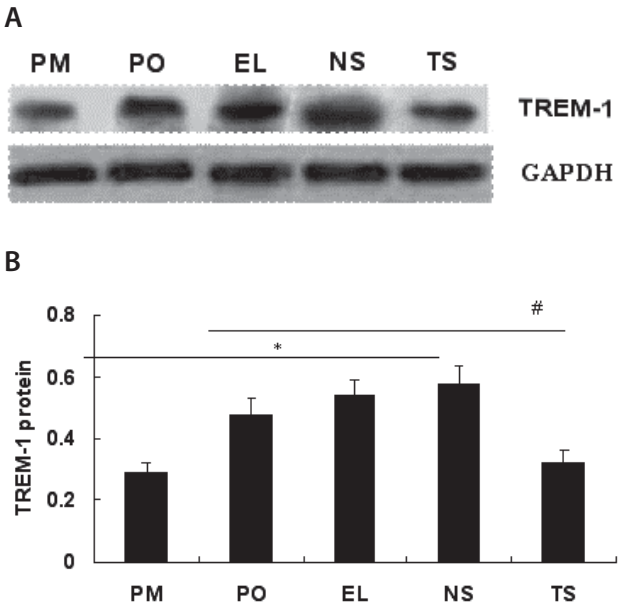

FIGURE 4. TREM-1 siRNA partially silenced the expression of TREM-1 protein in PMA-induced U937 cells. After PMA-induced U937 cells were transfected with TREM-1 siRNA (TS), negative siRNA (NS) or empty liposome (EL), and then treated with ox-LDL, the expression levels of TREM-1 protein were measured by Western blot. Untransfected U937 cells untreated (PM) or treated with ox-LDL (PO) were used as controls. Data have been shown as mean ± SD ($n = 5$). (A). Representative image showing the expression of TREM-1 and GAPDH proteins in U937 cells; (B). Quantitative analysis of the expression level of TREM-1 protein relative to GAPDH protein. *$p < 0.05$ *vs.* the PMA group (PM); $^{\#}$ $p < 0.05$ *vs.* the PMA+ox-LDL group (PO), Negative siRNA group (NS) or Empty liposome group (EL), respectively.

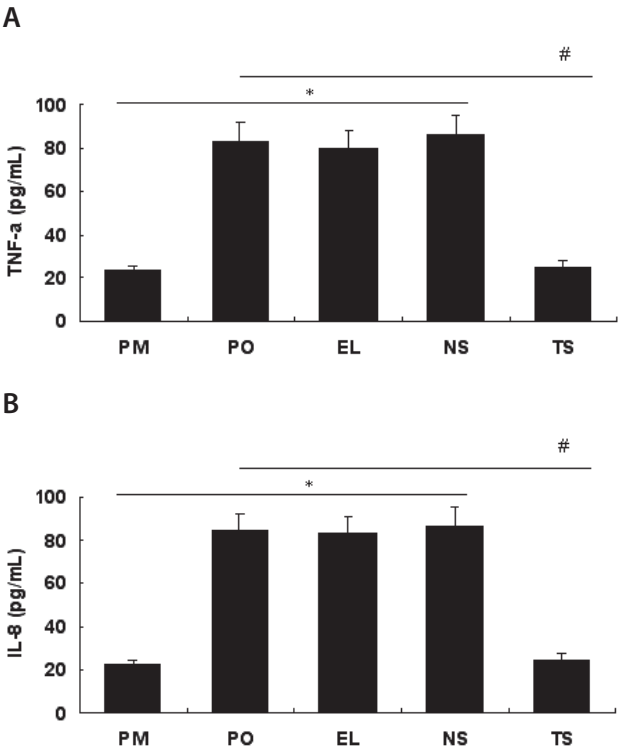

FIGURE 5. TREM-1 knockdown suppressed TNF-α and IL-8 production in U937 foam cells. After PMA-induced U937 cells were transfected with TREM-1 siRNA (TS), negative siRNA (NS) or empty liposome (EL), and then treated with ox-LDL, the levels of TNF-α (A) and IL-8 (B) secreted by these cells were measured by ELISA. Untransfected U937 cells untreated (PM) or treated with ox-LDL (PO) were used as controls. Data have been shown as mean ± SD ($n = 5$). *$p < 0.05$ *vs.* the PMA group (PM); $^{\#}$ $p < 0.05$ *vs.* the PMA+ox-LDL group (PO), Negative siRNA group (NS) or Empty liposome group (EL), respectively.

In contrast, no significant differences were noted in the expression levels of TREM-1 protein among untransfected U937 cells and U937 cells transfected with empty liposome or negative siRNA. Thus, TREM-1 was partially silenced by the corresponding siRNA in PMA-induced U937 cells.

TREM-1 knockdown suppressed TNF-α and IL-8 production in U937 foam cells

After PMA-induced U937 cells transfected with TREM-1 siRNA were treated with ox-LDL, the production of TNF-α and IL-8 in U937 foam cells was detected by ELISA. As shown in Figure 5 and Table 1, TREM-1 knockdown significantly inhibited ox-LDL-induced TNF-α and IL-8 secretion in U937 foam cells. In contrast, the levels of TNF-α and IL-8 in foam U937 cells transfected with empty liposome or negative siRNA were not significantly different from those detected in untransfected cells. Apparently, siRNA-mediated silencing of the TREM-1 gene was capable of significantly suppressing the production of TNF-α and IL-8 in U937 foam cells.

TREM-1 knockdown suppressed ox-LDL-induced up-regulation of PKC expression in U937 foam cells

To determine whether ox-LDL treatment alters the expression of PKC protein in PMA-induced U937 cells, Western blot was performed (Figure 6). The expression level of PKC protein in the PMA+ox-LDL group was significantly higher than that in the PMA group ($p<0.05$). However, TREM-1 knockdown significantly inhibited ox-LDL-induced up-regulation of PKC expression in U937 foam cells. In contrast, the expression levels of PKC protein in foam U937 cells transfected with empty liposome or negative siRNA were not significantly different from that detected in untransfected cells. Collectively, these results indicated that TREM-1 knockdown suppressed ox-LDL-induced up-regulation of PKC expression in U937 foam cells.

DISCUSSION

Infectious agents can contribute to the pathogenesis of atherosclerosis by promoting macrophage production of inflammatory cytokines [16]. Moreover, TREM-1 plays a critical role in monocyte/macrophage-mediated inflammatory responses to microbial infection [24]. Based on these observations, we hypothesized that TREM-1 may be involved in regulating the production of proinflammatory cytokines during

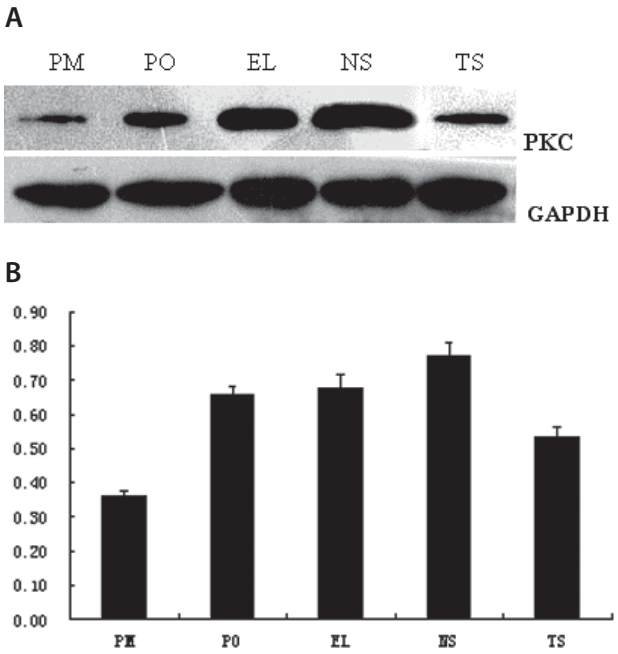

FIGURE 6. TREM-1 knockdown suppressed ox-LDL-induced up-regulation of PKC expression in U937 foam cells. After PMA-induced U937 cells were transfected with TREM-1 siRNA (TS), negative siRNA (NS) or empty liposome (EL), and then treated with ox-LDL, the expression levels of PKC in these cells were determined by Western blot. Untransfected U937 cells untreated (PM) or treated with ox-LDL (PO) were used as controls. Data have been shown as mean ± SD (n = 5). (A). Representative image showing the expression of TREM-1 and GAPDH proteins in U937 cells; (B). Quantitative analysis of the expression level of TREM-1 protein relative to GAPDH protein. *$p < 0.05$ *vs.* the PMA group (PM); $^{\#}$ $p < 0.05$ *vs.* the PMA+ox-LDL group (PO), Negative siRNA group (NS) or Empty liposome group (EL), respectively.

foam cell formation. In the present study, we demonstrated that ox-LDL treatment significantly up-regulate the expression of TREM-1 mRNA in PMA-induced macrophage-like cells, and TREM-1 knockdown remarkably inhibited ox-LDL-induced TNF-α and IL-8 secretion, suggesting that TREM-1 is a positive regulator of TNF-α and IL-8 production in U937 foam cells. Given that TNF-α and IL-8 are proinflammatory cytokines that play an important role during macrophage foam cell formation and atherosclerotic development and progression [13-15], these findings suggest a possible critical role of TREM-1 in the pathogenesis of atherosclerosis. Multiple studies have demonstrated that TNF-α and IL-8 are up-regulated in macrophage foam cells in atherosclerotic plaques and involved in the potentiation of atherosclerosis [7-15]. The activation of p38 mitogen-activated protein kinase (MAPK) and nuclear factor κB (NF-κB) may be implicated in the secretion of IL-8 in lipid-laden macrophages [8], while TNF-α production may depend on the activation of activator protein 1 (AP-1) [9], phosphoinositide 3-kinase (PI3K) and extracellular signal-regulated kinase (ERK) [6]. In the present study, we found that TREM-1 could control the release of TNF-α and IL-8 in U937 foam cells. Similarly, previous studies also showed that TREM-1-mediated TNF-α and IL-8 secretion was observed in monocytes/macrophages [21]. Although the mechanism underlying TREM-1-mediated release of IL-8 and TNF-α in U937 foam cells is still unclear, the connection between TREM-1 and the cytokine-inducing Toll-like receptor 4 (TLR4)/NF-κB pathway may provide a clue to this mechanism [25]. Yang et al. [26] found that blocking of TLR4 was able to substantially inhibit NF-κB activity and ox-LDL-induced IL-8 expression. Ornatowska et al. [27] demonstrated that TREM-1 silencing in macrophages resulted in decreased expression of key proteins in the TLR4 signaling pathway. Thus, it is reasonable that the TLR4/NF-κB signaling pathway might be involved in TREM-1-mediated TNF-α and IL-8 production in U937 foam cells. Protein kinase C (PKC) is a family of serine/threonine protein kinases that play a key role in the regulation of the inositol phosphate/diacylglycerol signalling pathway. Upon activation, PKC enzymes are translocated from the cytosol to the plasma membrane and exert diverse biological functions by phosphorylating target proteins. Feng et al. [28] found that PKC could promote the expression of scavenger receptor CD36 and lipid droplet-associated PAT-proteins in monocytes, thus contributing to foam cell formation. Oso et al. [29] demonstrated that inhibition of PKCbeta prevents LDL uptake and foam cell formation by reducing scavenger receptor an expression in human macrophages. Another study [30] indicated that PKC activation could modulate adipophilin-mediated lipid accumulation in THP-1 macrophages. In the present study, we discovered that the expression pattern of PKC in U937 foam cells was similar to that of TREM-1, suggesting that PKC activation may be involved in TREM-1-mediated IL8/TNF-α production in U937 foam cells. However, the mechanisms behind the link between PKC activation and TREM-1 link remain to be further studied. Of note, the PKC family consists of at least 12 isozymes that are divided into three subfamilies. Therefore, elucidation of the roles of different PKC isoforms in foam cell formation will lead to a better understanding of the pathogenesis of atherosclerosis. At present, the mechanism underlying ox-LDL-induced TREM-1 up-regulation remains elusive. Although a natural ligand for TREM-1 has not yet been identified, previous studies have shown that TREM-1 expression can be modulated *in vitro* and *in vivo* by various TLR ligands, including the gram-negative bacterial lipopolysaccharide, the primary ligand of TLR4 [31]. This raises the possibility that the TLR signaling pathway may also be involved in ox-LDL-induced TREM-1 up-regulation. Interestingly, TREM-1 and TLR ligands have been shown to induce inflammatory responses via intersecting and mutually stimulating pathways [21]. In addition, LDL oxidation is capable of inducing the formation of a number of highly reactive substances, some of

which may also directly mediate TREM-1 up-regulation. As stated above, macrophage foam cell formation is a characteristic feature of atherosclerotic plaques. Inhibition of foam cell formation and reduction of inflammatory cytokine production may be of therapeutic value in the treatment of atherosclerosis [5]. Our finding that TREM-1 controls the release of IL-8 and TNF-α in U937 foam cells defines a possible critical role of TREM-1 in the pathogenesis of atherosclerosis and implicates TREM-1 as a potential therapeutic target for the disease. In animals with LPS-induced endotoxemia, blockage of TREM-1 signaling by administration of either a soluble form of the TREM-1 molecule, small-molecule inhibitor or siRNA have been found to be able to improve animal survival [24, 32, 33]. If our results are verified *in vivo*, these approaches might also be applicable to the treatment of atherosclerosis.

CONCLUSION

In conclusion, the present study provides evidence that, in U937 foam cells, up-regulated expression of TREM-1 is concomitant with an increase in the levels of TNF-α and IL-8, and siRNA-mediated down-regulation of TREM-1 expression suppresses the production of TNF-α and IL-8. Apparently, TREM-1 can stimulate the release of TNF-α and IL-8 in U937 foam cells. These results suggest a critical role of TREM-1 in foam cell formation and the pathogenesis of atherosclerosis and may aid in the design and development of new strategies to combat atherosclerosis.

ACKNOWLEDGEMENTS

The authors thank Dr. Xiang-Jun Li and Medjaden Bioscience Limited for assisting in the preparation of this manuscript.

DECLARATION OF INTEREST

There was no conflict of interest in this study.

REFERENCES

[1] Libby P, Ridker PM, Maseri A. Inflammation and atherosclerosis. Circulation 2002; 105:1135-1143.
[2] Ross R. Atherosclerosis-an inflammatory disease. N Engl J Med 1999; 340:115-126.
[3] Woollard KJ, Geissmann F. Monocytes in atherosclerosis: subsets and functions. Nat Rev Cardiol 2010; 7:77-86.
[4] Bobryshev YV. Monocyte recruitment and foam cell formation in atherosclerosis. Micron 2006; 37:208-222.
[5] Li AC, Glass CK. The macrophage foam cell as a target for therapeutic intervention. Nat Med 2002; 8:1235-1242.
[6] Miller YI, Viriyakosol S, Worrall DS, Boullier A, Butler S, Witztum JL. Toll-like receptor 4–dependent and –independent cytokine secretion induced by minimally oxidized low-density lipoprotein in macrophages. Arterioscler Thromb Vasc Biol 2005; 25:1213.
[7] Terkeltaub R, Banka CL, Solan J, Santoro D, Brand K, Curtiss LK. Oxidized LDL induces monocytic cell expression of interleukin-8, a chemokine with T-lymphocyte chemotactic activity. Arterioscler Thromb 1994; 14:47-53.
[8] Hakala JK, Lindstedt KA, Kovanen PT, Pentikäinen MO. Low-density lipoprotein modified by macrophage-derived lysosomal hydrolases induces expression and secretion of IL-8 via p38 MAPK and NF-kappaB by human monocyte-derived macrophages. Arterioscler Thromb Vasc Biol 2006; 26(11):2504-9.
[9] Jovinge S, Ares MP, Kallin B, Nilsson J. Human monocytes/macrophages release TNF-alpha in response to Ox-LDL. Arterioscler Thromb Vasc Biol 1996; 16:1573-1579.
[10] Tipping PG, Hancock WW. Production of tumor necrosis factor and interleukin-1 by macrophages from human atheromatous plaques. Am J Pathol 1993; 142:1721-1728.
[11] Wang N, Tabas I, Winchester R, Ravalli S, Rabbani LE, Tall A. Interleukin-8 is induced by cholesterol loading of macrophages and expressed by macrophage foam cells in human atheroma. J Biol Chem 1996; 271:8837-8842.
[12] Rayment NB, Moss E, Faulkner L, Brickell PM, Davies MJ, Woolf N, et al. Synthesis of TNF alpha and TGF beta mRNA in the different micro-environments within atheromatous plaques. Cardiovasc Res 1996; 32:1123-1130.
[13] Gerszten RE, Garcia-Zepeda EA, Lim YC, Yoshida M, Ding HA, Gimbrone MA Jr, et al. MCP-1 and IL-8 trigger firm adhesion of monocytes to vascular endothelium under flow conditions. Nature 1999; 398:718-723.
[14] Boisvert WA, Santiago R, Curtiss LK, Terkeltaub RA. A leukocyte homologue of the IL-8 receptor CXCR-2 mediates the accumulation of macrophages in atherosclerotic lesions of LDL receptor-deficient mice. J Clin Invest 1998; 101:353-363.
[15] Persson J, Nilsson J, Lindholm MW. Interleukin-1beta and tumour necrosis factor-alpha impede neutral lipid turnover in macrophage-derived foam cells. BMC Immunol 2008; 9:70.
[16] Libby P, Egan D, Skarlatos S. Roles of infectious agents in atherosclerosis and restenosis: an assessment of the evidence and need for future research. Circulation 1997; 96:4095-4103.
[17] Dudding L, Haskill S, Clark BD, Auron PE, Sporn S, Huang ES. Cytomegalovirus infection stimulates expression of monocyte-associated mediator genes. J Immunol 1989; 143: 3343-3352.
[18] Deniset JF, Cheung PK, Dibrov E, Lee K, Steigerwald S, Pierce GN. Chlamydophila pneumoniae infection leads to smooth muscle cell proliferation and thickening in the coronary artery without contributions from a host immune response. Am J Pathol 2010; 176:1028-1037.
[19] Pellicano R, Fagoonee S. Helicobacter pylori and atherosclerosis: can current data be useful for clinical practice? Int J Cardiol 2008; 127:288-289.
[20] Liu SC, Tsai CT, Wu CK, Yu MF, Wu MZ, Lin LI, et al. Human parvovirus b19 infection in patients with coronary atherosclerosis. Arch Med Res 2009; 40:612-617.
[21] Bouchon A, Dietrich J, Colonna M. Cutting edge: inflammatory responses can be triggered by TREM-1, a novel receptor expressed on neutrophils and monocytes. J Immunol 2000; 164: 4991-4995.
[22] Klesney-Tait J, Turnbull IR, Colonna M. The TREM receptor family and signal integration. Nat Immunol 2006; 7: 1266-1273.
[23] Goulet AC, Einsphar JG, Alberts DS, Beas A, Burk C, Bhattacharyya A, et al. Analysis of cyclooxygenase 2 (COX-2) expression during malignant melanoma progression. Cancer Biol Ther 2003; 2:713-718.
[24] Bouchon A, Facchetti F, Weigand MA, Colonna M. TREM-1 amplifies inflammation and is a crucial mediator of septic shock. Nature 2001; 410:1103-1107.
[25] Klesney-Tait J, Colonna M. Uncovering the TREM-1-TLR connection. Am J Physiol Lung Cell Mol Physiol 2007; 293(6):L1374-6.
[26] Yang QW, Mou L, Lv FL, Wang JZ, Wang L, Zhou HJ, et al. Role of Toll-like receptor 4/NF-kappaB pathway in monocyte-endothelial adhesion induced by low shear stress and ox-LDL. Biorheology, 2005; 42(3):225-36.
[27] Ornatowska M, Azim AC, Wang X, Christman JW, Xiao L, Joo M, et al. Functional genomics of silencing TREM-1 on TLR4 signaling

in macrophages. Am J Physiol Lung Cell Mol Physiol 2007; 293(6): L1377-84.

[28] Feng J, Han J, Pearce SF, Silverstein RL, Gotto AM Jr, Hajjar DP, et al. Induction of CD36 expression by oxidized LDL and IL-4 by a common signaling pathway dependent on protein kinase C and PPAR-gamma. J Lipid Res 2000; 41:688-696.

[29] Osto E, Kouroedov A, Mocharla P, Akhmedov A, Besler C, Rohrer L, et al. Inhibition of protein kinase Cbeta prevents foam cell formation by reducing scavenger receptor A expression in human macrophages. Circulation 2008; 118:2174-2182.

[30] Wang ZQ, Yang YZ, Wang Z, Ren Z, Tang CK, Liu LS et al. Effects of PKC activity on lipid-accumulation mediated by Adipophilin in THP-1 Macrophage. Progress in Biochemmistry and Biophysics 2007; 34(10):1055-1064.

[31] Murakami Y, Kohsaka H, Kitasato H, Akahoshi T. Lipopolysaccharide-induced up-regulation of triggering receptor expressed on myeloid cells-1 expression on macrophages is regulated by endogenous prostaglandin E2. J Immunol 2007; 178:1144-1150.

[32] Gibot S, Kolopp-Sarda MN, Bene MC, Bollaert PE, Lozniewski A, Mory F, et al. A soluble form of the triggering receptor expressed on myeloid cells-1 modulates the inflammatory response in murine sepsis. J Exp Med 2004; 200:1419-1426.

[33] Gibot S, Massin F, Marcou M, Taylor V, Stidwill R, Wilson P et al. TREM-1 promotes survival during septic shock in mice. Eur J Immunol 2007; 37: 456-466.

Hsp 70, hsCRP and oxidative stress in patients with acute coronary syndromes

Ramazan Amanvermez[1*], Ethem Acar[2], Murat Günay[1], Ahmet Baydın[2], Türker Yardan[2], Yüksel Bek[3]

[1] Department of Biochemistry, School of Medicine, Ondokuz Mayıs University 55139 Samsun, Turkey. [2] Department of Emergency Medicine, School of Medicine, Ondokuz Mayıs University, 55139 Samsun, Turkey. [3] Department of Bioistatistic, School of Medicine, Ondokuz Mayıs University, 55139 Samsun, Turkey

Abstract

Acute coronary syndromes (ACS) like unstable angina (UA) and acute myocardial infarction (AMI) can lead to the morbidity and mortality. The diagnosis and management of patients with ACS in the earliest times after symptom onset are considerably important in the emergency service. Study aimed to investigate the serum levels of heat shock protein 70 (Hsp 70), high sensitivity C-reactive protein (hsCRP), total creatine kinase (CK) activity, creatine kinase MB (CK-MB), cardiac troponin I (cTnI), leukocyte count (WBCs) and markers of oxidative stress in the first hours of ACS and to view their diagnostic values. 70 patients with ACS after admission and 20 sex-matched healthy controls were included in this study. Serum Hsp 70, hsCRP, CK, CK-MB, cTnI, protein carbonyls, malondialdehyde as well as whole blood WBCs were measured. The level of hsCRP was statistically higher in patients with AMI and UA than that of control group (p<0.001). WBCs and oxidized protein levels were higher in AMI than in UA and control groups. cTnI was related to CK-MB in AMI and UA groups (r=0.731, r=0.806, p<0.001, respectively) and also related with hsCRP in UA group (r=0.824, p<0.001). The mean Hsp 70 level was higher by 32.2% in AMI and 12.7% in UA patients compared to control subjects. hsCRP may have a role in the inflammatory response after ACS. In addition to cTnI and CK-MB, WBCs and hsCRP may be useful as a marker for the identification of ACS patients with chest pain in early diagnosing.

KEY WORDS: acute coronary syndromes, Hsp 70, hs-CRP, oxidative stress

INTRODUCTION

Acute coronary syndromes include unstable angina and acute myocardial infarction in which myocardial ischemia and/or necrosis trigger the inflammation and subsequent repair processes. Oxidative stress and chronic inflammatory responses play a mysterious role in the initiation and progression of ACS [1-3]. Plaque rupture and subsequent thrombosis at the site of the plaque rupture are the most common underlying pathophysiologic mechanisms of ACS [4,5]. The definition of acute coronary syndrome depends on the specific characteristics of each element of the triad of clinical presentation (including a history of coronary artery disease), biochemical cardiac markers such as creatine kinase-MB isoenzme, cardiac troponins and electrocardiographic changes. Patients with ACS span a large spectrum of risk that progresses from UA to non-ST-elevation myocardial infarction and to ST-elevation myocardial infarction [6]. Detecting patients in the early hours of ACS is still a challenge for emergency physicians. For instance, the ECG is often non-diagnostic for acute chest pain, and in fact, the sensitivity of the baseline ECG for detecting AMI is only 60%, and up to 33% of patients with ACS have no chest pain [7]. Misdiagnosis has been reported to be the main cause of treatment delays [8]. In last decade, routine serum markers (CK-MB, cTnI and T, myoglobin) of myocardial injury in acute coronary cases reflect only the abnormalities of the inflammatory milieu and plaque rupture. However, novel identified serum substances are the components of vascular inflammation and/or atherosclerotic plaque instability have drawn recent attention for their ability to portend acute clinical events and their outcomes. Within a number of markers, hsCRP and Hsp 70 are suggested as a risk marker of ACS in the literature [9-12]. Little is known about the utility of these biomarkers in combination and relationship with the other markers. In this study, we investigated the serum levels of hsCRP, Hsp 70, total CK activity, CK-MB, cTnI, WBCs and markers of oxidative stress (protein carbonyls, a marker of protein oxidation; malondialdehyde, a marker of lipid peroxidation) in the first hours of ACS in patients who were admitted to the Emergency Department (ED) for typical chest pain and diagnosed as ACS. In addition, we review the diagnostic values of CK-MB, cTnI, hsCRP, Hsp 70 and WBCs in view of ROC (receiver operation characteristic) curve analysis in the early assess-

* Corresponding author: Ramazan Amanvermez,
Department of Biochemistry, School of Medicine, Ondokuz Mayıs University, TR - 55139 Samsun, Turkey
Phone: +90 362 3121919; ext: 2534
Fax: +90 362 4576041
e-mail: aramazan@omu.edu.tr, amanvermez55@yahoo.com

Submitted: 6. September 2011 / Accepted: 31. January 2012

ment (ie, within 4-6 h of symptom onset) of suspected ACS in the ED and critically review oxidative stress in ACS patients.

MATERIALS AND METHODS

Patients and Procedures

The local ethical committee approved procedures used in this study. Patients with ACS who attended the ED of Ondokuz Mayıs University Hospital were included in this prospective study after they had given informed consent. The patients with typical chest pain were enrolled in the study upon arrival to the ED within 4-6 h of the onset of symptoms. Typical chest pain was defined as squeezing pain over the precordial area radiating to the neck, arm, back or epigastric region accompanied by sweating, nausea, vomiting or syncope. Furthermore, this chest pain was no relieved by rest or no response by sublingual nitroglycerin. Atypical chest pain was defined as pleuritic, induced by palpation, confined to one point of the anterior chest wall, lasting only a few seconds or lasting for many hours [13]. Following initial clinical evaluation, all patients had a standard 12-lead ECG, and biochemical markers were assessed. Sex-matched twenty healthy volunteers with no chest pain or clinical evidence of heart disease served as controls. Histories, physical examination, chest radiography, ECG, exercise ECG testing and routine laboratory tests showed that the controls had no evidence of coronary heart disease. According to the changes in ECG findings and cardiac enzymes, patients were divided into two groups; a) myocardial infarction with ST elevation and without ST-elevation, and b) unstable angina pectoris. These groups were commonly classified under the category "acute coronary syndrome". Patients with typical chest pain ongoing >30 min, 2 mm ST-elevation in at least two adjacent precordial leads, >1 mm in standard leads were classified as "ST-elevation myocardial infarction". Patients without ST-elevation were classified as "non-ST-elevation myocardial infarction" or "unstable angina pectoris" according to the changes in CK-MB and cTnI levels [14]. When ACS was diagnosed, patients were admitted to the cardiac unit. All patients underwent coronary angiogram as a routine working up except healthy controls. Significant coronary artery disease was the presence of positive angiogram results at least 50% narrow in coronary artery.

Laboratory assays

Blood samples were taken from ACS patients upon arrival to the ED. Also, blood was taken from the control subjects. Leukocyte count was measured in the whole blood by LH-750 Beckman Coulter analyzer. The serum was separated by centrifugation from other venous blood sample, and then hsCRP, cTnI, total CK, and CK-MB (mass) analyzed by clinical chemistry laboratory and separated serum for the other tests stored at -80°C until analysis. Circulating hsp 70 was measured with ELISA kit (EKS-715, Stressgen) in the serum samples. Lipid peroxidation in serum was estimated spectrophotometrically by the tiobarbituric acid-reactive substance (TBARS) method with slight modifications and expressed in terms of malondialdehyde (MDA) [15]. Measurements of protein (carbonyl) oxidation in the serum samples were made by the method of Evans et al. [16] with slight modifications. Carbonyl concentration (nmol mg^{-1} of protein)= nmol ml^{-1} of carbonyl groups/protein concentration in mg ml^{-1}.

Statistical analysis

All statistical analysis was performed with SPSS software (SPSS, release 13.0, Inc, Chicago, ILL). Data was tested for normality assumption. They were not normally distributed. Therefore non-parametric statistical analyses were used for all comparisons. Kruskal-Wallis test was used to determine the statistical significance of the differences in the groups. Then Mann-Whitney-U test (with Bonferroni correction) was used for comparisons between groups. ROC curves for the variables which have significant effect on ACS drawn to indicate the diagnostic values of test variables. Also, we calculated the Spearman Correlation Coefficient between the levels of serum parameters. We summarized continuous variables with mean ± standard deviation, categorical variables with percentages. At the 0.05 significance level the means of any two groups marked with the same letters indicate statistically non significant groups for each serum parameter.

RESULTS

The general characteristics of the patients and control groups are shown in Table 1. As expected, all patients were more probably to have history of hypertension, diabetes, hyperlipidemia, smoking and family history of coronary heart disease than controls. As presented in Table 2, the mean level of Hsp 70 was higher by 32.2% in pa-

TABLE 1. Characteristics and risk factor profile in all study groups.

Characteristics	Group I: Acute Myocardial Infarction (n= 45)	Group II: Unstable Angina (n= 25)	Group III: Controls (n= 20)
Age, y (mean ± SD)	62.88 ± 12.98	58.24 ± 9.93	52.45±8.35
Male/Female, n	35/10	19/6	11/9
Coronary risk factors; n (%)			
Hypertension	22 (48.9%)	21 (84.0%)	0
Diabetes mellitus	15 (33.3%)	9 (36.0%)	0
Hyperlipidemia	12 (26.7%)	12 (48.0%)	0
Smoking	22 (48.9%)	14 (56.0%)	3 (15.0%)
Increased age (> 65 years)	25 (55.6%)	7 (28.0%)	0
Family history of coronary artery disease	4 (8.9%)	2 (8.0%)	0

TABLE 2. Serum Hsp 70, hsCRP, total CK, CK-MB, cTn I, WBCs, MDA and protein carbonyls levels in patients with coronary artery disease.

	Patients with coronary artery disease			
Parameters	Acute Myocardial Infarction (n= 45)	Unstable Angina (n= 25)	Healthy Controls (n= 20)	p*
Hsp 70 (ng/ml)	9.51 ± 11.34a	7.39 ± 4.32a	6.45 ± 0.87a	p>0.05
hs-CRP (mg/L)	48.58 ± 58.50a	38.25 ± 65.30a	3.15 ± 6.09b	p<0.001
total CK (U/L)	1098.13 ± 1891.04a	193.56 ± 236.81b	81.45 ± 39.46c	p<0.01
CK-MB (ng/ml)	79.38 ± 104.58a	13.02 ± 32.80b	0.70 ± 0.54c	p<0.001
cTn I (ng/ml)	29.16 ± 35.37a	3.53 ± 12.16b	0.03 ± 0.15c	p<0.001
WBCs (10^3/μL)	12086.6 ± 4518.4a	9488.0 ± 2772.9b	8340.0 ± 1994.5b	p<0.01
MDA (μmol/L)	0.804 ± 0.801a	1.086 ± 0.736 b	0.574 ± 0.342a	p<0.05
Protein carbonyls (nmol/mg protein)	3.28 ± 1.16a	2.25 ± 0.87b	2.09 ± 0.72b	p<0.05

*The different letters indicate statistically significant groups for each parameter.

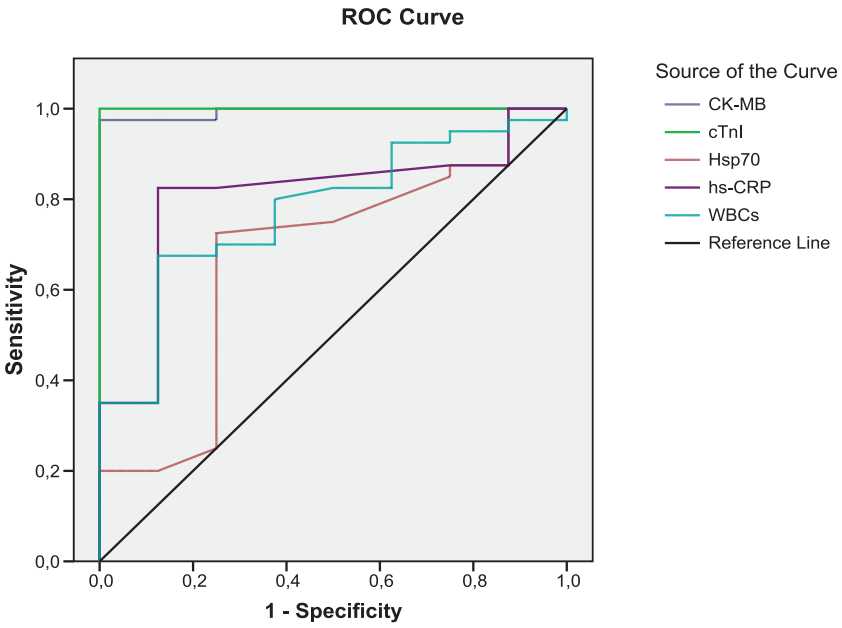

FIGURE 1. The diagnostic value of CK-MB, cTnI, Hsp70, hsCRP and WBCs tests to differentiate between AMI and UA groups

Legend for Fig. 1

Test Result Variable(s)	Area Under the Curve	Std. Error	P (b)	Asymptotic 95% Confidence Interval	
				Lower Bound	Upper Bound
CK-MB	.815	.055	<0.001	.707	.923
cTnI	.796	.056	<0.001	.685	.907
Hsp70	.665	.074	0.028	.521	.809
WBCs	.647	.070	0.051	.511	.783
Hs-CRP	.600	.074	0.183	.454	.746

[b]Null hypothesis: true area = 0.5

tients with AMI and 12.7% in patients with UA compared to control subjects. But no statistically difference was obtained for Hsp 70 levels among the groups (p>0.05). The levels of hsCRP in serum were significantly higher in patients with AMI and UA compared to control group (p<0.001). However, its mean value was found higher by 21.2% in patients with AMI when compared to UA group. Total CK levels were significantly elevated in patients with ACS as compared to levels in the control group (p<0.01). CK-MB and cTnI used to be the standard markers for diagnosing AMI; however, cTnI has proven more accurate in confirming or excluding AMI. The levels of these tests in serum were found significantly higher in patients with AMI when compared to control group (p<0.001). Also, CK-MB and cTnI levels were observed higher in patients with UA compared to control subjects. WBCs in AMI patients were measured over reference count (p<0.001). In addition, mean leukocyte counts in patients with UA were measured higher by 12.1% with respect to control group. Mean serum MDA was raised by 28,6% in patients with AMI and 47.1% in UA patients compared to control group. Similarly, serum protein carbonyls value was significantly increased in patients with AMI (p<0.05). However, its mean value was higher (by 7.1%) in patients with UA compared to control group. The Spearman's correlation coefficients of CK-MB and cTnI were significant in AMI and UA groups (r=0.731, r=0.806, p<0.001, respectively). Also, the correlation coefficient between hsCRP and cTnI was significant (r=0.824, p<0.001). We found statistically significant correlations between WBC and hsCRP in AMI and UA groups (r=0.34, p=0.035, r=0.58, p=0.003, respectively). Diagnostic values for CK-MB, cTnI, Hsp 70, hsCRP and WBCs to differentiate the groups were shown in Figures 1, 2, 3 and their legends.

DISCUSSION

Prompt recognition of a patient with an ACS is very important since appropriate therapy can markedly improve the prognosis of patients. New cardiac biomarkers have emerged as strong predictors of risk among patients presenting with ACS. Importantly, these biomarkers assess different pathophysiological mechanisms in myocardial ischemia: increases in cTnI indicate myocardial necrosis [17], CK-MB raises within 3-4 h of cardiac ischemia/necrosis [18], hsCRP, a marker of in-

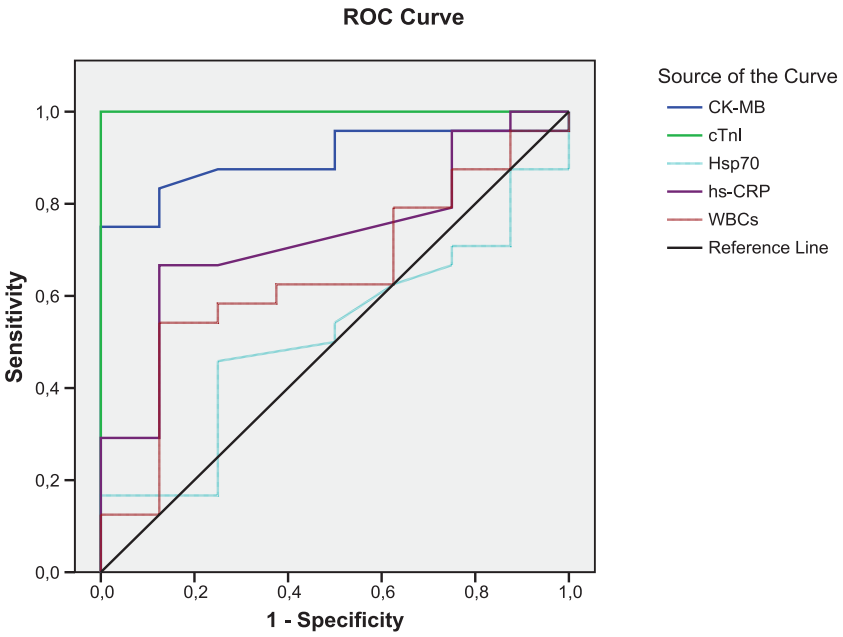

FIGURE 2. The diagnostic value of CK-MB, cTnI, Hsp70, hsCRP and WBCs tests to differentiate between AMI and control groups.

Legend for Fig. 2

Test Result Variable(s)	Area Under the Curve	Std. Error	P (b)	Asymptotic 95% Confidence Interval	
				Lower Bound	Upper Bound
cTnI	1.000	.000	<0.001	1.000	1.000
CK-MB	.994	.008	<0.001	.978	1.010
hsCRP	.806	.079	0.007	.652	.960
WBCs	.777	.081	0.014	.617	.936
Hsp70	.672	.108	0.128	.460	.884

[b]Null hypothesis: true area = 0.5

flammation, is increased in patients with ACS [19]. Elevations in WBCs have been associated with the development of coronary artery disease and AMI [20]. Hsp 70 levels are independently associated with a higher risk of ACS [11]. Usually, it is accepted that CK-MB and cTnI are considerably important as AMI indicators in patients with ACS along with chest pain and ECG findings. In our study, statistically significant differences were obtained for the levels of these tests between the groups (Table 2). CK-MB and cTnI are gold markers in detecting AMI patients among subjects with ACS. CK-MB may set to differentiate between AMI and UA in the first hours of ACS as shown in Figure 1 and legend. By the way, these tests were observed to be an elevation in UA patients when compared to healthy control group. As a result of this finding, both test levels in patients with ACS might be sensitive signs to change from UA to AMI. Because during acute presentation of symptoms, there is a more contemporary continuum of events that begin with plaque rupture or erosion that lead to UA, and may progress to non-Q wave and Q-wave AMI at any moment [21]. Along with these explanations, patients with UA prior to AMI may be evaluated by CK-MB and cTnI leakage, and less Q-wave activity than patients with AMI of sudden onset [22]. Some UA patients with an abnormal CK-MB, cTnI and hsCRP may imply a transient myocardial ischemia in relation to duration ischemic episodes. Frequently, these patients are at high immediate risk for cardiac events. A number of studies have noted that the pathophysiology of coronary artery disease involves inflammation [9, 23, 24]. The hsCRP assays can detect low-grade inflammatory activity within the vascular system, which helps predict the first or recurrent coronary events [9]. In the present study, serum hsCRP levels were determined to be higher in UA patients, and highest in AMI patients with respect to control individuals. Interestingly, its value rises in parallel to the levels of increased CK-MB and cTnI in UA and AMI patients as indicated in Table 2. In prior studies, Tanaka et al. [25] reported that patients with plaque rupture at the culprit site showed higher hsCRP levels in the acute phase of AMI. Liuzzo et al. [26] showed that patients presenting with UA who had increased plasma levels of CRP (≥3 mg/L). A scientific statement of the Centers for Disease Control and Prevention/American Heart Association proposed a cutoff of 10 mg/L as more suitable when the predictive value of CRP was assessed in ACS [27]. According to our findings, an increased hsCRP level in UA and AMI, in the absence of systemic inflammatory disease, is a more likely to reflect widespread activation of inflammatory cells. Also, Hansson has indicated that the levels of C-reactive protein and interleukin-6 are elevated in patients with UA and AMI, with high levels predicting worse prognosis [28]. The use of hsCRP may significantly add to our ability to correctly identify patients presenting with ACS who are at high risk for future cardiovascular events. In addition to CRP, the other marker of inflammation and plaque instability is WBC count. Elevations in leukocyte count have been associated with adverse clinical outcomes and a higher mortality rate in the setting of ACS [29]. Indeed, platelet activation and markers of inflammation have been associated with coronary artery disease and ACS [20]. In our study, WBC count was measured high in patients presenting AMI, however it was elevated (by 12.1%) in UA patients with respect to reference count. Madjit et al. [30] reported that leu-

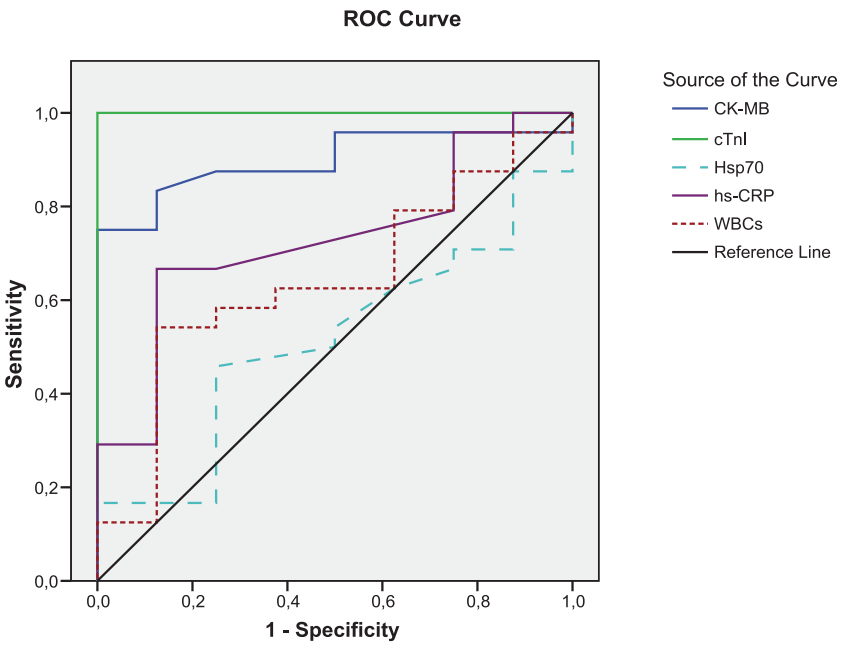

FIGURE 3. The diagnostic value of CK-MB, cTnI, Hsp70, hsCRP and WBCs tests to differentiate between UA and control groups.

Legend for Fig. 3

Test Result Variable(s)	Area Under the Curve	Std. Error	P (b)	Asymptotic 95% Confidence Interval	
				Lower Bound	Upper Bound
cTnI	1.000	.000	<0.001	1.000	1.000
CK-MB	.898	.055	<0.001	.790	1.007
Hs-CRP	.729	.096	0.056	.540	.918
WBCs	.641	.109	0.240	.428	.854
Hsp70	.513	.110	0.913	.297	.729

[b]Null hypothesis: true area = 0.5

kocytosis was an independent predictor of AMI. As a result of our study finding and literature reports [30, 31], leukocyte count in the first hours of ACS may be useful as diagnostic or prognostic indicator in patients with AMI or UA. On the other hand, an elevated leukocyte count and enhanced oxidative stress has been implicated in the pathogenesis of coronary artery disease and ACS [2, 3, 20, 32, 33]. Coronary atherosclerosis, the most common pathological process underlying cardiovascular disease, represents a state of heightened oxidative stress characterized by lipid and protein oxidation in vascular wall [34, 35]. In relation to this issue, findings of our study indicated that MDA was raised in the serum of UA patients and protein carbonyls in serum were increased in patients with AMI. Therefore, these results indicate the presence of oxidative stress in patients with ACS. Similarly, Serdar et al. [36] have demonstrated to increases serum lipid and protein oxidation in the first hours of ACS in patients with UA and AMI. Kostner et al. [32] have shown that lipid peroxidation in serum is significantly higher in UA as compared to patients with stable angina and to controls. Based on the results of scientific studies along with our findings, oxidative stress in ACS is an important event. It may lead to endothelial dysfunction and plaque disruption in patients. Heat shock proteins protect against cell damage and apoptosis. Their expression is up regulated upon exposure to stressful conditions such as ischemia, hypoxia, oxidative damage, mechanical shear stress, and inflammatory response. It has been shown that Hsp 70 protects cells against ischemic cardiac damage. Dybdahl et al. [12] had indicated that Hsp 70 was rapidly released into circulation after AMI. They have shown that circulating Hsp 70 is related to the extent of myocardial damage after admission to the emergency unit at six hours and suggested as a marker of myocardial injury. Valen et al. [22] reported that Hsp 70 (also called Hsp 72) was increased in atrial tissue of patients with UA. A recent work has demonstrated that plasma levels of Hsp 70 are markedly higher in patients with ACS within 12 h of the onset of symptoms than in the controls, and also Hsp 70 levels are higher in ACS than in stable angina [11]. However, mean serum level of Hsp 70 in the current study was higher in AMI and UA with respect to health controls. It seems to be Hsp 70 increases along with hsCRP in patients with ACS as shown in Table 2. Therefore, it might have a role in the inflammatory response against myocardial ischemia or necrosis.

CONCLUSIONS

As shown in Figures 1, 2, 3 and legends, ROC curve analyses indicated that CK-MB and cTnI provided the highest diagnostic accuracy for discriminating between patients in AMI and UA. After these tests, Hsp 70 has a higher diagnostic value for separating rather than WBCs and hsCRP (legend for Fig.1). The levels of cTnI and CK-MB have the highest diagnostic value for discriminating between individuals in AMI and health controls. According to ROC analysis results, WBCs and hsCRP have also high diagnostic accuracy with respect to control (legend for Figure 2). Patient population and healthy controls in this study are too small to allow any diagnostic and prognostic conclusions in ACS. Further investigation with large patient population and controls are required to confirm these findings in the prospective studies.

ACKNOWLEDGEMENTS

This study was supported partly by Ondokuz Mayıs University Research Fund, T.430 project.

DECLARATION OF INTEREST

The authors declare no conflict of interest for present study.

REFERENCES

[1] Inoue N, Kobayashi S, Yokoyama M. Oxidative stress and inflammation in plaque instability-role of vascular C-reactive protein. International Congress Series 2004; 1262: 71-74.
[2] Aukrust P, Berge RK, Ueland T, Aaser E, Damas JK, Wikeby L, et al. Interaction between chemokines and oxidative stress: possible pathogenic role in acute coronary syndromes. Journal of the American College of Cardiology 2001; 37(2): 485-491.
[3] Singh RB, Niaz MA, Sharma JP, Kumar R, Bishnoi I, Begom R. Plasma levels of antioxidant vitamins and oxidative stress in patients with acute myocardial infarction. Acta Cardiol 1994; 49(5): 441-452.
[4] Falk E, Shah PK, Fuster V. Coronary plaque disruption. Circulation 1995; 92: 657-671
[5] Fuster V, Badimon J, Chesebro JH, Fallon JT. Plaque rupture, thrombosis, and therapeutic implications. Haemostasis 1996; 26: 269–284.
[6] Armstrong EJ, Morrov DA, Sabatine MS. Inflammatory biomarkers in acute coronary syndromes: part I: introduction and cytokines. Circulation 2006; 113(6): e72-e75.
[7] Moe KT, Wong P. Current trends in diagnostic biomarkers of acute coronary syndrome. Ann Acad Med Singapore 2010; 39: 210-215.
[8] Dadkhah S, Sharain K, Sharain R, Kiabayan H, Foschi A, Zonia C, et al. The value of bedside cardiac multibiomarker assay in rapid and accurate diagnosis of acute coronary syndromes. Crit Pathw Cardiol 2007; 6: 76-84.
[9] Futterman LG, Lemberg L. High-sensitivity C-reactive protein is the most effective prognostic measurement of acute coronary events. American Journal of Critical Care 2002; 11(5): 482-486.
[10] Burke AP, Tracy RP, Kolodgie F, Malkom GT, Zieske A, Kutys R, et al. Elevated C-reactive protein values and atherosclerosis in sudden coronary death. Circulation 2002; 105 (17); 2019-2023.
[11] Zhang X, Xu Z, Zhou L, Chen Y, He M, Cheng L, et al. Plasma levels of Hsp 70 and anti-Hsp 70 antibody predict risk of acute coronary syndrome. Cell Stress and Chaperones 2010; 15(5): 675-686.
[12] Dybdahl B, Slordahl SA, Waage A, Kierulf P, Espevik T, Sundan A. Myocardial ischemia and the inflammatory response: release of heat shock protein 70 after myocardial infarction. Heart 2005; 91: 299-304.
[13] Cete Y, Eken C, Eray O, Goksu E, Kiyan S, Atilla R. The value of point-of-care fatty acid binding protein in patients with chest pain in determining myocardial infarction in the emergency setting. Hong Kong J Emerg Med 2010; 17: 224-229.
[14] Gururajan P, Gurumurthy P, Nayar P, Srinivasa Nageswara Rao G, Babu S, Cherian KM. Heart fatty acid binding protein (H-FABP) as a diagnostic biomarker in patients with acute coronary syndrome. Heart Lung Circ 2010; 19(11):660-664.
[15] Singh RP, Padmavathi B, Rao R. Modulatory influence of Adhatoda vesica leaf extract on the enzymes of xenobiotic metabolism, antioxidant status and lipid peroxidation in mice. Mol Cell Biochem 2000; 213: 99-109.
[16] Evans P, Lyras L, Halliwell B. Measurement of protein carbonyls in human brain tissue. Methods Enzymol 1999; 300: 145-156.
[17] Adams JE 3rd, Bodor GS, Dávila-Román VG, Delmez JA, Apple FS, Ladenson JH. et al. Cardiac troponin I. A marker with high specificity for cardiac injury. Circulation 1993; 88: 101-106.
[18] Dekker MS, Mosterd A, Hof AWJ, Hoes AW. Novel biochemical markers in suspected acute coronary syndrome: systemic review and critical appraisal. Heart 2010; 96:1001-1010.
[19] Scirica BM, Morrow DA, Cannon CP, De Lemos JA, Murphy S, Sabatine MS, et al. Clinical application of C-reactive protein across the spectrum of acute coronary syndromes. Clinical Chemistry 2007; 53(10): 1800-1807.
[20] Furman MI, Gore JM, Anderson FA, Budaj A, Goodman SG, Avezum A, et al. Elevated leukocyte count and adverse hospital events in patients with acute coronary syndromes: Findings from the Global Registry of Acute Coronary Events. Am Heart J 2004;147:42-48.
[21] Wu AH, Ford L. Release of cardiac troponin in acute coronary syndromes: ischemia or necrosis? Clin Chim Acta 1999; 284: 161-174.
[22] Valen G, Hansson GK, Dumitrescu A, Vaage J. Unstable ungina activates myocardial heat shock protein 72, endothelial nitric oxide synthase, and transcription factors NFκB and AP-1. Cardiovascular Research 2000; 47: 49-56.
[23] Ross R. Atherosclerosis- an inflammatory disease. N Engl J Med 1999; 340: 115-126.
[24] Blake GJ, Ridker PM. C-raeactive protein and other inflammatory risk markers in acute coronary syndromes. J Am Coll Cardiol 2003; 41 (4 Suppl S): 37S-42S.
[25] Tanaka A, Shimada K, Sano T, Namba M, Sakamota T, Nishida Y, et al. Multible plaque rupture and C-reactive protein in acute myocardial infarction. J Am Coll Cardiol 2005; 45 (10): 1594-1599.
[26] Liuzzo G, Biasucci LM, Gallimore JR, Grillo RL, Rebuzzi AG, Pepys MB, et al. The prognostic value of C-reactive protein and serum amyloid a protein in severe unstable angina. N Engl J Med 1994;331:417-424.
[27] Pearson TA, Mensah GA, Alexander RW, Anderson JL, Cannon RO, Criqui M, et al. Markers of inflammation and cardiovascular disease: application to clinical and public health practice: a statement for healthcare professionals from the Centers for Disease Control and Prevention and the American Heart Association. Circulation 2003; 107: 499-511.
[28] Hansson GK. Inflammation, atherosclerosis, and coronary artery disease. N Engl J Med. 2005;352(16):1685-95.
[29] Panteghini M. Role and importance of biochemical markers in clinical cardiology. European Heart Journal 2004; 25: 1187-1196.
[30] Madjid M, Awan I, Willerson JT, Casscells SW. Leukocyte count and coronary heart disease: implications for risk assessment. J Am Coll Cardiol. 2004;44(10):1945-56.
[31] Menon V, Lessard D, Yarzebski J, Furman MI, Gore JM, Goldberg RJ. Leukocytosis and adverse hospital outcomes after acute myocardial infarction. Am J Cardiol 2003; 92: 368-372.
[32] Kostner K, Hornykewycz S, Yang P, Neunteufl T, Glogar D, Weidinger F, et al. Is oxidative stres causally linked to unstable angina pectoris? A study in 100 CAD patients and matched controls. Cardiovascular Research 1997; 36: 330-336.
[33] Misra MK, Sarwat M, Bhakuni P, Tuteja R, Tuteja N. Oxidative stres and ischemic myocardial syndromes. Med Sci Monit 2009; 15(10): 209-219.
[34] Stocker R, Keaney JF Jr. Role of oxidative modifications in atherosclerosis. Physiol Rev 2004; 84(4): 1381-1478.
[35] Stocker R, Keaney JF Jr. New insights on oxidative stress in the artery wall. J Thromb Haemost 2005;3(8):1825-1834.
[36] Serdar Z, Serdar A, Altin A, Eryilmaz U, Albayrak S. The relation between oxidant and antioxidant parameters and severity of acute coronary sydromes. Acta Cardiol 2007; 62(4): 373-380.

Isolation of a potent antibiotic producer bacterium, especially against MRSA, from northern region of the Persian Gulf

Esmaeil Darabpour[1], Mohammad Roayaei Ardakani[1]*, Hossein Motamedi[1], Mohammad Taghi Ronagh[2]

[1] Department of Biology, Faculty of Science, Shahid Chamran University, Ahvaz, Iran. [2] Department of Marine Ecology, Marine Science & Technology University, Khorramshahr, Iran

Abstract

Nowadays, emergence and prevalence of MRSA (Methicillin Resistant *Staphylococcus aureus*) strain have become a great global concern in 21st century, so, it is necessary to discover new antibiotics against this pathogen. The aim of this study was isolation and evaluation marine bacteria from the Persian Gulf in order to finding antibiotic compounds against some pathogenic bacteria. For this purpose, water and sediment samples were collected from the Persian Gulf during March to October 2009. The antibacterial activity of the isolated bacteria was assessed using disc diffusion method. The Growth Curve Interference (GCI) parameter against MRSA was determined for the high potential antibiotic producing strain. The most important factors affecting fermentation conditions in antibiotic production were also optimized. Definite identification of intended isolate was confirmed by 16S rRNA sequencing. Altogether, 51 bacterial colony was isolated and among them only 3 bacterium showed antibacterial activity. *Pseudoalteromonas piscicida* PG-01 isolated from a sediment sample was chosen as the best antibiotic producing strain. This strain was effective against all tested Gram-positive bacteria, had good anti-MRSA activity and also GCI value against MRSA was two times lower than MIC value. Among the optimized fermentation parameters, carbon and nitrogen sources play major role in efficacy of optimized antibiotic production. Ultrastructural study on the effect of intended antibiotic compounds on MRSA using TEM revealed that the target site for this compound is cell wall. Considering the antibacterial effect of PG-01 strain especially against MRSA, intended antibiotic compounds can gives hope for treatment of diseases caused by multi-drug resistant bacteria.

KEY WORDS: MRSA, natural antimicrobial, *Pseudoalteromonas piscicida* PG-01, marine environment

INTRODUCTION

Despite the use of antibiotics for nearly eight decades, infectious diseases continue to have an impact on human health and cause morbidity and mortality worldwide. In recent decades, the growing emergence of multi-drug resistant bacteria (MDRB) has caused one of the major challenges for infectious disease treatment. Methicillin Resistant *Staphylococcus aureus* (MRSA) causes a wide range of diseases from skin infections to invasive diseases such as necrotizing pneumonia, has become one of the greatest challenges for modern antimicrobial therapy in both industries and developing countries, particularly because due to multi-drug resistant strains. Presently, three different types of MRSA have been described: hospital-acquired MRSA (HA-MRSA), community-acquired MRSA (CA-MRSA) and lifestock-associated MRSA (LA-MRSA). These strains are world-widely distributed and cause medication failure in clinical cases. MRSA strains have acquired a mobile genetic element called staphylococcal cassette chromosome (SCC*mec*), carrying *mec*A encoding a penicillin-binding protein (PBP2a) with low affinity to beta-lactam antibiotics [1, 2]. The most frequent SCC*mec* types found in hospital isolates are I, II and III; also type IV is associated with community-acquired strains. Now, however, nosocomial infections are major problem around the world due to increasing bacterial resistance to classical antimicrobials and searching for new antibacterials with new antibacterial mechanisms is of great urgent. From the early 1960s, research groups began to concentrate on the oceans for novel bioactive compounds [3]. Marine microorganisms can be considered as an untapped source of new bioactive molecules because 1) certain classes of marine bacteria have developed unique adaptation mechanisms [4] to the physiological, physical, chemical and biological conditions e.g., salinity, pressure, temperature, and depletion of micronutrients found in the oceans, which is reflected in their physiology and biochemical properties [2, 5]; 2) competition among microbes for space and food [6] in some marine niches especially about of the particle associ-

* Corresponding author: Mohammad Roayaei Ardakani, Department of Biology, Faculty of Science, Shahid Chamran University, Ahvaz, Iran.
Tel/Fax: 0098 611-3331045
e-mail: ismal_dar@yahoo.com; roayaei_m@yahoo.com

Submitted: 16. November 2011 / Accepted: 26. January 2012

ated bacteria and sediment inhabiting bacteria has exerted a driving force on bacterial selection leading to new adaptive strategies and the synthesis of new metabolites, and 3) some bacteria have developed certain adaptation mechanisms resulting in production of bioactive metabolites which may be useful for their defense against predators such as protozoans. Furthermore, more than 95% of earth's biosphere is oceans and during the past five decades more than 10,000 marine metabolites have been isolated and characterized, which 18% of these bioactive compounds were obtained from bacterial sources [3]. Today, one of the main goals of the marine biotechnology is finding natural substances originated from marine microorganisms with pharmaceutical applications such as anti-cancer, anti-infection and anti-inflammation activities. Till now, several marine-derived antibiotics with anti-MRSA activity has been reported. These novel antibiotics have been isolated from five genera of marine bacteria including *Pseudoalteromonas, Pesudomonas, Bacillus, Marinospora*, and *Streptomyces* [7]. Persian Gulf, in southwest Asia, is a relatively shallow and extension of Indian Ocean located between Iran and the Arabian Peninsula; it is bordered by Iran on the entire north-eastern coastline. This study mainly focused on 1) isolation and identification of potent antibiotic producer bacteria, especially against MRSA, from the northern regions of Persian Gulf, 2), optimization of antibiotic production and preliminary purification and characterization of intended antibiotic compound, and 3) determination the mechanism of action for intended antibiotic compound against MRSA using Transmission Electron Microscopy (TEM).

MATERIALS AND METHODS

Sample collection

During March to October 2009, 3 sampling regions in Persian Gulf were selected (Figure 1) and samples of coastal water; surface water, deep water, coastal sediment, bed sediment and mangrove forest sediment were collected from 17 study sites in some northern area of Persian Gulf. Water samples were collected using sterilized-niskin bottle (using 70% ethanol prior to sampling); subsequently, samples were collected in sterilized glass bottles. Sediment samples were collected by sterilized van veen grab in to sterilized plastic bags. These samples were kept at 4˚C (placed on ice) until delivery to laboratory.

Isolation procedure

In order to isolation of marine bacteria from water samples, 8 µl of samples were spread on agar plates with marine agar 2216 (Himedia, India). Sediment samples (1 g) were transferred to test tube containing 1ml of sterilized sea water, vigorously mixed, and finally ten fold serial dilutions were prepared and aliquots (20 µl) of each dilution were spread

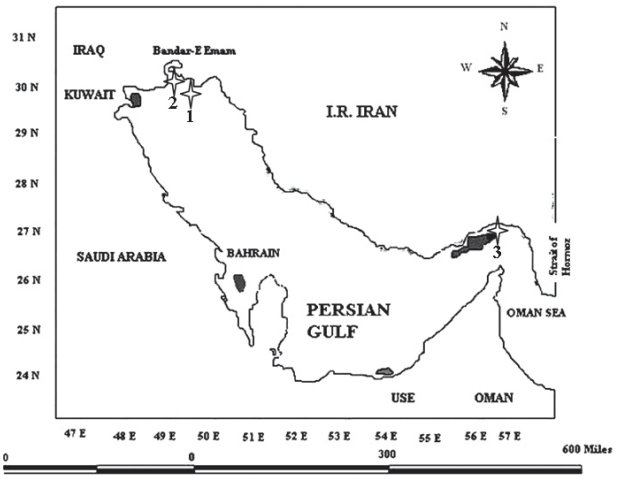

FIGURE 1. Map of sampling sites in the Persian Gulf. 1: Bahrakan port, 2: Mahshahr port, 3: Qeshm Island

on the entire surface of marine agar 2216 [8]. Isolation of marine bacteria from both water and sediment samples was performed using pour plate technique, too. The inoculated plates were incubated at 24, 30 and 37˚C for 3-5 days, developed colonies were purified by repeatedly subculturing on marine agar and finally, those colonies with distinct characteristics such as pigmentation, size, opacity, elevation, margin and surface were chosen for further processing [9].

Screening of isolates for antibacterial activity

All of the bacterial isolates from different samples were screened for the production of antimicrobial substances by primary screening method. Pure colonies were grown in maine broth medium (MB) (Laboratorios CONDA, Spain) at 30˚C for 5-7 days. The broth cultures were centrifuged at 10000 rpm for 15 min at 4˚C, and the cell free supernatants were filtered through 0.22 µm pore size filter (Millipore, Italy) and it was surveyed for antibacterial activity. Antibacterial activity was assayed by standard agar disk diffusion test against standard test organisms including *Staphylococcus aureus* (ATCC 6538), *Staphylococcus epidermidis* (ATCC 12228), *Bacillus subtilis* (ATCC 12711), *Listeria monocytogenes* (ATCC 19112), *Escherichia coli* (ATCC 11303), *Pseudomonas aeruginosa* (ATCC 27853), *Salmonella typhi* (ATCC 19430), and with Methicillin Resistant *Staphylococcus aureus* (MRSA) as clinical strain. Standard bacterial strains were obtained from Iranian Research Organization for Science and Technology (IROST) and MRSA that was also MDR (multi-drug resistant) was collected from the Golestan Hospital, Ahavz, Iran. Tested bacteria were cultured in Muller Hinton Broth (MHB, Merck, Germany) medium at 37˚C for 5-8 h until adjusted to the 0.5 Mc Farland turbidity (10^8 cfu/ml) [10]. 100 µl of these suspensions was inoculated on Muller Hinton Agar (MHA, Merck, Germany) plates as lawn culture by sterile cotton swab and remained for 15 min for absorption of ex-

cess moisture. The sterile filter paper discs (6 mm diameter) [11] were saturated by 50 µl of cell free supernatants of the marine isolates and then were placed on lawn cultures. After a diffusion period of 1h, the plates were incubated at 37˚C for 24h and the inhibition zone around each disc was measured in mm. This experiment was carried out in triplicate.

Antibacterial activity of the highest potential producer

After primary screening, the isolate responsible for the greatest zone of inhibition was chosen for further study. In order to test the antibacterial activity, after 3 days of incubation, the broth culture was centrifuged at 8000 rpm for 15 min at 4˚C, and then supernatant was extracted using equal volume of ethyl acetate. Solvent was removed at 37˚C. The dried crude extract was dissolved in ethyl acetate at concentration of 50 mg/ml. The antibacterial activity of the obtained raw extract was evaluated at this concentration using disc diffusion method against Gram-positive microorganisms including *S. aureus* (ATCC 6538), *S. epidermidis* (ATCC 12228), *B. subtilis* (ATCC 12711), *L. monocytogenes* (ATCC 19112), MRSA, and *L. monocytogenes* (clinical isolate) and Gram-negative bacteria including *E. coli* (ATCC 11303), *P. aeruginosa* (ATCC 27853), *S. typhi* (ATCC 19430), *Bordetella bronchiseptica* (clinical isolate) and *Brucella melitensis* (clinical isolate). The clinical isolates were prepared from the Golestan Hospital, Ahvaz, Iran. A disc soaked in ethyl acetate was kept as negative control. The following antibiotics were used as control (µg/disc): vancomycin (VA) 30 µg, methicillin (MT) 5 µg, nitrofurantoin (FM) 300 µg, penicillin (P) 10 µg, and colistin (CL) 10 µg. All of these synthetic antibiotic discs were produced by Difco, USA. The MIC (Minimal Inhibitory Concentration) of the antimicrobial agent from the best producer strain was determined against two somewhat important and more sensitive bacteria by macro broth dilution assay method [12,13]. MBC (Minimal Inhibitory Concentration) was also determined.

Determination of GCI (Growth Curve Interference) parameter

GCI is a parameter which defined as the lowest concentration of an antibiotic compound that modifies the growth curve of a tested pathogen comparing to a control without antibiotic [14]. Tested pathogen in this study was MRSA. For determination of GCI, MIC was determined by the macro broth dilution assay method. At first, 15 ml of extract at four concentrations including equal to MIC and sub-MICs was prepared. In the next step, four flasks containing 15 ml Muller Hinton Broth medium of 0.5 Mc Farland turbidity of MRSA culture was prepared. Finally, each of the prepared different extracts were added to above flasks and then incubated at 37˚C on a rotatory shaker; biomass accumulation was measured from 0 till 10 h (every 1 h) by spectrophotometry reading of optical density (OD) at 600 nm until tested bacterium was entered in stationary and death phase of growth. A flask containing 30 ml MHB with the 0.5 Mc Farland turbidity of MRSA but without extract was used as control. Related curves were drawn and GCI was determined.

Optimization of the culture conditions and processing parameters for antibiotic production

The preliminary fermentation conditions for production of antibiotic by PG-01 isolate was prepared in Marine Broth (as control medium) by incubating at 30˚C for 3 days. Also, a synthetic medium containing of glucose (primary carbon source) 1 g/l and peptone (primary nitrogen source) 5 g/l of sterilized-sea water with initial pH 7.5 was prepared in order to achievement a medium as an alternative for Marine Broth (as un-optimized medium). The required sea water for the optimization process was collected from a site with 2 km distance from seashore and then sterilized by 0.22 µm Millipore filter. Furthermore, in order to access to the optimum NaCl concentration, both seawater and distilled water were separately used for preparation of synthetic medium. Optimization process for antibacterial compound production was studied based on carbon and nitrogen sources, optimum temperature, optimum initial pH, optimum NaCl concentration and optimum incubation time. In these experiments one variable was changed at a time but in order to achieve a suitable medium for antibiotic production by this marine isolate, once a factor will be optimized it was used for further optimization process; the carbon source and NaCl concentration were the first and the last optimized factors, respectively. The bacterium was grown at different conditions such as different temperatures (25, 28, 31, 34, 37, 40 and 43˚C), pH values (6, 6.5, 7, 7.5, 8, 8.5 and 9), NaCl concentration (0, 0.5, 1, 1.5, 2, 2.5, 3, 3.5, 4, 6, 8 and 10% (w/v)), various carbon sources (sorbitol, dextrose, galactose, fructose, glycerol, xylose, glucose and starch), various nitrogen sources (peptone, tryptone, yeast extract, meat extract, KNO_3, casein, L-arginine and tyrosine) and different incubation times (12, 24, 36, 48, 60, 72, 84, 96 and 120 h), and then the efficiency of the optimized parameters was discovered using disc diffusion method against MRSA [15]. For anti-MRSA assay, 35 µl of the filter-sterilized (0.45 µm) supernatant prepared from each of the harvested samples from production media under optimized conditions was tested. Also, the best solvent for the antibiotic extraction was optimized.

Kinetics of growth and antibiotic production

Co-variation between bacterial growth and antibiotic production was investigated in a batch system. The culture was undertaken in marine broth medium. A 10 ml inoculum prepared from a fresh overnight culture (was grown in a 250 Erlenmeyer containing 100 ml medium on a rotary

shaker at 30˚C, 140 rpm) was inoculated in this medium and incubated at 37˚C on a rotatory shaker (140 rpm). Cell growth was measured at OD_{600}. Samples were harvested from production media at 2-h intervals from 0 till 6h and 4h intervals from 6h till stationary and death phase of growth. Supernatants were harvested from these samples by centrifugation at 8000 rpm at 4˚C for 10 min and subsequently were sterilized by filtration 0.45 µm and then used for antibacterial assay. Anti-MRSA activity of the harvested samples was assessed using disc diffusion method [16].

Purification of antibacterial compound

To reveal the antimicrobial constituents clearly by bioautography, the supernatant and the raw ethyl acetate extract (prepared from broth culture) possessing antibacterial activity were partially purified by TLC plates (Merck, Germany) using n-butanol: acetic acid: distilled water (v/v 4:4:1) as mobile phases. The separated components were visualized under visible and ultraviolet light (254 and 366 nm). The retardation factor (R_f) values of the spots were also determined. For bioautographic analysis, developed TLC plate were dried overnight and the respective bands were scraped out separately along with silica and dissolved in ethyl acetate, and then centrifuged at 5000 rpm for 4 min and supernatants were passed from filter (0.45 µm) [17] . All of the bands were subjected to antibacterial activity assay against MRSA using disc diffusion method and also their activity was compared with the whole extract. Oxytetracycline was used as control.

Thermal and enzymatic stability of the intended antibacterial compound

For determining the effect of temperature on stability of the antibiotic, 1 ml of supernatant was harvested from broth culture and was added to sterile screw capped ampoules and treated at 4˚C in refrigerator for 24h, at 25, 37, 56, 70 and 90˚C in a water bath for 30 min and at 120˚C in autoclave for 15 min [18, 19]. Enzymatic stability was also examined by treatment of 200 µl of supernatant by 20 µl from each of pepsin (Merck, Germany), Proteinase K (Fermentas, Canada) and Pancreatin enzymes (Philip Harris, UK) at 100 mg/ml final concentration [20]. Finally, the residual antibacterial activity of heat- and enzymatic-treated samples was determined by measurement of the inhibition zone against MRSA. Untreated preparations were used as controls. For all enzymes a positive enzymatic effect was demonstrated by the lack of an inhibition halo around the enzyme-impregnated paper [21].

Determination the site of antibacterial compound accumulation

In order to finding the possible intra-cellular location of the intended active compounds with anti-MRSA activity, 5 ml of broth culture (containing whole cell) was harvested form 3 day's age culture and then sonicated (Bandelin Sonoplus, Germany) at 120 MHz for 40 s at 4˚C [22]. 1 ml of this sonicated sample was filter-sterilized using 0.45 µm filter. An un-sonicated sample was prepared, too. Finally, for antibacterial activity assay, 35 µl of both samples was tested against MRSA using disc diffusion method [21].

Ultrastructural study on the effect of intended antibacterial compound against MRSA

Determination the mechanism of action of intended antibacterial compound on MRSA was done by Transmission Electron Microscope (TEM) (Philips, Netherlands). After determination of MIC value of the ethyl acetate extract of PG-01 isolate, MRSA cells were grown in MHB medium to 0.5 Mc Farland turbidity, then immediately these cells were treated with MIC concentration (40 mg/ml) and sub-MIC concentrations (37, 34 and 30 mg/ml) for 7 h. Samples were harvested at 2, 4 and 7 h. Finally, all of the samples were mixed together on a vortex mixer and centrifuged at 4500 rpm, and then the cells were fixed in 4% glutaraldehyde [23]. MRSA cells without the extract were considered as control [24] . Then, treated and control cells were post-fixed in 1% osmium tetroxide. Washing was done by sodium cacodylate buffer and then these samples were dehydrated in gradualed gold ethanol series (30-100%) [25]. Dried cell blocks were infiltrated by epoxy resin and Ultrathin sections were prepared. Subsequently, the sections were stained by Uranyl acetate and lead citrate. Ultimately, the ultrathin sections were analyzed using TEM.

Strain identification with 16S rRNA gene sequencing

The highest potential antibiotic producer strain (PG-01 isolate) was selected for molecular identification by 16S rRNA sequencing. In order to genomic DNA extraction, a single colony of intended bacterium was subcultured in MB at 30°C for 48 h and DNA was extracted by a commercial kit (Gen Fanavaran, Iran), according to the manufacture instructions. Full length sequence of 16S rRNA gene was amplified from the isolated genomic DNA using the following universal bacterial 16S rRNA primers: Forward strand: 5′-CCGAATTCGTCGACAACAGAGTTTGATCCTGGCTCAG and Reverse strand: CCCGGGATCCAAGCTTACGGTTACCTTGTTACGACTT-5′ [26]. Polymerase chain reaction (PCR) was performed in a 50 µl mix reaction containing 50 mM MgCl2, 10 mM of each deoxynucleoside triphosphates (dATP, dTTP, dGTP and dCTP), 10×PCR buffer, 10 ρmol/µl of forward and reverse primers and 5 U of Taq polymerase. The PCR thermal profile was consisted of denaturation at 94˚C for 5 min followed by 30 cycles of amplification, each consisting of denaturation at 94˚C for 1 min, annealing at 62˚C for 40 sec, and elongation at 72˚C for 2.5 min. A fi-

nal elongation step at 72˚C for 20 min was also included. The Electrophoresis of PCR product was done on 1% agarose gel for 55 min at 95 v. PCR product was sequenced by Gen Fanavaran biotech corp. The obtained sequences were compared in BLAST analysis with available data of Genbank, NCBI. Finally, phylogenetic tree was constructed by CLC Main Workbench 6.0 software program using the neighbour-joining algorithm [27]. Also, the obtained sequence from PG-01 isolate was compared to the sequence of its closest phylogenetic neighbour strain by chimera check/pintail program (http://www.bioinformatics-toolkit.org/Web-Pintail/).

Phenotypic characterization of PG-01 isolate

Different characteristics of the PG-01 isolate including Gram stain, pigmentation, motility and utilization of different carbon sources were determined. Morphological study of this isolate was done using scanning electron microscopy (SEM). A single colony of antibiotic producer bacterium from 24h culture on marine agar was dissolved in 5 ml sterile distilled-water and subsequently 2 µl from this suspension was harvested and fixed in 1% glutaraldehyde and then, cells were dehydrated using a graded acetone series. Finally the air-dried prepared sample was coated by silver for 7 min and surface morphology was studied by a Leo1455 Vp scanning electron microscope.

RESULTS

Fifty one bacterial isolates were isolated from different seawater and sediment samples collected from Persian Gulf. The 2, 9, 13, 3, 18 and 6 isolates were obtained from coastal water, surface water, deep water, coastal sediment, bed sediment and mangrove forest sediment, respectively (Table 1). Of these, three stains have the capability of antibiotic production (Table 1) which were named as PG-01, PG-02 and PG-03 isolates. The PG-01 and PG-02 isolates were from bed sediment (at a depth of 10 m) and surface water, respectively and both samples were collected from Mahshahr port, north of Persian Gulf. But PG-03 was isolated from a mangrove forest sediment sample collected from Qeshm Island, south of Persian Gulf. These three bacteria were maintained at 15˚C on marine agar slants and frozen in marine broth with 20% glycerol. Primary assays showed that PG-01 and PG-02 were effective only against tested Gram-positive bacteria while PG-03 isolate presented a low level of antibacterial activity against some Gram-positive and Gram-negative bacteria. However, PG-01 strain considered as the most potent antibiotic producer isolate; it was effective on all of the tested Gram-positive bacteria and the obtained DIZ (Diameter of inhibition zone) of this strain comparing to the PG-02 and PG-03 isolates was remarkable (Table 2). The obtained raw extract from the PG-01 isolate was effective against all tested Gram-positive bacteria while Gram-negative bacteria showed resistance to it (Table 3). Among tested pathogens, *S. aureus* ATCC and MRSA were the most sensitive strains to this extract; however, its antibacterial activity against other Gram-positive bacteria was remarkable, too. Furthermore, *L. monocytogenes* was the most resistant Gram-positive bacterium to the PG-01 extract. All tested clinical

TABLE 1. Number of bacterial strains isolated from different samples collected from the northern regions of Persian Gulf

Sampling site	Number of bacterial strains isolated from different marine samples						Isolated strain (No.)	Strain with antibacterial activity (No.)
	coastal water	surface water	deep water	coastal sediment	bed sediment	mangrove forest sediment		
Bahrakan port	-	2	4	1	4	-	11	0
Mahshahr port	-	4	5	-	7	-	16	2
Qeshm island	2	3	4	2	7	6	24	1

TABLE 2. Results of the determination of spectrum and potential activity of three antibacterial compound producer bacteria isolated from Persian Gulf.

Marine strain	Sample (origin)	Spectrum activity	Antibacterial activity
PG-01	Bed sediment	Gram-positive	+++
PG-02	Surface water	Gram-positive	++
PG-03	mangrove forest sediment	Gram-positive and negative	++

(+): DIZ > 9 mm; (++): Against Gram-positive bacteria: DIZ:9-14 mm; (++): Against Gram-negative bacteria: DIZ:9-12 mm; (+++): Against Gram-positive bacteria: DIZ>14 mm; (+++): Against Gram-negative bacteria: DIZ> 12 mm

FIGURE 2. Anti-MRSA activity of PG-01 strain extract compared with vancomycin. (The diameter of disc is 6 mm)

TABLE 3. Antibacterial activity of ethyl acetate extract of *Pseudoalteromonas piscicida* PG-01 against some clinical and standard pathogens compared with commercial antibiotics.

	Concentration of extract (mg/ml) PG-01			Antibiotic disc		
Bacterial species	50	MT	VA	P	FM	CL
Gram-positive bacteria						
MRSA	32	R	20	R	23	R
L. monocytogenes	14	R	17	R	16	R
S. aureus ATCC	34	13	18	12	23	R
S. epidermidis ATCC	25	15	15	R	28	R
B. subtilis ATCC	23	18	24	13	23	14
L. monocytogenes ATCC	15	11	R	R	14	R
Gram-negative bacteria						
B. bronchiseptica	R	30	R	R	17	R
Br. melitensis	R	R	R	R	28	R
E. coli ATCC	R	R	18	R	R	R
P. aeruginosa ATCC	R	R	R	R	R	R
S. typhi ATCC	R	R	10	R	20	R

*(6mm) diameter disc
R: Resistant

pathogenic bacteria were MDR strains; also among standard strains, except *S. aureus* ATCC and *B. subtilis* ATCC, other bacteria were MDR strains. All the tested pathogenic microorganisms, except *B. subtilis* ATCC, were resistant to colistin; meanwhile most of the tested clinical pathogenic bacteria revealed resistance to penicillin and methicillin. *P. aeruginosa* ATCC was the most resistant bacterium. The diameter of the inhibition zones for vancomycin and PG-01 against MRSA were 20 and 32 mm, respectively (Figure 2 and Table 3). MIC and MBC values for ethyl acetate extract of PG-01 broth culture against MRSA were 30 and 60 mg/ml, respectively. Meanwhile MIC and MBC values against *B. subtilis* ATCC were the same (20 mg/ml). Antibacterial activity of indented antibacterial compound against MRSA was maintained with sub-MIC concentrations even with two times below the MIC value (GCI: 20 mg/ml) (Figure 3). In the presence of the PG-01 extract at 40, 50 and 60 mg/ml concentrations, the growth curve of MRSA was not reach to stationary

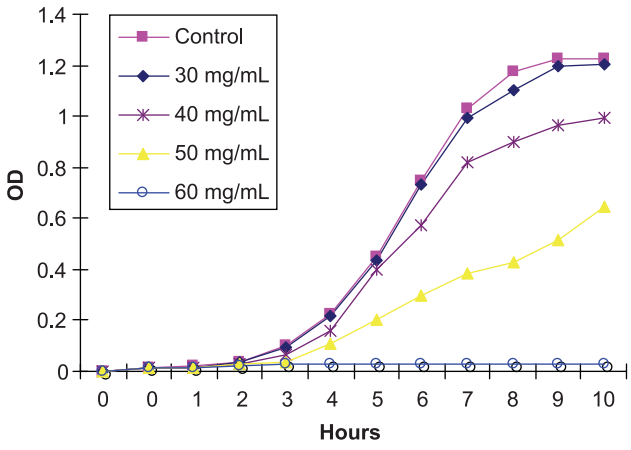

FIGURE 3. Determination of GCI parameter for P*seudoalteromonas piscicida* PG-01 broth culture extract against MRSA.

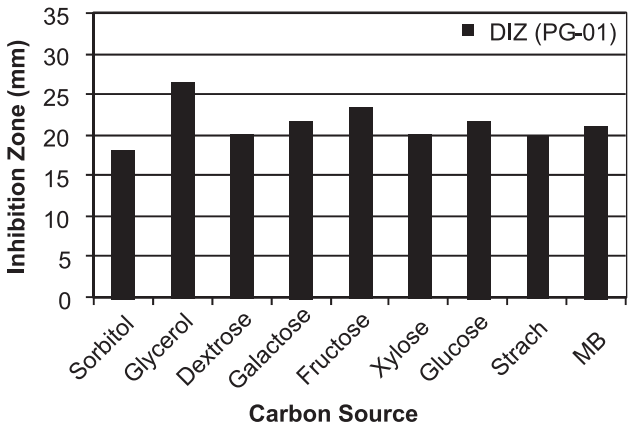

FIGURE 4. Effect of various carbon sources on antibiotic production. (The diameter of disc is 6 mm), DIZ: Diameter of Inhibition Zone

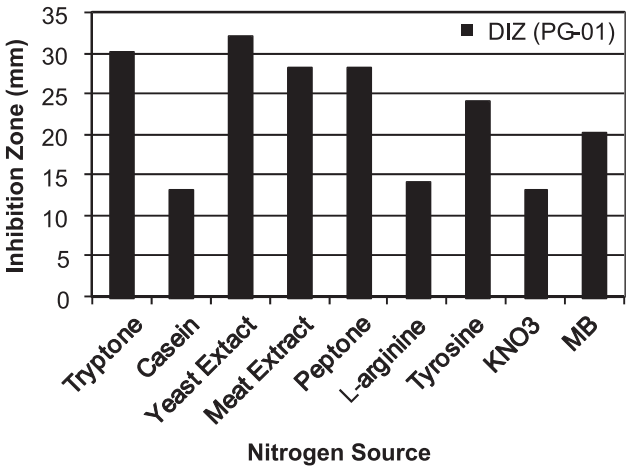

FIGURE 5. Effect of various nitrogen sources on antibiotic production; (The diameter of disc is 6 mm), DIZ: Diameter of Inhibition Zone

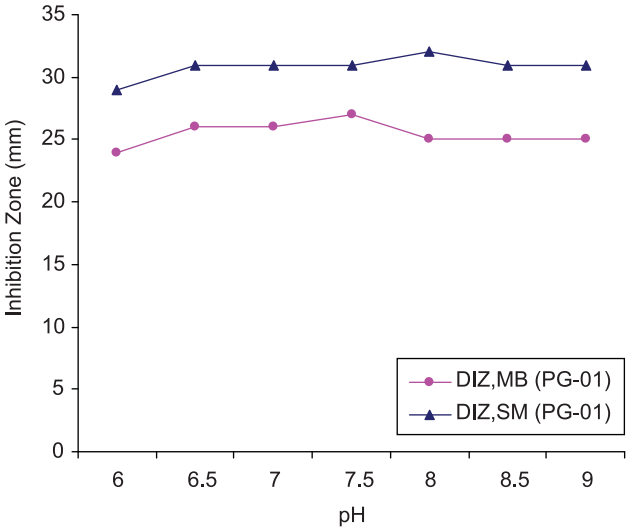

FIGURE 6. Effect of pH on antibiotic production. (The diameter of disc is 6 mm), MB: Marine Broth, SM: Synthetic Medium, DIZ: Diameter of Inhibition Zone

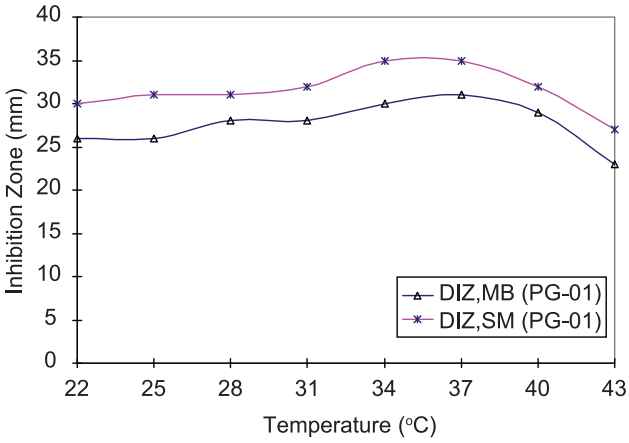

FIGURE 7. Effect of temperature on antibiotic production. (The diameter of disc is 6 mm), MB: Marine Broth, SM: Synthetic Medium, DIZ: Diameter of Inhibition Zone

phase. Also, partially interference in growth curve was observed at 30 mg/ml concentration compared to control. The optimization results revealed that glycerol and yeast extract are the best carbon and nitrogen sources for production of antibiotic by PG-01 isolate, respectively, (Figures 4 and 5). In the case of synthetic medium the maximum antibiotic activity was achieved at initial pH 8 (Figure 6), at temperature 34-37˚C (Figure 7), 0% NaCl (w/v) (Figure 8), and 48 h incubation time (Figure 9). For marine broth medium, the optimum conditions for the antibiotic production were initial pH 7.5, temperature 37˚C (Figure 7), 2% NaCl (w/v) (Figure 8), and 60 h incubation time (Figure 9). Antibacterial activity of harvested samples was observed after 12h for both production medium, but at this time DIZ for the harvested sample from marine broth and synthetic medium were 14 and 25 mm, respectively (Figure 9). The best NaCl concentration for antibiotic production by PG-01 isolate in synthetic medium prepared by distilled water was 2% (w/v) while about of synthetic medium prepared with natural seawater adding of NaCl even at the lowest concentration cause to blocking of the antibiotic production by PG-01 isolate (Figure 8). Also, ethyl acetate was chosen as the best solvent for antibiotic extraction (Figure 10). Sorbitol as carbon source presented the lowest efficiency for antibiotic production by this isolate; furthermore, casein and KNO_3 were the least effective nitrogen sources for production by PG-01 isolate. About of the temperature optimization, the lowest antibiotic production was observed at 43°C. Among the optimized fermentation parameters, carbon and nitrogen sources have a significant effect on antibiotic production while pH has only a slight favorable effect on production. On the other hand, NaCl concentration was found as a

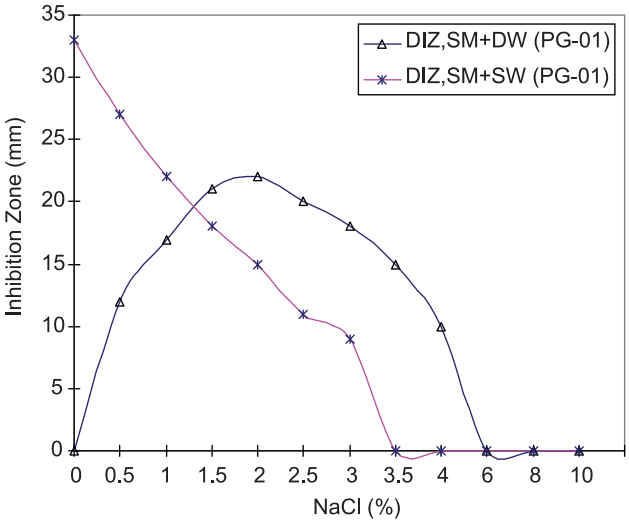

FIGURE 8. Effect of salinity on antibiotic production. (The diameter of disc is 6 mm), DW: Distilled Water / SW: Sea Water, DIZ: Diameter of Inhibition Zone

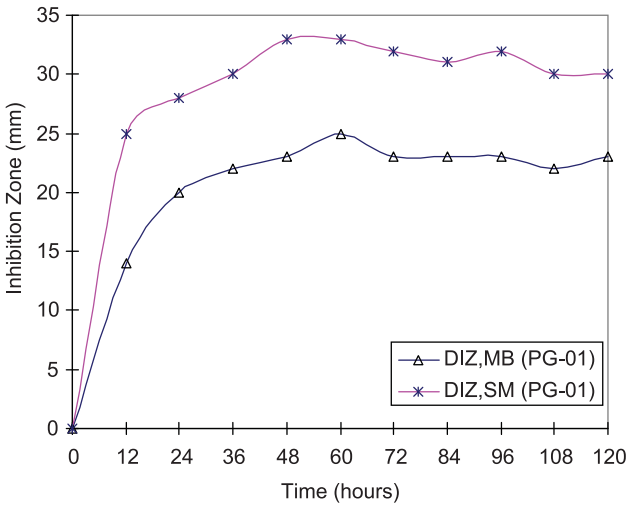

FIGURE 9. Effect of incubation time on antibiotic production. (The diameter of disc is 6 mm), MB: Marine Broth. SM: Synthetic Medium, DIZ: Diameter of Inhibition Zone

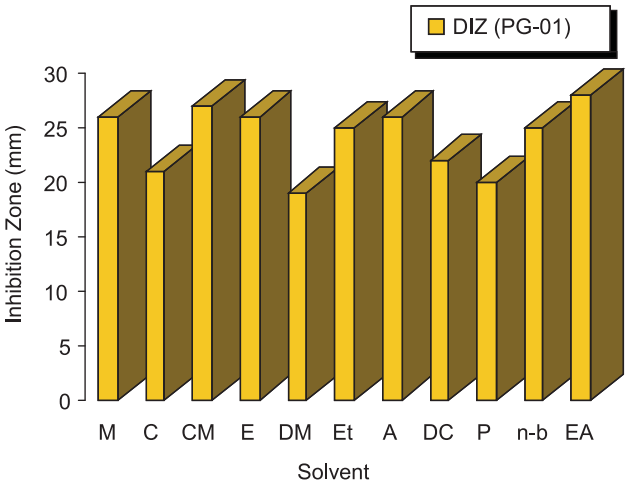

FIGURE 10. Optimization of solvent for antibiotic extraction
M: Methanol, **C**: Chloroform, **CM**: Chloroform-Methanol (1:2 (v/v)), **E**: Ethanol, **DM**: DMSO, **Et**: Ether, **A**: Aceton, **DC**: Dichloromethane, **P**: Propanol, **n-b**: n-butanol, **EA**: Ethyl Acetate. (The diameter of disc is 6 mm), DIZ: Diameter of Inhibition Zone

TABLE 4. Results of determination of R_f values and anti-MRSA activity for each of the separated bands using TLC

Spot	R_f	DIZ (mm)
6A	0/77	10
6B	0/91	R
7A	0/95	24
8A	0/44	17

TABLE 5. Antibacterial activity of anti-MRSA compound produced by *Pseudoalteromonas piscicida* PG-01 after enzymatic treatment

Strain	Control	Pancreatin	Pepsin	Proteinase K
PG-01	22	11	22	22

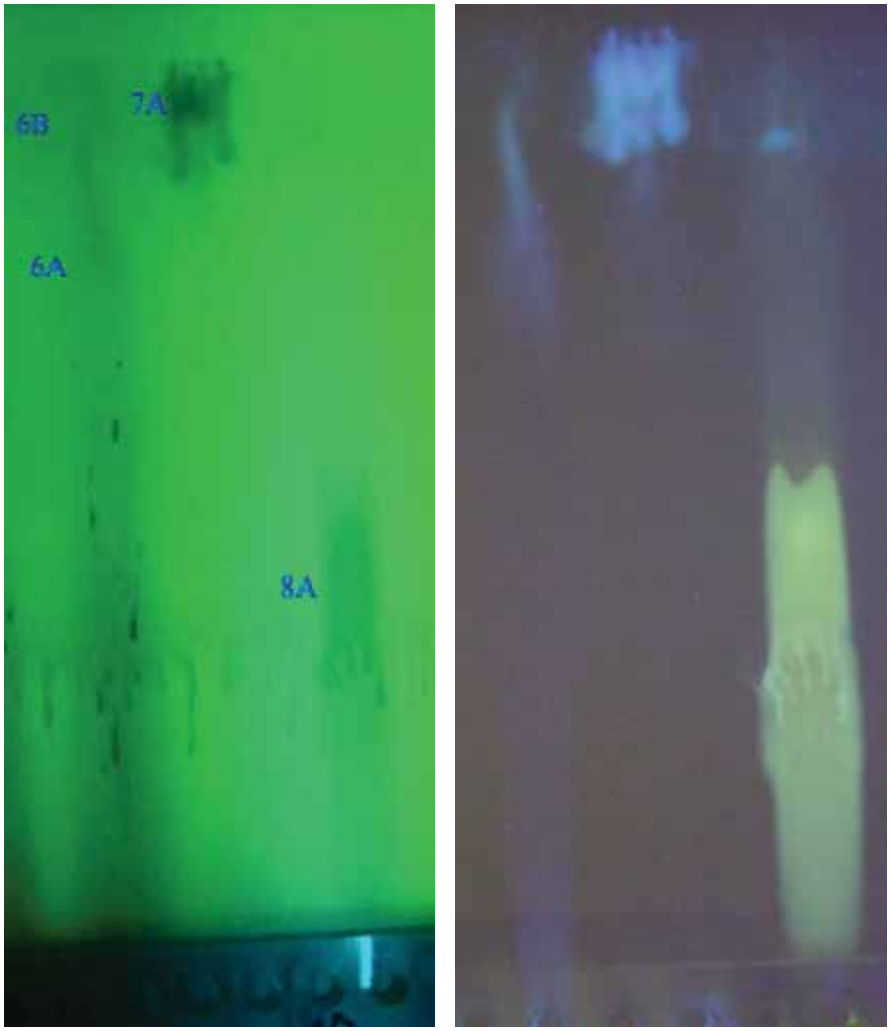

FIGURE 11. TLC analysis for the supernatant and ethyl acetate extract samples of *Pseudoalteromonas piscicida* PG-01
a: Tlc (visualized at 254 nm) , **b:** Tlc (visualized at 366 nm), 6: Sample 6 (the supernatant sample prepared from broth culture), 7: Sample 7 (extract sample prepared from broth culture), 8: Sample 8 (Oxytetracycline as control), A and B: Separated bands

critical factor on the antibiotic production. In general, antibacterial activity (inhibition zone diameter) of PG-01 against MRSA at un-optimized (marine broth) and optimized (synthetic medium) conditions was 16 and 31 mm, respectively. PG-01 isolate was found to produce only one antimicrobial component by bioautography. Results from bioautographic analysis revealed that the two spots 6A and 7A which were obtained from supernatant and extract, respectively were presented anti-MRSA activity (Table 4, Figure 11); however, the spot 7A with a R_f value of 0.95 exhibited the strongest antibacterial activity against MRSA so that when activity of this component was assessed against MRSA compared to the whole extract, the obtained DIZ values were relatively equal. Likewise, the intended two active components and oxytetracycline have remarkably different polarities (Figure 11 a, b). Thermostability studies exhibited that this antibacterial substance was a thermostable compound. However, the antibacterial activity remained unaltered after treatment at 4-90˚C, it started to decrease after being autoclaved (121˚C) but even at this temperature it didn't completely loose its activity too (Figure 12). The anti-MRSA activity of this antibacterial compound was decreased only

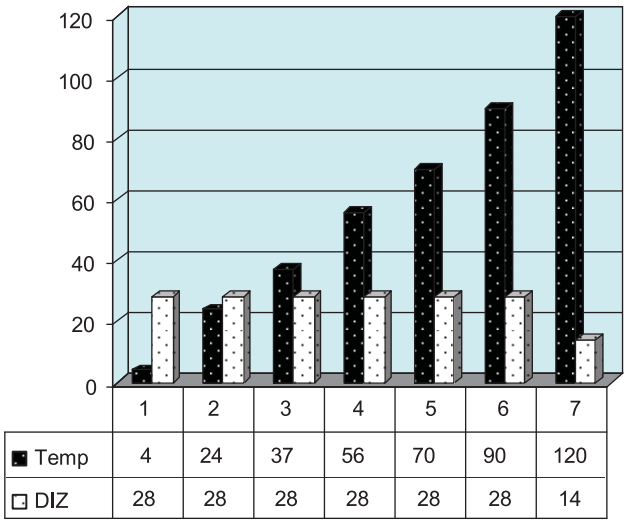

	1	2	3	4	5	6	7
Temp	4	24	37	56	70	90	120
DIZ	28	28	28	28	28	28	14

FIGURE 12. Results of heat treatment of an anti-MRSA compound produced by *Pseudoalteromonas piscicida* PG-01, (The diameter of disc is 6 mm), Temp: Temperature (°C)

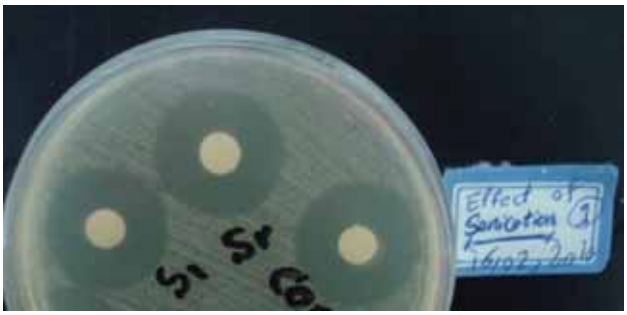

FIGURE 13. The obtained results from sonication treatment of broth culture (containing whole cell) of PG-01 isolate; as we can see, inhibitory activity of the treated sample against MRSA remained unaltered, that is to say, there is no intracellular anti-MRSA compound in the cells of PG-01 isolate. S1: Sample (un-filtered), S2: Sample (filtered), Con: Control (un-sonicated)

after treatment with Pancreatin by 50% compared with control (22 mm) (Table 5). Based on these findings, the active molecule may not be proteinaceous in nature, but a glycolipid nature for this antibiotic can be suggested. Sonication treatment indicated no intracellular active compound, because inhibitory activity of the treated sample against MRSA remained unaltered (Figure 13). So, it can be concluded that the antibacterial compound produced by PG-01 is completely secretory. TEM results of ultrathin section of MRSA treated with the antibacterial compound produced by PG-01 isolate were shown in Figure 14. A comparison of transmission electron micrograph results of the treated cells with untreated cells, revealed deformities caused in the cell wall structure (weakened and deformed cell wall) by this marine-derived antibacterial compound while un-treated cells have a thick and intact cell wall (Figure 14). Lysis of cell with residual membranes and empty protoplasmic space and numerous membrane blebs are shown in Figure 15, too. So, the target site for antibacterial compound produced by PG-01 isolate is cell wall and this antibacterial compound can be considered as a bactericidal agent against MRSA. In the case of treated cells, also, because of decrease in the thickness of the cell wall we can see that the electron density of this part is decreased. Considering growth of PG-01 and time course of its antibacterial compound production revealed that the growth of intended marine isolate increased exponentially at 4 to 28h of incubation (Figure 16). The anti-MRSA activity of the culture supernatant was detectable as early as at 12 h of incubation and reached the highest activity at 100h of incubation (Figure 16). So, in marine broth culture, production of antibacterial compound with PG-01 isolate was started in the early stage of logarithmic phase and increased to a maximal production level until the stationary phase; that it can be said that antibacterial production occurs during the whole growth phase.

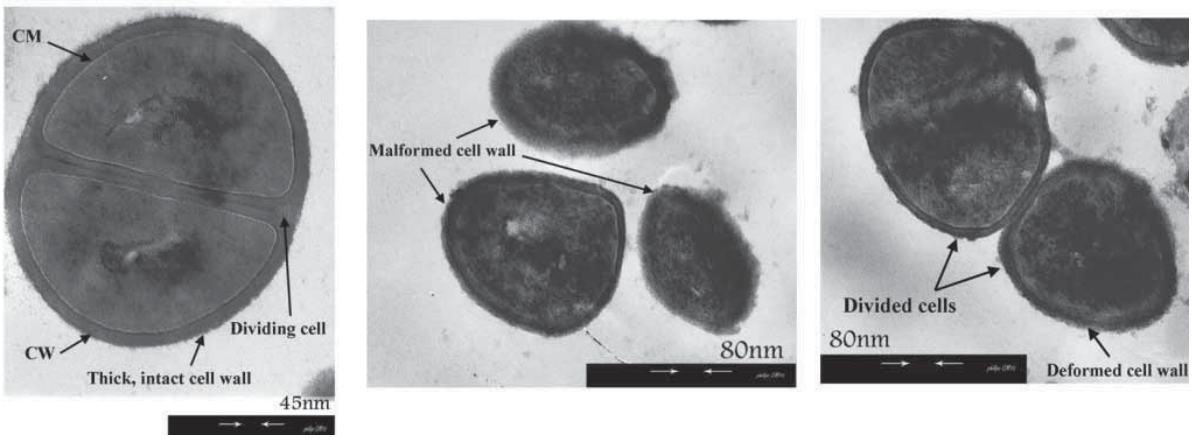

(a) **(b)** **(c)**

FIGURE 14. Transmision electron micrographs of MRSA. **a** Cell grown in the absence of antibacterial compound produced by *Pseudoalteromonas piscicida* PG-01; **b, c** Cells grown in the presence of antibacterial compound produced by *Pseudoalteromonas piscicida* PG-01

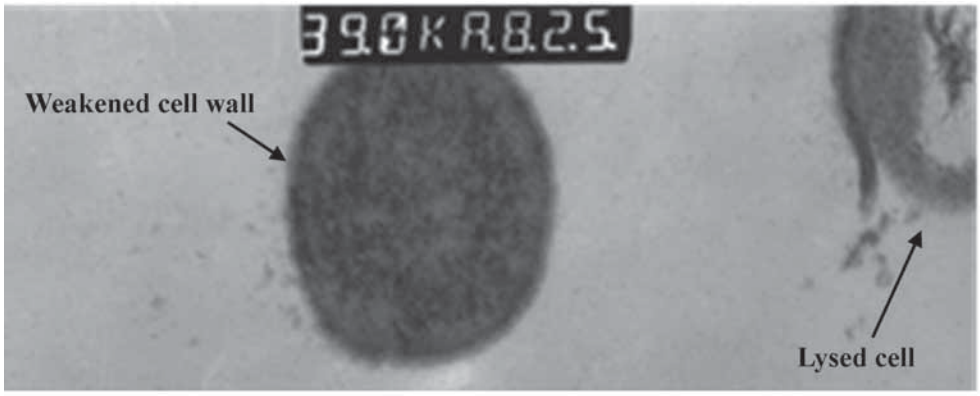

FIGURE 15. Transmision electron micrographs of MRSA; **a** cell with weakened cell wall; **b** lysis of cell due to bactericidal effect of antibiotic produced by PG-01 Strain.

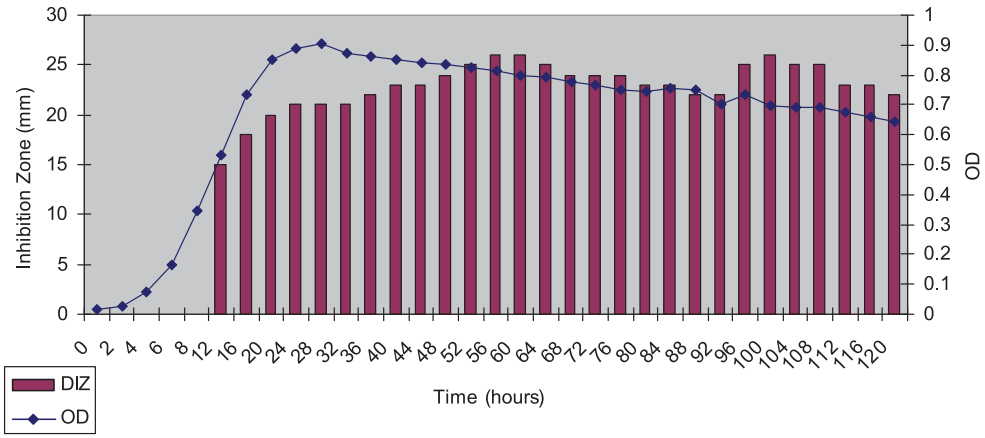

FIGURE 16. Results of Co-variation between cell growth of *Pseudoalteromonas piscicida* PG-01 and its antibiotic production

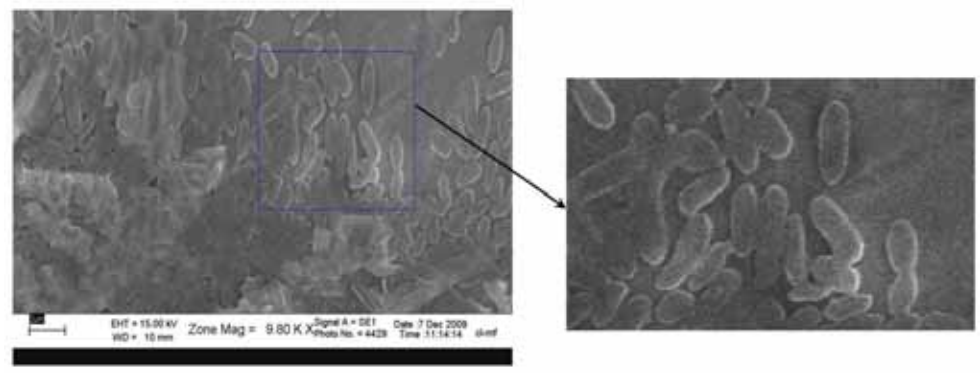

FIGURE 17. Scanning electron micrographs of PG-01 isolate in order to study of its morphology. (**a, b**)

The marine PG-01 isolate was Gram-negative, motile, catalase positive and strictly aerobe. The colonies of this isolate on marine agar were smooth, convex, and brownish with entire edges. The SEM micrograph results presented that this marine isolate is typically a rod-shape bacterium and its surface is smooth (Figure 17 a, b). This isolate didn't growth on more than 5% (w/v) NaCl concentration and also, was able to utilize a range of carbohydrates such as D-glucose, xylose, and maltose and glycerol as carbon substrates. Furthermore, this strain was resistant to the commercial antibiotics including polymixin B, tetracycline, and penicillin. In molecular diagnosis, a 1500 bp PCR product was amplified successfully (Figure 18) and on the basis of the BLAST search, the PG-01 isolate showed the highest 16S rRNA gene sequence similarity (97%) to *Pseudoalteromonas piscicida* 1314. The phylogenetic tree analysis showed also that this isolate had the most phylogenetic homogeneity with *P. piscicida*; the other two *Pseudoalteromonas* species including *P. viridis* and *P. rubra* were placed within the intra-cluster branches related to the location of PG-01 isolate (Figure 19). Also, the mean of the observed nucleotide differences between *Pseudoalteromonas piscicida* PG-01 and 1314 (Figure 20) was 1.24%, and is roughly equivalent to evolutionary distance. The 16S rRNA gene sequence of PG-01 strain was deposited in GenBank with accession number JF737768.

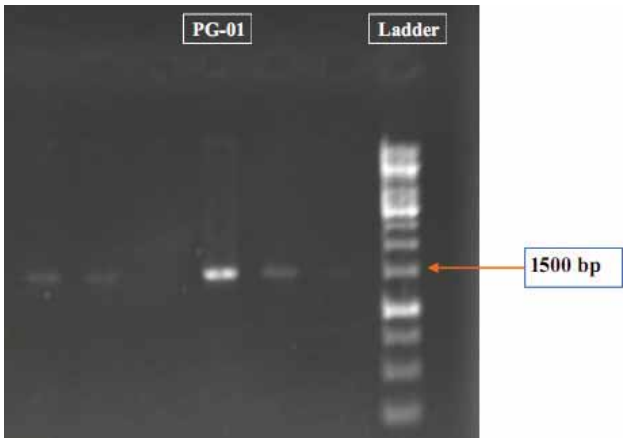

FIGURE 18. Agarose gel electrophoresis of amplified 16S rRNA fragment (1500 bp) of PG-01 isolate.

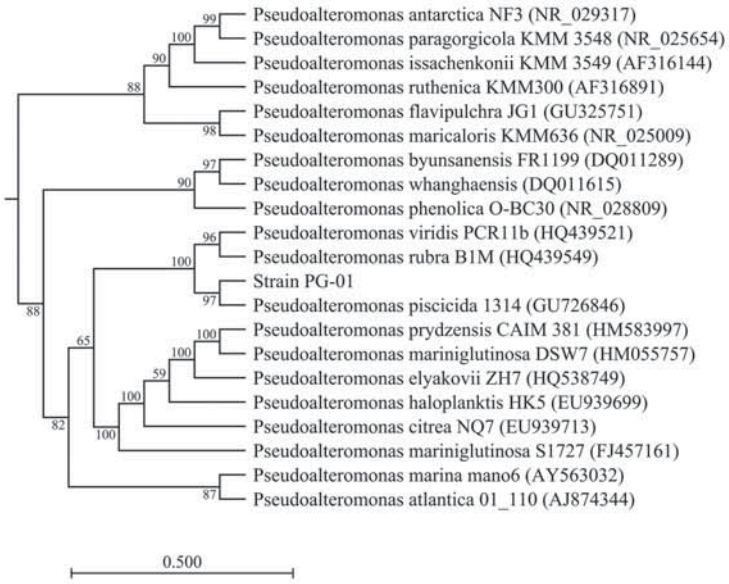

FIGURE 19. Phylogenetic relationships of Strain PG-01 and some related *Pseudoalteromonas* species on the basis of 16S rRNA gene sequence analysis. Numbers at branch nodes are bootstrap values (expressed as a percentage of 1000 replicates) based on the neighbour-joining algorithm. Bar represents approximately 0.5 % nucleotide sequence difference.

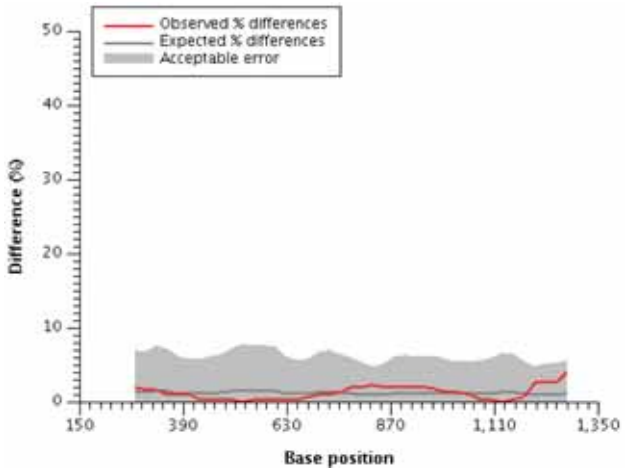

FIGURE 20. Variation in % difference between *P. piscicida* 1314 (1372 nt) and *P. piscicida* PG-01 (1248 nt) determined with a 300 base sliding window, moving 25 bases at a time along the sequences.

DISCUSSION

During two previous decades, studying about marine microorganisms has been raised significantly due to their very high capability of producing secondary metabolites. In fact, the strong selective pressure resulted from competition between bacteria in the marine environment for space and nutrition and also metabolic and physiological differences between marine and terrestrial microorganisms arising from different conditions in marine would result in that these microorganisms produce a great amount of natural products applicable in medicine and industry [6]. The emergence and dissemination of resistant pathogenic bacteria to current antibiotics particularly MRSA (Methicillin Resistant *Staphylococcus aureus*) has become a great global concern in 21st century, especially for the hospitalized patients. Today, vancomycin has become the drug of choice for treating MRSA infections; however, treatment failures, adverse side effects and the emergence of vancomycin resistant bacteria are leading to urgent needs for alternative anti-MRSA therapies [28]. So, it seems that finding new antibiotic against this rebel pathogen named superbug, especially from natural resources is vital. Marine ecosystem as an untapped resource can be surveyed for natural antimicrobials. For the first time, antibiotic production by marine bacteria has been documented by Rosenfeld and Zobell, 1946 [29]. It is noticeable that a sea with somewhat special climate such as Persian Gulf with relatively high temperature (average 35˚C) and salinity (~4%) must be more focused to finding new and special natural metabolites. Meanwhile, Persian Gulf is a rich source of marine micro- and macro-organisms with high biodiversity. In our research, two of the three obtained marine antibiotic producer bacteria were isolated from sediment samples; this result may be due to existence of competition on space and nutrients at this habitant. However, there are many reports that marine colonized bacteria consist a percentage of antibiotic producing bacteria higher than observed in free-living state isolated from marine environment [30]. The activity of the crude extract of PG-01 strain was restricted to Gram-positive bacteria; however, it was highly active against human pathogenic strains, including clinical and standard strains. This difference may be due to several possible reasons such as permeability barrier provided by the presence of cell wall with multilayer structure in Gram negative bacteria or the membrane accumulation mechanisms or pres-

ence of enzymes in periplasmic space which are able to break down foreign molecules introduced from outside [31]. All of the studied pathogenic clinical strains were MDR bacteria even against the well-known synthetic antibiotics; furthermore, nearly 55% of all isolates studied were resistant to methicillin. Also, it seams that penicillin and colistin must be gradually go away form the effective antibiotics list. Based on the obtained results from GCI parameter determination, antibacterial activity of intended antibacterial compound against MRSA was maintained with sub-MIC concentrations, this outcome has a pharmaceutical importance about using antibacterial compound, especially for treatment of high-risk patients and also preventing of emergence of new antibiotic resistances. Results from optimization process revealed that among the optimized fermentation parameters, carbon and nitrogen source or C/N ratio plays the most important role in efficacy of optimization for antibiotic production by intended marine strain. Glycerol and yeast extract were chosen as optimum carbon and nitrogen sources for antibiotic production by *Pseudoalteromonas piscicida* PG-01; there are several reports about selection of these substrates as the best sources in order to antibiotic production by different bacteria [32, 33]. Considering of these results, the culture of this strain in complex medium revealed more than 100% higher antibiotic production compared to marine broth. Commonly, chemically defined media as production media aren't used in industrial fermentation process to obtain high yields and hence this improvement of cultivation parameters is one of the main objectives in industrial research [34]; So, the obtained result from optimization is very usable for improving supply of the intended marine antibiotic for its industrial production in future. The results of heat and enzymatic treatment show that the active constituent of the antibacterial compound produced by *Pseudoalteromonas piscicida* PG-01 is thermostable substance and also is not sensitive to tested proteolytic enzymes; so, this antibacterial compound maybe not peptide in nature. However, this marine antibiotic compound loose its activity by 50 % when treated by pancreatin; since this enzyme has amylase, lipase and proteinase activity, a glycolipid nature of active molecule can be suggested. On the other hand, the findings obtained from the solvent optimization revealed that some solvents specific for lipid extraction such as Chloroform-Methanol (1:2 [vol/vol] had a excellent efficiency for extraction of antibiotic produced by PG-01, suggests that there was substantial lipid fraction in this inhibitory substance. TLC and bioautography results revealed that the intended antimicrobial compound and oxytetracycline are with remarkably different polarities; consequently they have different antimicrobial profiles. In study the co-variation between cell growth and antimicrobial compound production test, we found that production of antibiotic with PG-01 strain was started at the mid-logarithmic phase while the most of the antimicrobials as secondary metabolites usually will be produced at the late exponential or stationary phase; however there are several reports that indicates antibiotic production can be triggered at the early stages of cell growth [8, 35]. Moreover, with alteration in culture condition such as carbon source and so on, production of secondary metabolites may be started at the logarithmic growth phase; that is to say, under this condition in logarithmic phase, cell division will be stopped and subsequently antibiotic production will be occurred [35, 36]. TEM results showed that the target site for antibacterial compound produced by *Pseudoalteromonas Piscicida* PG-01 is cell wall; so, this antibiotic compound can be considered as a bactericidal agent against MRSA and can give hope for treatment of diseases caused by this rebel pathogen. It seems likely this antibacterial substance deforms the cell wall of target cells, influnce proton motive force and subsquently increase osmotic pressure due to influx of water and finally cell lysis occurs [25]. This strain was characterized by both biochemical and as well as molecular methods. The PG-01 isolate exhibited some phenotypic differences from its closest phylogenetic neighbor *P. piscicida* strain that noted in Bergey's manual for systematic of bacteriology [37] including ability to grow at 40°C, produces a brownish diffusible pigment, inability to use of ammonia, and ability to nitrate reduction. However, based on Phylogenetic analysis of the 16S rRNA gene sequencing and phenotypic characteristics, this marine isolate maybe proposed to represent a novel species or sub-species of the *Pseudoalteromonas* genus, we named as *P. piscicida* PG-01. It has been reported that different strains belonging to *Pseudoalteromonas sp.* have antibacterial activity, antiviral activity and agarolytic activities [38]. Finally, determination of the structures and pharmacological study of the active compound produced by intended marine bacterium is necessary that will be reported in future.

CONCLUSION

In conclusion, The PG-01 strain exhibited antibacterial activity against all tested Gram-positive bacteria. PG-01 isolate had good anti-MRSA activity and also GCI value against MRSA was two times lower than MIC value. Among the optimized fermentation parameters, carbon and nitrogen sources found to have a significant effect on antibacterial compound production by intended marine bacterium. TLC results for ethyl acetate extract of PG-01 showed that there is only a single fraction with antibacterial activity. We found that intended marine antibacterial compound is no proteinaceus in nature; also, it is completely secretory and has extra-cellular location.

Ultrastructral study on the effect of intended antibacterial compound on MRSA using TEM revealed that the target site for this is cell wall. Finally, *P. piscicida* PG-01 can be regarded as a valuable strain for discovery of new weapon in fighting against multi-drug resistant bacteria, especially MRSA.

ACKNOWLEDGMENTS

The authors wish to thank the vice chancellor for research of Shahid Chamran University, Ahvaz, Iran, for the research grant and financial support.

DECLARATION OF INTEREST

The authors declare no conflict of interest for this study.

REFERENCES

[1] Katayama Y, Ito T, Hiramatsu K. A new class of genetic element, staphylococcus cassette chromosome mec, encodes methicillin resistance in *Staphylococcus aureus*. Antimicrob Agents Chemother. 2000;44(6):1549-55
[2] Utsui Y, Yokota T. Role of an altered penicillin-binding protein in methicillin- and cephem-resistant *Staphylococcusaureus*. Antimicrob Agents Chemother 1985; 28:397-403.
[3] Bhatnagar I, Kim SK. Immense essence of excellence: marine microbial bioactive compounds. Mar Drugs 2010; 8: 2673-2701.
[4] Schäberle FT, Goralski E, Neu E, Erol O, Hölzl G, Dörmann P, et al. Marine Myxobacteria as a source of antibiotics -- comparison of physiology, polyketide-type genes and antibiotic production of three new isolates of *Enhygromyxa salina*. Mar Drugs 2010; 8: 2466-2479.
[5] Carvalho CCCR, Fernandes P. Production of metabolites as bacterial responses to the marine environment. Mar Drugs 2010; 8: 705-727.
[6] Zheng L, Han X, Chen H, Lin W, Yan X. Marine bacteria associated with marine microorganisms: the potential antimicrobial resources. Ann Microbiol 2005; 55:119-124.
[7] Rahman H, Austin B, Mitchell WJ, Morris PC, Jamieson DJ, Adams DR et al. Novel anti-infective compounds from marine bacteria. Mar Drugs 2010; 8:498-518.
[8] Brinkhoff T, Bach G, Heidorn T, Liang L, Schlingloff A, Simon M. Antibiotic production by a Roseobacter clade-affiliated species from the German Wadden Sea and its antagonistic effects on indigenous isolates. Appl Environ Microbiol 2004;70: 2560-2565.
[9] Yeon SH, Jeong WJ, Park JS. The diversity of culturable organotrophic bacteria from local solar salterns. J Microbiol 2005; 43:1-10.
[10] Asthana RK, Deepali, Tripathi MK, Srivastava A, Singh AP, Singh SP. Isolation and identification of a new antibacterial entity from the Antarctic *Cyanobacterium Nostoc* CCC 537. J Appl Phycol 2009; 21:81-88.
[11] Xiong H, Qi S, Ying XuY, Miao L, Qian P. Antibiotic and antifouling compound production by the marine-derived fungus Cladosporium sp. F14. J Hydro-environ Res 2008;2: 264-270.
[12] NCCLS. Performance Standards for Antimicrobial Susceptibility Testing; Ninth Informational Supplement. NCCLS document M100-S9. National Committee for Clinical Laboratory Standards, Wayne, PA, 2008; pp. 120-126.
[13] Motamedi H, Darabpour E, Gholipour M, Seyyednejad SM. In vitro assay for the anti-brucella activity of medicinal plants against tetracycline-resistant *Br. melitensis*. J Zhejiang Univ-SCIENCE B 2010;11: 506-511.
[14] Castillo A, Liebana J, Lopez E, Baca P, Liebana JM, Liebana MJ et al. Interference of antibiotics in the growth curves of oral streptococci. Int J Antimicrob Agent 2006; 27:263-266.
[15] Vijayan KK, Bright SIS, Jayaprakash NS, Alavandi S, Somnath PS, Preetha R et al. A brackishwater isolate of Pseudomonas PS-102, a potential antagonistic bacterium against pathogenic vibrios in penaeid and non-penaeid rearing systems. Aquaculture 2006; 251:192-200.
[16] Shibl AM, Al-Sowaygh IA. Antibiotic inhibition of protease production by Pseudomonas aeruginosa. J Med Microbiol 1980;13: 345-349.
[17] El-Naggar MY, El-Assar SA, Abdul-Gawad SM. Meroparamycin production by newly isolated *Streptomyces* sp. strain MAR01: taxonomy, fermentation, purification and structural elucidation. J Microbiol 2006; 44: 432-438.
[18] Manilal A, Sujith S, Selvin J, Shakir C, Kiran GS. Antibacterial activity of Falkenbergia hillebrandii (Born) from the Indian coast against human pathogens. Int J Exp Bot 2009; 78:161-166.
[19] Amin M, Kalantar E, Mohammad-Saeid N, Ahsan B. Antibacterial effect and physicochemical properties of essential oil of *Zataria multiflora* Boiss. Asian Pac J Trop Med 2010; 3:439-442.
[20] Mirhossini M, Nahvi I, Emtiazi G, Tavasoli M. Incidence and antibiotic susceptibility of bacteriocin-producing lactic acid bacteria from dairy products. Int J Dairy Technol 2008; 61: 391-396.
[21] Braja JL, Lemos ML, Toranzo AE. Purification and characterization of an antibacterial substance produced by a marine *Alteromonas* species. Antimicrob Agent Chemoter 1989;33:1674-1679.
[22] McArthur M, Bibb MJ. Manipulating and understanding antibiotic production in *Streptomyces coelicolor* A3 (2) with decoy oligonucleotides. Proc Natl Acas Sci 2008;105:1020-1025.
[23] Guignard B, Entenza JM, Moreillon P. β lactams against methcillin resistant *Staphylococcus aureus*. Curr Opin Pharmacol 2005;5: 479-489.
[24] Kersten A, Poitschek C, Rauch S, Aberer E. Effects of penicillin, ceftriaxone, and doxycycline on morphology of *Borrelia burgdorferi*. Antimicrob Agent Chemoter 1995; 39:1127-1133.
[25] Chen H, Chan SC, Lee JC, Chang CC, Murugan M, Jack RW. Transmission Electron *Microscopic* observations of membrane effects of antibiotic Cecropin B on *Escherichia coli*. Microsc Res Tech 2003; 62:423-430.
[26] Papizadeh M, Roayaei Ardakani M, Ebrahimipour G, Motamedi H. Utilization of dibenzothiophene as sulfur source by Microbacterium sp. NISOC-06. World J Microbiol Biotechnol 2010; 26:1195-1200.
[27] Saitou N, Nei M. The neighbor-joining method: a new method for reconstructing phylogenetic trees. Mol Biol Evol 1987; 4:406-425.
[28] Chopra I. Antibiotic resistance in *Staphylococcus aureus*: concerns, causes and cures. Expert Rev Anti Infect Ther 2003;1: 45-55.
[29] Asha Devi NK, Balakrishnan K, Gopal R, Padmavathy S. *Bacillus clausii* MB9 from the east coast regions of India: Isolation, biochemical characterization and antimicrobial potentials. Curr Sci 2008;95:5-10.
[30] Armstrong E, Yan L, Boyd KG, Wright PC, Burgess JG. The symbiotic role of marine microbes on living surfaces. Hydrobiol 2001;461: 37-40.
[31] Motamedi H, Darabpour E, Gholipour M, Seyyednejad SM. Antibacterial effect of ethanolic and meyhanolic extract of *Plantago ovata* and *Oliveria decumbens* endemic in Iran against some pathogenic bacteria. Int J Pharmacol 2010;6: 117-122.
[32] Preetha R, Jayaprakash NS, Philip R, Singh ISB. Optimization of carbon and nitrogen sources and growth factors for the production of an aquaculture probiotic (Pseudomonas MCCB 103) using response surface methodology. J Appl Microbiol 2007; 102:1043-1051.
[33] El-Banna NM. Effect of carbon source on the antimicrobial activity of *Corynebacterium kutscheri* and *Corynebacterium xerosis*. Afric J Biotechnol 2006; 5:833-835.
[34] Nair R, Murphy T, Roy I, Keshavarz T. Optimization studies on multiple elicitor addition in microbial systems: *P. chrysogenum* and *B. Licheniformis*. Chem Eng Trans 2008; 14:373–380.

[35] Oyama M, Kubota K. Induction of antibiotic production by protease in Bacillus brevis (ATCC 8185). J Biochem 1993; 3: 637-641.
[36] Dewi AS. Biologically active secondary metabolites from tropical marine invertebrates. MSc Thesis. University of British Columbia. Canada. 2009; pp. 43-72.
[37] Garrity GM, Bell JA, Lilburn TI. Pseudoalteromonas. In:, Bergey's manual of systematic bacteriology. Bownan JP and McMeekin TA, editors. 2nd Edition, New Yourk: Springer, 2006; pp. 467-477.
[38] Castillo CSD, Wahid MI, Takeshi Y, Taizo S. Isolation and inhibitory effect of anti-Vibrio substances from Pseudoalteromonas sp. A1-J11 isolated from the coastal sea water of Kagoshima Bay. Fish Sci 2008;74: 174-179.

Clinical implications of cellular stress responses

Borut Poljšak[1], Irina Milisav[1,2*]

[1] Faculty of Health Sciences, University of Ljubljana, Zdravstvena pot 5, SI-1000 Ljubljana, Slovenia. [2] Institute of Pathophysiology, Faculty of Medicine, University of Ljubljana, Zaloška 4, SI-1000 Ljubljana, Slovenia

Abstract

Cellular stress response is a reaction to changes or fluctuations of extracellular conditions that damage the structure and function of macromolecules. Different stressors trigger different cellular responses, namely induce cell repair mechanisms, induce cell responses that result in temporary adaptation to some stressors, induce autophagy or trigger cell death. Inability to repair the damage or exposure to prolonged stress may contribute to aging. Persistent cell stress often enhances susceptibility to cancer and aging associated diseases. Cells and tissues are increasingly being used for transplantations and other novel therapeutic methods in which the quality and well being of cells is of paramount importance for the treatment to succeed. Therefore, discovering the mechanisms of cellular stress responses and the ability to detect and ameliorate them is important in prevention of development of disorders developed by persistent stress and for the success of transplantation and other cell related methods of regenerative medicine.

KEY WORDS: Cell stress, adaptive response, aging, transplantation, cancer, cardiovascular disease

Types of cellular stress responses

Cells are exposed to many internal and external stimuli when they are a part of a normal tissue or when they grow in culture, some of which induce stress. Stressors can trigger a variety of stress responses. Depending on the severity and duration of stress encountered, the cells either re-establish cellular homeostasis to the former state or adopt an altered state in the new environment. For example, stressors can damage intracellular macromolecules, including proteins, DNA, RNAs and lipids. This results either in cell reparation or cell death. Less severe stress may change cellular responses to subsequent environmental signals [1]. There are four basic types of responses (Figure 1). The stressors can (1) induce cell repair mechanisms, (2) induce cell responses that result in temporary adaptation, (3) induce autophagy or (4) trigger cell death [2]. Most of the responses are intended to restore the normal physiology of cells; in the process, they can use considerable amounts of resources. The responses that result in temporary adaptation to stress are reported the least systematically. Nevertheless, many biological and biomedical disciplines independently documented adaptive responses of organisms after the exposure of low doses of stressors [3]. For example, a low dose of mutagen would protect against damage from a subsequent exposure to the same, and sometimes differ-

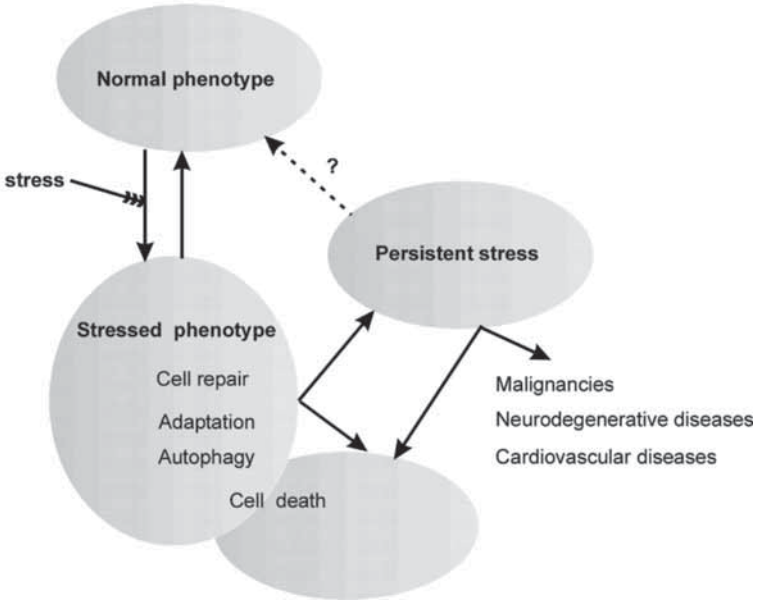

FIGURE 1. Cellular responses to stress and their consequences
Stress can induce the changes from normal to stressed cell phenotype. Characteristic are one or more of the folowing pathways: the induction of cell repair mechanisms, cell responses that result in temporary adaptation, autophagy or cell death. Most of these responses can restore the normal physiology of cells; failure to do so result in prolonged stress or cell death. Prolonged stress enhances the susceptibility to cancer and to aging associated diseases.

* Corresponding author: Irina Milisav,
Institute of Pathophysiology, Faculty of Medicine, University of Ljubljana, Zaloška 4, SI-1000 Ljubljana, Slovenia
Tel: +386-1-543-7089; Fax: +386-1-543-7021
e-mail: irina.milisav@mf.uni-lj.si

Submitted: 15 February 2012 / Accepted: 26 March 2012

ent, mutagen [4, 5]. Adaptive response was also observed in the field of epidemiology; initially on alcohol consumption and various parameters of cardiovascular diseases [6]. Other examples of adaptation to low doses of stressors include the reports on the effects of low doses of radiation [7], ischaemia [8] and other chemicals [9]. Also, anti-aging and life-prolonging effects of many stressors, such as e.g. calorie restriction, point in the same direction [10]. The above papers only reported observations of the connection of low dose of stressor to adaptation. The report by Nipic et al. [1] demonstrated the first mechanism behind the cellular adaptation to stress; the adaptation to stress results in inhibition of apoptosis triggering by caspase-9 in stress phenotype. Therefore there is no triggering of apoptosis through one of the two main apoptotic triggering pathways (i.e. intrinsic pathway) in the stress phenotype. Nevertheless, the suitable triggers can still trigger apoptosis through different pathways [1]. The question remains whether different types of stressors result in the same phenotype, or better whether the adaptation to one type of stress would protect the cells and organisms to moderate amounts of other stressors as well? Various types of low dose of external stressors induce the adaptation to stress from yeast to higher organisms [11, 12] (Figure 2). Whether the adaptation to various stressors results in the same or in different types of cellular and organismal responses remains to be determined in future. The connection between the intracellular (intrinsic) stressor and potential adaptation is even more difficult to establish. Stressors can trigger cellular responses, from within cells and by the immune system. The stress responses of non-immune cells are described sometimes as an intrinsic stress response, while the stress responses of the immune system are called extrinsic stress response [13]. The latter functions by signaling with cytokines and clonal selection of cells. The transcription of many of the genes that participate in immune response is regulated by NF-κB, which is a growth and division-promoting factor and can thus turn into an oncogene. The intrinsic stresses can be DNA damage, hypoxia, low levels of glucose and amino acids, interference with mitochondrial and ribosomal biogenesis, the action of some toxins, etc. The transcription factor transformation-related protein 53 (p53) responds to such stressors. p53 also regulates many genes that prevent DNA damage or help in the DNA repair. Hypoxia, glucose levels and mitochondrial and ribosomal biogenesis are regulated by the interactions of the p53 pathway genes with the insulin-like growth factor 1 (IGF-1)/mTOR pathways and the regulation of the endosomal compartment by p53-induced genes [14]. In addition to its functions as a transcription factor in the nuclei, cytoplasmic p53 has transcription independent activities [15]. p53 is inactive in unstressed cells. Stress signal results in higher levels of p53, through

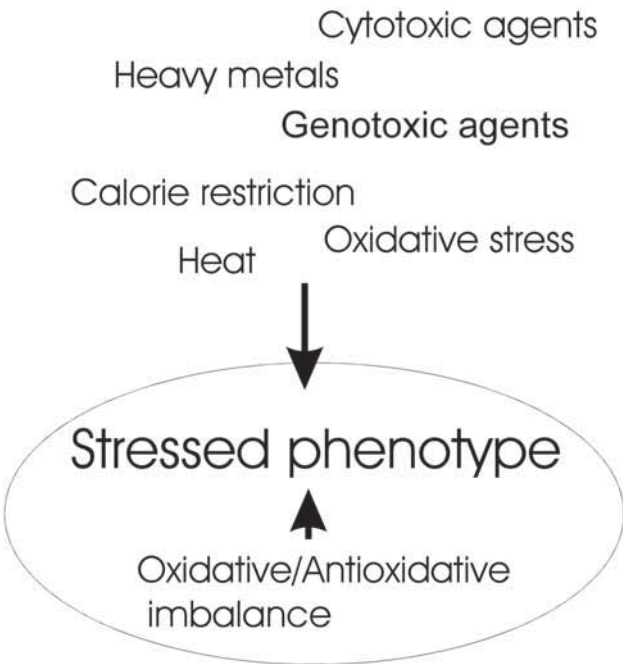

FIGURE 2. External and internal stressors can induce cellular adaptation to stress. Potent inducers of cellular stress from within and outside the cells are excessive amounts of oxidants. As some oxidants (reactive oxygen species) are needed for proper functioning of the organism, it is the oxidative/antioxidative imbalance that results in cellular stress [19].

post-translational modifications, which are selectively activated by different stress signals. This leads to transcription of different sets of genes resulting in cell cycle arrest, apoptosis or the cells loose the ability to divide (are senescent). The activation of p53 or NF-κB including pathways are mutually exclusive within the cells. The activation of p53 results in slowing glycolysis and restoring oxidative phosphorylation, while the activation of NF-κB pathway activates cell division and utilizes large amounts of glucose and predominant use of glycolysis [13]. Studying the adaptation to stresses is extremely important for the field of medicine, both for basic medical science and clinical practice. The contribution of stress responses to aging and disease development will be described in this paper. Testing for the possible adaptation to stress can improve the design and models of studies in different fields: in pharmacology how safe and effective doses of drugs are determined (and tested), how environmental, occupational and consumer exposure standards are derived and how risks and benefits are assessed.

Stress and aging

Accumulation of damaged macromolecular structures over time was long recognized to lead to aging. There are many studies, which link the decline in the effectiveness and integration of stress responses to ageing and the development of age-related diseases [16]. Modulation of mitochondrial and metabolic functions and mobilization of macromolecular

maintenance and repair leads to life extension in modeling organisms. The mitochondrial free radical theory of aging implies that aging is caused by damage of macromolecules by mitochondrial reactive oxygen species (ROS) [17]. Whether ROS damage is an initial trigger or the main effector of the aging process is a topic of current debates [18]. Certainly, the aging process results from a loss of homeostasis due to accumulation of molecular damage to DNA, proteins and lipids. However, the transient generation of ROS, within boundaries, seems to be essential to maintain the cellular homeostasis during physiological and stress conditions. This is supported by the observations of the importance of proper oxidative/antioxidative balance for health and longevity [19]. The administration of antioxidants to various species of invertebrates and humans did not result in anticipated beneficial effects. On the other hand, low amounts of ROS may act as secondary messengers in cells; the studies in *C. elegans* and rodents have even reported that the increased production of ROS in young animals resulted in life extension [20, 21, 22]. This may be an evidence of the beneficial role of stress responses. Needles to say that higher amounts of ROS exposure may be involved in aging and disease progression and in such cases the toxicity of ROS participates in creating a damage, which is well documented in aging and neurodegenerative diseases [23].

Stress and chronic diseases

Excessive amounts of ROS, overloading of the peroxidized polyunsaturated fatty acids (hydroxynonenals), products of cholesterol oxidation, mutations favoring protein misfolding, altered glycosylation, etc. may cause a severe stress and lead to accumulation of unfolded or misfolded proteins in brain cells [24]. The so called 'aggregated proteins' accumulation is a hallmark of many neurodegenerative diseases, like Alzheimer's, Parkinson's, Huntingdon's, amyotrophic lateral sclerosis and Friedereich's ataxia [24, 25]. Cell stress and stress proteins have a profound effect in triggering/developing the cardiovascular diseases, too. It was first observed in 1970's that the patients infected with *Mycobacterium tuberculosis* or *M. leprae* have antibodies to an antigen, which was identified subsequently as heat shock protein (Hsp60). It is now confirmed that Hsp60 and other chaperones, like Hsp10, Hsp70 and Hsp90 family members are strong imunogens and immunomodulators in experimental models of arthritis, diabetes and atherosclerosis [26]. Apart from the potent intracellular role of Hsp proteins as facilitators of correct protein folding and re-folding of misfolded proteins, many of them are potent activators of immune cells and may act as adjuvants and as immunogens, possibly as in the case of Mycobacterial infection. Atherogenesis may be driven by cross reactive immunity to bacterial Hsp60 proteins. Namely, the host Hsp60 proteins are expressed on the stressed endothelial cells. The exposure to long term severe non-lethal stress may therefore result in pathology.

Cellular adaptation to stress in tumor and normal cells

The accumulation of damage over long-term enhances the susceptibility to aging-associated illnesses, described above, and also to cancer (Figure 1). Rudolf Virchow observed the connection between chronic inflammation and cancer in 1863 [27]. It still stands that the increased risk of malignancy is connected to chronic inflammation caused either by chemical and physical agents or autoimmune and inflammatory reactions of uncertain aetiology. Prolonged stress therefore may result in malignancy. The well known examples include the connection of prolonged exposure to silica, asbestos and cigarette smoke to the increased risk of developing bronchial cancer; chronic infections with *H. pylori* and *Papillomavirus* and the risk of developing gastric and cervical cancers, respectively, etc [27]. When normally growing cells are in contact with carcinogens, they may respond by undergoing growth arrest, apoptosis or necrosis. Also, a population of genetically modified cells may emerge with intrinsic or induced resistance to apoptosis [28]. Control of intracellular concentration of ROS seems critical for the survival of cancer cells. For example, the acute increases in intracellular concentrations of ROS may cause the inhibition of glycolysis and divert the glucose flux into the pentose phosphate pathway in human lung cancer cells [29]. This generates sufficient antioxidant response for detoxification of ROS, therefore enables the cancer cells to withstand the initial oxidative stress and subsequently enables their proliferation. The epithelial cells detached from the extracellular matrix would normally not survive, as such cells lose the ability to take up glucose, which result in ATP deficiency. The detached epithelial cells can be rescued through two different pathways [30]. The expression of cancer promoting oncogene ErbB2 restores the cell's ability to take up glucose and reduces the levels of ROS through the antioxidant-generating pentose phosphate pathway. Alternatively, the ATP deficiency could be rescued by antioxidant treatment, which stimulates fatty acid oxidation otherwise inhibited by detachment-induced ROS. The latter cell rescue occurs without the rescue of glucose uptake. Therefore, the perturbation of oxidant/antioxidant balance (the lowering of oxidative stress) promotes the survival of pre-initiated tumor cells even detached from the extracellular matrix environment by altering metabolic regulation, which results in enhanced malignancy [30]. To summarize, pre-cancer cells may lead to neoplasia as a result of their altered growth/death ratio, due to disrupted cell cycle control, genomic instability or altered metabolism. Even tumor cells can become more invasive if they are pre-exposed to stress, i.e. preconditioned. Acutely hypoxic tumor

cells were found to be more metastatic then normoxic [31]. Patients with hypoxic primary tumors have an increased frequency of locoregional treatment failure, increased incidence of distant metastases and poor disease-free and survival rates [32]. Mice exposed to acute cyclic hypoxia showed increased incidence of pulmonary metastases, their primary tumors have increased blood perfusion, microvascular density and expression of vascular endothelial growth factor-A. Preconditioning against the proteins induced as the consequence of stress responses may improve the outcome of cancer therapy in experimental models. Neutralization of vascular endothelial growth factor (VEGF) in endothelial cells by specific antibody could enhance the anti-tumor activity of carboplatin in an *in vivo* ovarian cancer model [33]. On the other hand, decreasing the stress response in tumor cells by preconditioning them with various agents is often explored in experimental models with the aim of developing the method to increase the susceptibility of tumor cells to treatment. For example, the abolition of stress-induced protein synthesis by cycloheximide sensitizes leukemia cells to anthracyclins, the currently successful anticancer drugs [34]. In conclusion, the connection between chronic inflammation and cancerogenesis is known for over hundred years; one of the recently established hallmarks of cancer is the presence of stress phenotypes [35].

Stress and transplantation

As discussed above, the adaptation of normal cells to stress is beneficial in the short term and can be detrimental in the long term. There are medical procedures during which the cellular resistance to stress is beneficial, for example, when handling the cells and tissues for transplants. Also, the transplanted cells must thrive *in vivo* at the site of transplantation, in spite of the fact that the stress factors, which caused the deterioration of original cells, may be still present at the site of transplantation. The increased survival of cells in experimental models is attempted often through preconditioning of transplanted cells with chemical agents and by gene transfer [36-39]. The preconditioning of retinal pigment epithelial cells by limited exposure to non-lethal oxidative stress results in protection against subsequent H_2O_2-induced cell death [40]. Such preconditioning of retinal cells may improve the survival of these cells after the transplantation into the environment with increased oxidative stress. Therefore, such preconditioning is potentially important as a basis for the development of new treatment procedures. Preconditioning has a physiological role, too. Some of the cells in the organism need appropriate stress in order to function properly. For example, vascular endothelial cells need appropriate physical stimuli to maintain their structure and function [41]. The vascular endothelial cells of liver, the sinusoidal vascular endothelial cells, have small pores, through which shear stress is applied to hepatocytes as well. There is an almost constant shear stress in undamaged liver. Remodeling of sinusoidal structures was observed in the liver culture exposed to either no shear stress or to high shear stress, compared to the tissue exposed to moderate shear stress [41]. This find seems to have important implications for medical procedures on liver. Rapidly increased portal flow producing high shear stress may occur after massive liver resection or during ischemia/reperfusion in liver transplantation [41]. The increased portal flow may result in postoperative hepatic insufficiency in serious cases. Also, when a small-for-size graft is implanted in adult living donor liver transplantation, the increased portal flow after reperfusion (in the small graft) contributes to the poor prognosis following the transplantation. Therefore, perioperative flow management during the surgical procedures on liver is important and may improve the postoperative result.

CONCLUSIONS

Encountering the stressors is the normal consequence of living in a fluctuating environment; therefore, the cells have developed mechanisms to ameliorate the stress or to adapt to it. This is achieved through the repair of damage, adaptation, reuse of resources and a limited cell death. Living with stressors is unavoidable in the life of organisms and cells, thus the cells have to divert at least some of their resources from other pathways, to deal with the consequences of stressors. Our cells are well adapted to exposure to a mild stress for a short time. In contrast there are potentially serious consequences of exposure to the prolonged stress. Cellular stress can at least contribute to, or even trigger, many diseases and malignant transformations and has an important role in aging. To ameliorate or repair these processes the cells are being used in cell therapies and regenerative medicine. For maximal therapeutic success it is important to use the cells in the best condition possible or those adapted to stress. Discovering the detailed mechanisms of stress responses, some of which are described here, will improve the assessment of the condition of transplanted cells and to better their handling and transplant survival rates. Even more important, the knowledge of cell stress responses is important for the well being of normal cells and may form a basis for development of preventional measures and treatments of diseases significantly influenced by persistent stress, like cancer and neurodegenerative diseases.

DECLARATION OF INTEREST

We have no conflict of interest to declare.

REFERENCES

[1] Nipic D, Pirc A, Banic B, Suput D, Milisav I. Preapoptotic cell stress response of primary hepatocytes. Hepatology. 2010; 51(6):2140-2151.

[2] Milisav I. Cellular Stress Responses, Advances in Regenerative Medicine, Sabine Wislet-Gendebien (Ed.), ISBN: 978-953-307-732-1, InTech, 2011. Available from: http://www.intechopen.com/articles/show/title/cellular-stress-responses

[3] Calabrese EJ. Getting the dose–response wrong: why hormesis became marginalized and the threshold model accepted. Arch. Toxicol. 2009; 83(3): 227-247.

[4] Samson L, Cairns J. A new pathway for DNA repair in Escherichia coli. Nature 1977 267(5608):281-283.

[5] Samson L, Schwartz JL. Evidence for an adaptive DNA repair pathway in CHO and human skin fibroblast cell lines. Nature 1980 287(5785):861-863.

[6] Marmot MG, Rose G, Shipley MJ, Thomas BJ. Alcohol and mortality: a U-shaped curve. Lancet. 1981;1 (8220 Pt 1):580-583.

[7] Olivieri G, Bodycote J, Wolff S. Adaptive response of human lymphocytes to low concentrations of radioactive thymidine. Science. 1984; 223(4636):594-597.

[8] Murry CE, Jennings RB, Reimer KA. Preconditioning with ischaemia: a delay of lethal cellinjury in ischaemic myocardium. Circulation 74(5): 1124-1136.

[9] Ugazio G, Koch RR, Recknagel RO. Mechanism of protection against carbon tetrachloride by prior carbon tetrachloride administration. Exp Mol Pathol. 1972; 16(3):281-285.

[10] Huffman DM. Exercise as a calorie restriction mimetic: implications for improving healthy aging and longevity. Interdiscip Top Gerontol. 2010; 37:157-174.

[11] Costa V, Moradas-Ferreira P. Oxidative stress and signal transduction in Saccharomyces cerevisiae: insights into ageing, apoptosis and diseases. Mol. Aspects Med. 2001; 22(4-5):217-246.

[12] Ristow M, Zarse K. How increased oxidative stress promotes longevity and metabolic health: The concept of mitochondrial hormesis (mitohormesis). Exp. Gerontol. 2010;45(6):410-418.

[13] Ak P, Levine AJ. p53 and NF-κB: different strategies for responding to stress lead to a functional antagonism. FASEB J. 2010;24(10):3643-3652.

[14] Sengupta S, Peterson TR, Sabatini DM. Regulation of the mTOR complex 1 pathway by nutrients, growth factors, and stress. Mol Cell. 2010; 40(2):310-322.

[15] Speidel D. Transcription-independent p53 apoptosis: an alternative route to death. Trends Cell Biol. 2010;20(1):14-24.

[16] Haigis MC, Yankner BA. The aging stress response. Mol Cell. 2010;40(2):333-344.

[17] Harman D. The biologic clock: the mitochondria? J Am Geriatr Soc. 1972; 20(4):145-147.

[18] Hekimi S, Lapointe J, Wen Y. Taking a "good" look at free radicals in the aging process. Trends Cell Biol. 2011;21(10):569-576.

[19] Poljsak B, Milisav I. The neglected significance of "antioxidative stress". read Oxid Med Cell Longev. 2012; 2012: 480895. doi: 10.1155/2012/480895.

[20] Yang W, Hekimi S. A mitochondrial superoxide signal triggers increased longevity in Caenorhabditis elegans. PLoS Biol. 2010;8(12):e1000556.

[21] Andziak B, O'Connor TP, Qi W, DeWaal EM, Pierce A, Chaudhuri AR, et al. High oxidative damage levels in the longest-living rodent, the naked mole-rat. Aging Cell 2006;5(6):463-471.

[22] Pérez VI, Van Remmen H, Bokov A, Epstein CJ, Vijg J, Richardson A. The overexpression of major antioxidant enzymes does not extend the lifespan of mice. Aging Cell. 2009;8(1):73-75.

[23] Haigis MC, Yankner BA. The aging stress response. Mol Cell. 2010;40(2):333-344.

[24] Calabrese V, Guagliano E, Sapienza M, Panebianco M, Calafato S, Puleo E. et al. Redox regulation of cellular stress response in aging and neurodegenerative disorders: role of vitagenes. Neurochem Res 2007;32(4-5):757-373.

[25] Petrozzi L, Ricci G, Giglioli NJ, Siciliano G, Mancuso M. Mitochondria and neurodegeneration. Biosci Rep. 2007;27(1-3):87-104.

[26] Shamaei-Tousi A, Halcox JP, Henderson B. Stressing the obvious? Cell stress and cell stress proteins in cardiovascular disease. Cardiovasc Res. 2007;74(1):19-28.

[27] Balkwill F, Mantovani A. Inflammation and cancer: back to Virchow? Lancet. 2001; 357(9255):539-545.

[28] Carlisle DL, Pritchard DE, Singh J, Owens BM, Blankenship LJ, Orenstein JM, Patierno SR. Apoptosis and P53 induction in human lung fibroblasts exposed to chromium (VI): effect of ascorbate and tocopherol. Toxicol Sci. 2000;55(1):60-68.

[29] Anastasiou D, Poulogiannis G, Asara JM, Boxer MB, Jiang JK, Shen M, et. al. Inhibition of pyruvate kinase M2 by reactive oxygen species contributes to cellular antioxidant responses. Science., 2011; 334(6060): 1278-1283.

[30] Schafer ZT. Antioxidant and oncogene rescue of metabolic defects caused by loss of matrix attachment. Nature, 2009; 461: 109-113.

[31] Rofstad EK, Gaustad JV, Egeland TA, Mathiesen B, Galappathi K. Tumors exposed to acute cyclic hypoxic stress show enhanced angiogenesis, perfusion and metastatic dissemination. Int J Cancer. 2010;127(7):1535-1546.

[32] Vaupel P, Mayer A. Hypoxia in cancer: significance and impact on clinical outcome. Cancer Metastasis Rev. 2007;26(2):225-239.

[33] Wild R, Dings RP, Subramanian I, Ramakrishnan S. Carboplatin selectively induces the VEGF stress response in endothelial cells: Potentiation of antitumor activity by combination treatment with antibody to VEGF. Int J Cancer. 2004;110(3):343-351

[34] Gausdal G, Gjertsen BT, McCormack E, Van Damme P, Hovland R, Krakstad C. et al. Abolition of stress-induced protein synthesis sensitizes leukemia cells to anthracycline-induced death. Blood. 2008;111(5):2866-2877

[35] Leung AK, Sharp PA. MicroRNA functions in stress responses. Mol Cell. 2010; 40(2):205-215.

[36] Harrison EM, Sharpe E, Bellamy CO, McNally SJ, Devey L, Garden OJ. et al. Heat shock protein 90-binding agents protect renal cells from oxidative stress and reduce kidney ischemia-reperfusion injury. Am J Physiol Renal Physiol 2008;295(2):F397-405.

[37] Wang X, Zhao T, Huang W, Wang T, Qian J, Xu M. et al. Hsp20-engineered mesenchymal stem cells are resistant to oxidative stress via enhanced activation of Akt and increased secretion of growth factors. Stem Cells. 2009; 27(12):3021-3031.

[38] Hynes SO, McCabe C, O'Brien T. β cell protection by inhibition of iNOS through lentiviral vector-based strategies. Methods Mol Biol. 2011;704:153-168.

[39] Chou J, Greig NH, Reiner D, Hoffer BJ, Wang Y. Enhanced survival of dopaminergic neuronal transplants in hemi-Parkinsonian rats by the p53 inactivator PFT-α. Cell Transplant 2011; 20(9):1351-1359.

[40] Sharma RK, Netland PA, Kedrov MA, Johnson DA. Preconditioning protects the retinal pigment epithelium cells from oxidative stress-induced cell death. Acta Ophthalmol 2009;87(1):82-88.

[41] Torii T, Miyazawa M, Koyama I. Effect of continuous application of shear stress on liver tissue: continuous application of appropriate shear stress has advantage in protection of liver tissue. Transplant Proc. 2005;37(10):4575-4578.

Xanthomas of the stomach: a report of two cases

Bojana M. Andrejić[1*], Snežana V. Božanić[2,3], Nenad S. Šolajić[2,3], Matilda A. Djolai[1,2], Aleksandra M. Levakov[1,2]

[1] Department of Histology and Embryology, Faculty of Medicine, Hajduk Veljkova 3 Novi Sad, Serbia. [2] Center for Pathology and Histology, Clinical Center of Vojvodina,Hajduk Veljkova 1, Novi Sad, Serbia. [3] Department of Pathology, Faculty of Medicine, Hajduk Veljkova 3,Novi Sad, Serbia

Abstract

Gastrointestinal tract xanthomas are non tumor, well demarcated mucosal lesions that consist of foamy histiocytes, most commonly diagnosed in the stomach. The histologic appearance of xanthomas can resemble certain malignant lesions. After retrospective data base search, we have encountered only 2 cases of xanthomas, both in the antral part of the stomach. Lamina propria of the mucosa contained rare, chronic inflammatory infiltrate and clusters of oval and polygonal cells with abundant, foamy cytoplasm. The cytoplasm of described cells did not show the presence of mucin (Periodic acid-Schiff (PAS) and Alcian blue staining). The cells showed distinct cytoplasmic CD68 positivity and CKMNF116 negativity, which confirmed the diagnosis of xanthoma. Given the frequent association of xanthomas and known precancerous lesions of gastric mucosa, and occasional coexistence of malignant change, we need to pay attention to its diagnosis, and it is advisable to use both histochemical and immunohistochemical methods.

KEY WORDS: xanthoma, stomach, differential diagnosis, CD68 antigen, cytokeratin MNF116.

INTRODUCTION

Xanthomas of the gastrointestinal system are tumor-like lesions that occur in the form of yellow to white, well demarcated mucosal nodules or plaques. Histologically, xanthomas consist of clusters of foamy histiocytes containing lipid [1]. In the gastrointestinal tract xanthomas are mostly diagnosed in the lamina propria of the stomach, mainly in the antrum and pyloric region, while the esophagus, small and large intestine are very rare localizations [2]. The incidence of gastric xanthomas detected at endoscopy varies from 0.018% in Europe to 0.80% in China. Analysis of autopsy material by Kimura et al. that targeted examination of the presence of gastric xanthomas, found data on the incidence of 58%, as opposed to Feyrter et al. who determined an incidental finding of gastric xanthomas at autopsy with a frequency of 1.9% [3, 4]. The histologic appearance of xanthomas can resemble certain malignant lesions [2, 5] such as clear cell type of carcinoid tumors [2, 3] and signet ring cell type adenocarcinoma [2]. Although this is a benign lesion, considering the differential diagnosis of this entity, we found it important to draw attention to the morphological and immunophenotypic characteristics of gastric xanthomas.

* Corresponding author: Bojana Andrejić
Hajduk Veljkova 6, 21000 Novi Sad
email: andrejic.bojana@gmail.com
phone: +381631669300

Submitted: 17. January 2012 / Accepted 5. March 2012

MATERIAL AND METHODS

A retrospective chart review was performed (january 1st 2006– August 1st 2011) at the tertiary medical center (Clinical Center of Vojvodina, Center for Pathology and Histology) in order to find out the number of diagnosed xanthomas and study their histomorphological features. The data were obtained from pathohistological reports of the patients who underwent biopsy sampling of mucosa the stomach during upper gastrointestinal tract endoscopy procedures. In the mentioned period, only two cases of gastric xanthomas were diagnosed (in 2007 and 2011). Biopsy specimens reported in Case 1 were fixed in 4% formalin and in Case 2 in 70% alcohol. After fixation material was dehydrated in alcohol and embedded in paraffin. Sections 4-5μm thick were stained with hematoxylin and eosin (HE) and Giemsa methods.

CASE 1

A 28 years old female patient, during the upper gastrointestinal endoscopy, has been diagnosed with a polyp of the stomach and suspicion of celiac disease. Biopsy material sampled during the endoscopy was sent to histopathological analysis. Biopsy sample of the duodenal mucosa by its histological characteristics did not confirm the presence of celiac disease. Sample taken from the stomach was a papillary, superficial part of the gastric mucosa, mainly from the foveolar layer. Superficial and foveolar epithelia of gastric type were pre-

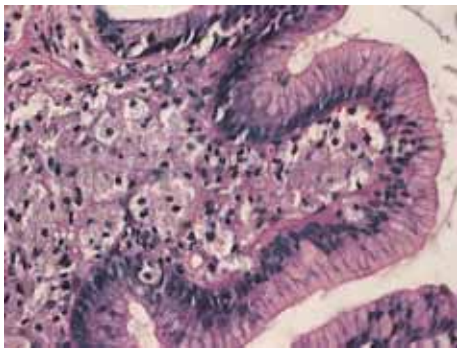

FIGURE 1. Gastric xanthoma cells with abundant foamy cytoplasm and centrally located nuclei (HE, x400).

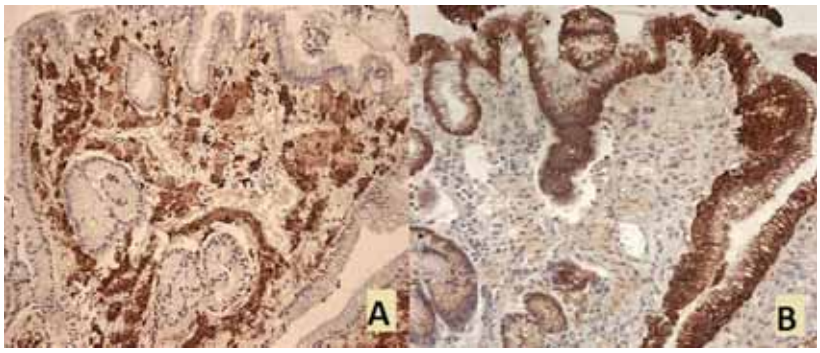

FIGURE 2. Immunohistochemistry of the xanthoma; (A) microphotograph showing diffuse cytoplasmic expression of CD68; (B) microphotography showing CKMNF116 – negative xanthoma cells.

served, without signs of intestinal metaplasia or Helicobacter pylori (H. pylori). Antral type glands specific for that region were located only at the edges of the sample. In the lamina propria there was a rare, chronic inflammatory infiltrate of lymphocytes and plasma cells, along with the clusters of oval and polygonal cells. Cytoplasm of polygonal cells was abundant, foamy and eosinophilic and these cells contained hyperchromatic, oval to round nuclei of uniform size (Figure 1). In order to confirm the diagnosis and rule out the possibility that the described cells were malignant epithelial cells, the material has been subsequently stained using histochemical methods Periodic acid-Schiff (PAS) and Alcian blue and immunohistochemically using antibodies to CD68 and CKMNF116 (Dako). The cytoplasm of the described cells did not show the presence of mucin. The cells showed distinct cytoplasmic positivity to CD68 (Figure 2A) and negativity to CKMNF116 (Figure 2B). This histochemical and immunohistochemical profile confirmed the absence of carcinoma cells. Histomorphological characteristics of the examined material indicated the xanthoma of gastric mucosa. We stated a definite diagnosis of gastric xanthoma. Because we did not have accesses to a fresh specimen (it was embedded in paraffin entirely) frozen sections were not available and the presence of fat vacuoles inside cells could not be shown by histochemical staining (Sudan black and Oil red).

CASE 2

The patient was a man aged 77 years, with no clinical data available. Three biopsy samples were taken from the stomach: antral mucosa, mucosa of the corpus and a sample from a submucosal lesion of the antrum that on the endoscopic examination gave the impression of adipose tissue. Histological examination of the gastric mucosa in the antrum and in the corpus showed mild atrophy and lymphocytic infiltration, without the presence of intestinal metaplasia and H. pylori. Third sample was a slightly papillary, polipoid sample of gastric mucosa. The lamina propria was entirely crowded with large, polygonal cells with abundant, foamy cytoplasm

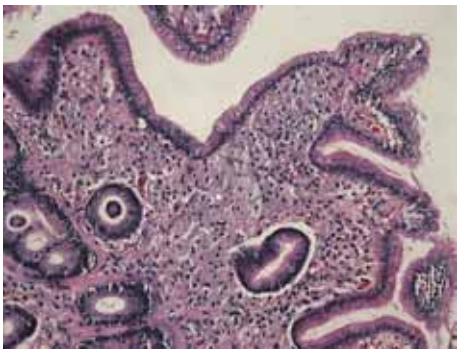

FIGURE 3. Gastric xanthoma (HE, 200x).

filled with numerous vesicles (Figure 3). Cytoplasm of these cells was negative when stained with PAS and Alcian blue methods. Gastric glands have not been observed in this specimen. (Immunohistochemical staining was not performed on this specimen due to inadequate alcohol fixation.)

DISCUSSION

Although gastric xanthoma was first described by Orth back in the 1887, its etiology and clinical significance are still unclear [4]. Data on the frequency of gastrointestinal xanthomas and the linkage with the more frequent manifestation in a particular sex are significantly different in the literature [2, 6]. The vast majority of authors agree that the xanthomas typically occur in the stomach (70%), mostly in the antral region (76%) [2, 3]. Both cases that we have encountered were gastric xanthomas, located in the antrum of the stomach, which is in accordance with the literature data. This type of change is common in the elderly (incidence of 53.3% in the age group of 40-60 years) although it can be seen in people of all age [3]. In our case, the lesion was diagnosed in female patient aged 28 years, and in elderly male patient aged 77 years, both in the antral part of the gastric mucosa. The etiology of gastrointestinal tract xanthomas is not fully understood although it is believed that the mucosa affected by certain pathological processes is more susceptible to their occurrence [6, 7].

Yi et al. believe that the transformation of macrophages into foamy cells can be induced by phagocytosis of H. pylori bacteria, which penetrate into the lamina propria [7]. This data was confirmed by the finding of H. pylori antigens in the cytoplasm of foamy cells even in cases where the presence of bacteria in the mucosa was not detected [8]. In both our cases H. pylori was not observed. During the repair of damaged mucosa debris rich in lipid materials is produced, and phagocytosed by tissue macrophages and thus form the foamy cells [2, 3, 4, 7]. Yi et al. indicate that the mucosal atrophy is significantly associated with the presence of xanthomas [7]. As sample of the 28 years old patient did not contain the full thickness of the mucosa, and antral glands were located in a small number only on the edge of the section, the presence of atrophy could not be assessed. Mild atrophy was detected in antrum and the corpus of the stomach in the 77 year old patient, but in the specimen that contained foamy cells glands were not present. None of the other precancerous pathological processes that make the lining more susceptible to the emergence of xanthomas (active gastritis, ulcers, intestinal metaplasia, gastric resection) were not present in our patients [9]. Linkage between patient's lipid metabolism and cutaneous xanthelasma is widely accepted [3, 6]. The data about the connection lipid metabolism disorders and gastrointestinal tract xanthomas is inconclusive [4, 7]. Patients presented here were referred by physicians from other institutions (and other cities on a territory of Vojvodina) for endoscopic examinations so the clinical data on the values of serum lipid levels, in our cases could not be obtained. Endoscopically and histologically gastric xanthomas may resemble malignant tumors of the stomach in terms of a significant histopathologic differential diagnosis problem [6]. In addition to the morphological features that can resemble cancer, Muraoka et al. reported on the case of early gastric cancer and xanthomas where xanthoma cells and cancerous cells were in contact with each other, but with clear immunophenotypic differences [10]. They have proven that xanthoma cells did not originate from tissue macrophages, but from activated monocytes that pass from the bloodstream under the influence of various factors and inflammatory mediators [10]. In our cases, the possibility of the presence of malignant epithelial mucinous cells was rejected based on histochemical staining which clearly proved the absence of mucin in both cases, while in the case of 28 year old patient and immunohistochemical negativity of CKMNF116 showed that these cells are not of epithelial origin. CD68 positivity proved them to be macrophage cells. These histochemical and immunohistochemical profile of xanthoma cells is consistent with the allegations of the literature [3, 5, 6].

CONCLUSION

Given the frequent association of xanthomas and known precancerous lesions of gastric mucosa, and occasional coexistence of malignant change, we need to pay attention to diagnosis of xanthomas. It is advisable to use histochemical and immunohistochemical methods to confirm the diagnosis of xanthomas and eliminate the possibility of gastric malignancy. In our case, xanthoma was diagnosed in a young female, in the absence of associated etiologic factors and mucosal damage. In the elderly male patient mild atrophy was present but as the data on lipid status of both of our patients was not collected, it is possible that the appearance of xanthomas was associated with disorders of lipid metabolism.

ACKNOWLEDGEMENTS

This work was supported by The Ministry of Science and Technological development of the Republic of Serbia (grant number 41012).

DECLARATION OF INTEREST

None to declare.

REFERENCES

[1] Rosai J. Rosai and Ackerman's Surgical Pathology, 9th ed. Philadelphia: Elsevier Inc; 2004.
[2] Gürsoy S, Yurci A, Torun E, Soyuer I, Güven K, Özbakir O et al. An uncommon lesion: gastric xanthelasma. Turk J Gastroenterol 2005; 16(3):167-170.
[3] Gencosmanogly R, Sen-Oran E, Kurtkaya-Yapicier O, Tozun N. Xanthelasmas of the upper gastrointestinal tract. J Gastroenterol 2004; 39:215-219.
[4] Nostrant T. Review. Gastroenterol Hepatol 2010; 6(3):183-184.
[5] Hirasaki S, Kubo M, Inoue A. Gastric hyperplastic polyp associated with proliferation of xanthoma cells observed by magnification narrow-band imaging endoscopy. Gastroenterology Research and Practice 2009; 2009:845260.
[6] Jansen HJ, van Krieken JH, Römkens THE. Yelow-white lesions in the upper gastrointestinal tract. Neth J Med 2009; 67(10):360-361.
[7] Yi SY. Dislipidemia and H. pylori in gastric xanthomatosis. World J Gastroenterol 2007; 13(34):4598-601.
[8] Isomoto H, Mizuta Y, Inoue K, Matsuo T, Hayakawa T, Miyazaki M et al. A close relationship between Helicobacter pylori infection and gastric xanthoma. Scand J Gastroenterol 1999; 34(4):346-52.
[9] Vukobrat-Bijedić Z, Radović S, Husić-Selimović A, Gornjaković S. Incomplete intestinal metaplasia as an indicator for early detection of gastric carcinomain the events of helicobacter pylori positive chronic atrophic gastritis. Bosn J Basic Med Sci 2006; 6(4):48-53.
[10] Muraoka A, Suehiro I, Fujii M, Ueno H, Hayashi S, Shimizu K et al. Type II early gastric cancer with proliferation of xanthoma cells. J Gastroenterol 1998; 33(3):326-9.

General anaesthesia in an adult patient with Morquio syndrom with emphasis on airway issues

Lajla Kadic*, Jacques J. Driessen

Department of Anesthesiology, Radboud University Nijmegen Medical, Centre, Huispost 630, route 633, Postbus 9101, 6500 HB Nijmegen, The Netherlands

Abstract

Patients with Morquio syndrome possess a number of characteristics which may complicate an anaesthetic procedure. The most important is that a deposition of mucopolysaccharides in the soft tissues of the oro-pharynx distorts the airway, making the airway management difficult, while the atlanto-axial instability puts these patients at risk of subluxation and quadriparesis.

As the endotracheal intubation in Morquio syndrome patients may be difficult or even impossible, we recommend the technique of awake fiberoptic intubation to be considered.

Our approach to awake fiberoptic intubation in an adult patient is described in this case report.

KEY WORDS: Morquio syndrome, mucopolysaccharidosis, neck instability, general anesthesia, fiberoptic intubation

INTRODUCTION

The mucopolysaccharidoses (MPS) are a family of lysosomal storage diseases that result in abnormal accumulation of glycosaminoglycans throughout the body. There is a broad spectrum in severety of expression of the musculoskeletal and neurological manifestations of these diseases, ranging from an early and obvious presentation, with rapid degeneration and death, to a nearly asymptomatic phenotype and normal life expectancy [1]. The Morquio–Brailsford syndrome, known as mucopolysaccharidosis type IV (MPS IV), is listed as a "rare disease" by the Office of Rare Diseases of National Institutes of Health, with a prevalence of 1/ 200 000-250 000 people. This deficiency leads to accumulation of keratin sulfate and chondroitin-6-sulfate in connective tissue, skeletal system und teeth [2]. Infiltration of the tissues may lead to anaesthetic problems. This includes distortion of upper airway anatomy with a large tongue and dental abnormalities which makes the endotracheal intubation difficult or impossible [3, 4]. Spinal abnormalities are common. Atlantoaxial instability with resultant myelopathy and spastic quadriparesis has been described in both, MPS IV and MPS VI. Cervical fixation at the occiput–to-C2 level is frequently needed in these patients and in fact profilactic occipito-cevical fusion has been strongly advocated for patients with Morquio syndrome independent of neurological symptoms [1, 5]. Cardiac abnormalities may be present. Aortic regurgitation is the most commonly observed valvular abnormality in patients with Morquio syndrome. However, few reports have been published describing cardiac surgery in patients with mucopolisaccharidosis, including Morquio syndrome, because valve disease becomes usually symptomatic only late in the course of these diseases [5]. MPS IV induced thoracic cage deformity, kyphoscoliosis, may reduce the long volumes and cause ventilation-perfusion mismatch [6]. Unlike other forms of mucopolysaccharoidoses, MPS IV patients

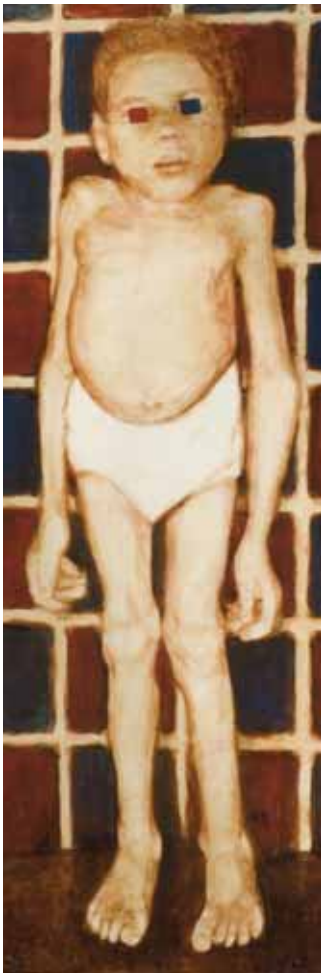

FIGURE 1. An art adapted photo of a typical Morquio syndrome patient by Peter Romberg

* Corresponding author: Lajla Kadic, Department of Anesthesiology, Radboud University Nijmegen Medical Centre, Huispost 630, route 633, Postbus 9101, 6500 HB Nijmegen, The Netherlands
Phone: +31 24 36 67255; Fax: +31 24 35 40462
e-mail: L.Kadic@anes.umcn.nl

Submitted: 31. October 2011 / Accepted: 9. March 2012

have and retain normal intelligence throughout life [1]. As the patients with mucopolysaccharoidosis are being referred to hospital for surgery more frequently compared to average population, it is important to gain basic knowledge of the disease in spite of the low incidence of the syndrome [7]. An (art adapted) photo of a typical Morquio syndrome patient is attached as Figure 1.

CASE REPORT

A 31 year old man, with Morquio syndrome presented at our Orthopaedic Department with the pain on the hips, limiting his walking ability to maximally 10 minutes. Bilateral coxarthrosis with deformity of the joints was diagnosed. A unilateral, total hip replacement had to be performed on the right side first and after the period of revalidation, on the left, as well. His length was 170 cm and weight 79 kg. The patient had a large head which seemed to be positioned on his thorax because of extremely short neck. Inspection of the mouth showed a large tongue with a Mallampati score III. Past history revealed cervical stabilization by the posterior spondylodesis C0-C2. Recent radiological investigation of cervical spine detected abnormal shape and insufficient height of vertebral corpora and some degenerative changes (Figure 2. and 3.) Radiological examination of lumbar spine showed typical scoliosis and torsion, with low height and wide corpora. Cardiology report was normal and the lung function test revealed slight diffusion problems. He used no other drugs except pain medication (paracetamol and diclofenac). During preoperative evaluation it became clear that unsuccessful spinal anaesthesia for a recent minor procedure precluded use of this technique again. The remaining option was awake (sedated) fiberoptic intubation (AFI). Every step of AFI was explained to the patient and emphasized the importance of his cooperation. Enough time was planned for the preparations. The patient was given an infusion and connected to standard monitoring. To relieve the anxiety and to achieve some amnesia, 2 mg of midazolam was given intravenously. As it may prove very difficult (or impossible) to accomplish an oral AFI intubation, due to a narrow space between the large tongue and the pharynx wall and the sharp angle that has to be made by the scope towards the glottic opening, we prepared the nasal route as well. A vasoconstrictor, 0,5% xilometazoline nose drops were given first, followed by 2% lidocaine gel (2 cm) in each nostril. The tongue and the pharynx were prepared by spraying 4-6 ml of 2% lidocaine. After a few minutes it was possible to place de tong depressor deep enough to anesthetize the back of the tong and pharynx wall by spraying another 4-6 ml of 2% lidocaine spray, asking the patient to take a deep breath simultaneously. We avoid higher concentration of local anes-

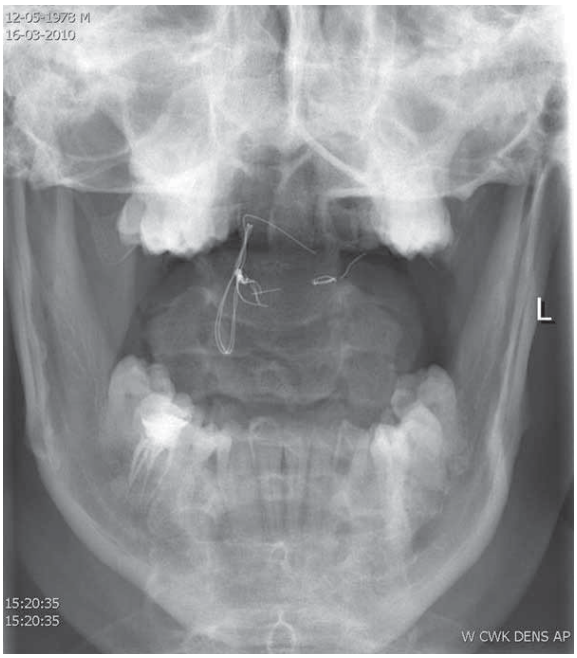

FIGURE 2. RTG photo of dens, preoperative.

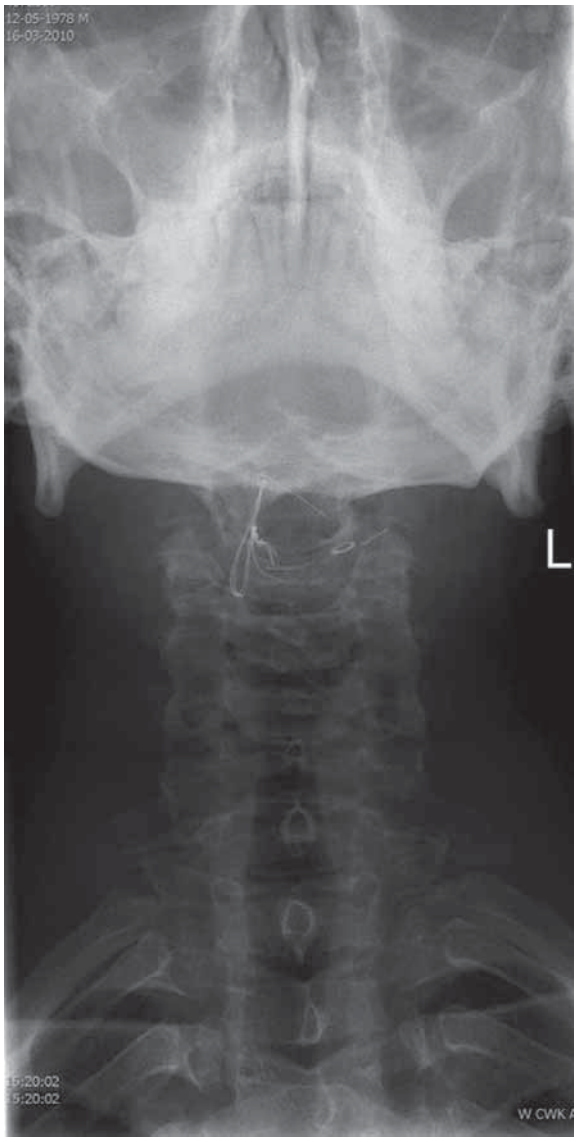

FIGURE 3. RTG photo of cervical spine, preoperative.

thetic because it causes more irritation of the mucosa. After a few more minutes we checked the sensitivity of nasal and pharyngeal surface by touching it. Patient felt no discomfort and an Ovassapian intubating oro-pharyngeal airway was inserted easily. Nasal oxygen prongs were placed with the flow of 3 liter /min. Intravenous sedation was started by propofol continuous infusion 2mg/kg and remifentanyl 0,05 μg/kg/min. Antisialogog, atropine 0,5 mg was administered intravenously. The patient continued to breath spontaneously, felt comfortable and remained cooperative. The fiberscope was prepared so that an epidural catheter (with three standard side-openings at the end) was threaded via the working channel to be used for spraying the vocal cords. The fiberscope was passed via the intubating airway and the vocal cords appeared in view after some chin-lift maneuver. We used spray-as-you-go technique to anesthetize the vocal cords with 2 ml of 2% lidocaine. That provoked some coughing. After waiting for about 30 seconds, the fiberscope was passed through the glottis until the carina and the endotracheal tube railroaded to trachea. The tube position was confirmed by auscultation and capnography and general anesthesia induced. The operation was uneventful and awake extubation followed.

DISCUSSION

The Morquio –Brailsford syndrome is a progressive disorder of connective tissue. It is known as mucopolysaccharidosis type IV. The various enzymatic defects lead to accumulation of keratin sulfate and chondroitin-6-sulfate in connective tissue, skeletal system und teeth, brain, heart, liver, spleen and tracheobronchial tree, leading to characteristic physical appearance and resulting in end-organ disfunction [2]. The basic diagnostic test is the detection of excessive amount of these substances in urine. The airway issues by patients with Morquio syndrome are frequently complicated by cervical spine instability and the risk of subluxation (cord trans-section in a child reported in literature) [2]. Radiological investigation should be performed before the operation and the problems discussed with the radiologist and neurosurgeon, in case of elective surgery. In case of an emergency, the approach to the airway and the cervical spine should follow the guidelines used for patients with suspected cervical spine injury (rigid collar). The neck fixation increases the difficulty of the airway management. In addition to the airway issues, preoperative pulmonary testing should be performed in these patients. Respiratory function can be compromised by chronic respiratory disease, recurrent pulmonary infections, obstructive sleep apnea and kyphoscoliosis leading to restrictive lung. Cardiac infiltration may lead to myocardial dysfunction, coronary artery lesions and valvular dysfunction. The most important problems concerning the airway management are based on intracellular accumulation of mucopolysaccharides resulting in macroglossia, limited mouth opening due to involvement of temporo-mandibular joints, short neck and subglotic narrowing. These elements may lead to "cannot intubate -cannot ventilate situation" [2]. Oral fiberoptic technique might be difficult due to large, heavy, anteriorly placed, "hanging epiglotis" (sometimes resting on the tong base) making the passage of the fibrescope towards the glotic opening impossible. Nasal fiberoptic technique is strait forward, but might be difficult related to mucopolisaccharoide infiltration in the nasopharynx, with the increased risk of bleeding. Careful preoperative airway examination should be done to predict and evaluate the possible problems. When the airway risk is present, loco-regional technique should be applied if possible. However, the use of spinal anesthesia can be difficult due to progressive scoliosis. Also the optimal dose of local anesthetic is difficult to predict due to (heavy) growth retardation in some of these patients. Regardless of the technique chosen, all necessary equipment to deal with difficult airway should be readily available in case of complications or failure. There is also a controversy about the appropriate means of induction. Some anaesthesiologists prefer the use of intravenous and others of inhalational agents (especially in children), but most of the authors suggest to avoid the use of muscle-relaxants. The relaxation of the supraglottic tissue may preclude effective bag-mask ventilation [3]. Endo-tracheal intubation using fiberoptic technique, being minimally invasive and allowing neutral head position is strongly recommended in these patients [4]. Attention to maximize the respiratory function postoperative is essential to avoid the obstruction and postoperative respiratory failure.

CONCLUSION

In conclusion, we recommend the technique of awake, fiberoptic intubation to be considered in adult patients with Morquio syndrome. Oral fibreoptic approach, as less traumatic, should be the first choice, keeping in mind that nasal route might be needed, and should be prepared as well. We strongly recommend not to use muscle relaxants, as they may impair the efficacy of a bag-mask ventilation, leading to can-not -intubate can-not-ventilate situation.

DECLARATION OF INTERESTS

There are no competing interests amongst the authors and there is not going to be any forthcoming presentation.

REFERENCES

[1] White KK, Steinman S, Mubarak SJ. Cervical stenosis and spastic quadriparesis in Morquio disease (MPS IV). A case report with twenty-six-year follow-up. J Bone Joint Surg Am. 2009; 91(2): 438-442

[2] Gösele S, Dithmar S, Holz FG, Völcker HE. Late diagnosis of Morquio syndrome. Clinical histopathological findings in a rare mucopolysaccharidosis. Klin Monbl Augenheilkd 2000; 217(2):114-117

[3] Tobias JD. Anesthetic care for the child with Morquio syndrome: general versus regional anesthesia. J Clin Anesth 1999; 11(3): 242-246

[4] McLaughlin AM, Farooq M, Donnelly MB, Foley K. Anaesthetic considerations of adults with Morquio's syndrome - a case report. BMC Anesthesiol. 2010 Feb 26;10: 2

[5] Pagel PS, Almassi GH.Perioperative implications of Morquio syndrome in a 31-year-old woman undergoing aortic valve replacement. J Cardiothorac Vasc Anesth 2009; 23(6):855-857

[6] Morgan KA, Rehman MA, Schwartz RE. Morquio's syndrome and its anaesthetic considerations. Paediatr Anaesth 2002; 12(7): 641-644

[7] Bartz HJ, Wiesner L, Wappler F. Anaesthetic management of patients with mucopolysaccharidosis IV presenting for major orthopaedic surgery. Acta Anaesthesiol Scand 1999; 43(6):679-683

Prostatic carcinoma bilateral iris metastases

Tatjana S. Sarenac[1]*, Mirjana A. Janicijevic-Petrovic[1], Suncica B. Sreckovic[1], Milan R. Radovanovic[2], Dejan D. Vulovic[2], Katarina M. Janicijevic[2]

[1] Clinic of Ophthalmology, Clinical Centre Kragujevac, Zmaj Jovina 30, 34000 Kragujevac, Serbia. [2] Medical faculty, University of Kragujevac, Svetozara Markovica 69, 34000 Kragujevac, Serbia

Abstract

We described a patient with bilateral iris metastases resulted from prostatic cancer. Slit lamp and ultrasonography examination of the both eye demonstrated tumor of the iris, as an amelanotic vascular mass located on the superior temporal quadrant.

On open biopsy revealed undifferentiated tissue that stained strongly positive for prostate carcinoma, confirming the diagnosis of metastasis prostate adenocarcinoma. Early diagnostic procedures are essential for the causal therapy of prostate carcinoma as the primary neoplasm.

KEY WORDS: iris metastases, prostate carcinoma, diagnosis

INTRODUCTION

The first case of choroidal metastases of prostate carcinoma was described in 1872. by Perls [1]. The predominant sources of metastatic carcinoma to the choroid are lung in men and breast in women [2]. The iris metastases are uncommon and they represent 12 % of all adult uveal metastases [3]. It is well known that prostatic carcinoma metastases are the most common metastases in the eye, but they are very rare at the iris. Each diagnosis must be viewed with scepticism unless there is histological and if possible hystochemical confirmation. Slit lamp examination indicated on iris pseudo tumor or non-specific increasing of tissue [4]. The aim of this manuscript is to represent the case on iris metastases of prostatic cancer with biopsy confirmation that had a strong prostate-specific staining [5].

CASE REPORT

A 69 years old man was admitted to the Clinic of Ophthalmology, Clinical Centre of Kragujevac in Serbia with the signs of increased intraocular pressure and with inflammation in anterior chamber of both eyes (Figure 1a). Duration of the symptoms was more than one month. Ophthalmological examination showed inflammation in anterior chamber with endothelial precipitates and tumor on the iris. Neoplasm was located at 11-h on the basis of the iris of right eye and on the 02-h on the basis of the left eye. Gonioscopy showed angle tumor infiltration. Fundus examination was regular. The best corrected visual acuity on the right eye was 10/20, and on the left eye was 18/20. Intraocular pressure measurements were: 42 mm Hg - right eye and 33 mm Hg - left eye. Ultrasonography of the both eyes was regular (Figure 1b). Anamnesis dates showed that patient was treated from prostatic carcinoma by hormonal therapy during the five years. Also, he was examined every year (blood examinations, tumor markers, lung radiography, abdomen ultrasonography, CT of the brain, sceletal scintigraphy). There were no metastases. Later, he was treated with chemotherapy. After urological examination, tumor was detected on digital rectal examination, and the serum prostate-specific antigen level was 126 ng/ml. Prostate biopsy was consistent with adenocarcinoma, Gleason score 8. Hormones therapy was suggested again (Figure 1). Skin metastases were detected and skin biopsy was performed (Figure 1c). Prostate cancer metastases was verified. Patient was treated with medicament antiglaucomatous drugs (carbo anhydrasis inhibitor, beta-blockers, etc) and with corticosteroids. Intraocular pressure was well regulated and pain disappeared. An open biopsy indicates on undifferentiated tissue that stained strongly positive for prostatic-specific acid phosphatase, confirming the diagnosis of metastases of prostatic carcinoma. Immunohystochemical studies were strongly positive for prostatic cancer. The patient was referred to oncologist for detailed prostatic examination. Native graphy indicated for neoplasm of prostate. Later examination showed positive regional lymph nodes. Definitive diagnosis was: Glaucoma sec. Tumor intra bulbare sec. A biopsy of the iris

* Corresponding author: Tatjana Sarenac,
Clinic of Ophthalmology, Clinical Centre Kragujevac,
Zmaj Jovina 30, 34000 Kragujevac, Serbia
Phone: +381 62 21 99 15; Fax: +381 34 37 00 73
e-mail: tvoja.tanja@yahoo.com

Submitted: 4 December 2011 / Accepted: 14 February 2012

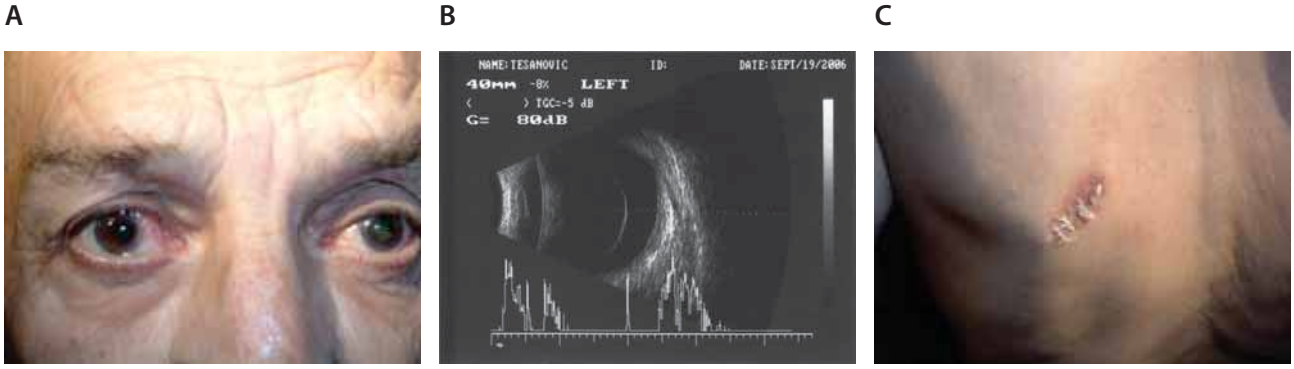

FIGURE 1. Iris metastases of the both eyes (A); Ultrasonography of the left eye (B); Subcutaneus metastases (C);

mass on both eyes showed inflammatory and cellular atypical infiltration strongly positive of prostatic carcinoma staining.

DISCUSSION

In 12 – 31 % eye metastases are the first sing of cancer disease [1, 2]. The incidence of metastases to the iris among patients with prostate carcinoma has been reported to vary between 8 - 10 % [2]. Prostate carcinoma is the most common primary cancer to cause metastases in the iris [3]. The first sign of prostatic carcinoma can be iris metastases [4]. Diagnosis of this disease entity requires a high clinical suspicion. Our patient complained of the visual loss, eye pain, watering, skin tumors, etc. [5]. He had a positive history with cancer. Ultrasonography, CT and MRI examinations are the modalities of diagnosis [6]. The iris metastases were amelanotic tumors with moderate dilated vessels and in growing to anterior chamber and iridocorneal angle (Figure 1). Inflammatory reaction in the anterior chamber was presented. An excision biopsy remains the gold standard and showed invasive lobular cancer of prostate [7]. Radiography examinations showed thickening in the region of the prostata but no mass lesion. The histopathology report showed positive cavity margins with focal lobular carcinoma in situ. A total prostatectomy was not planed, because of tumor dimension and surround infiltration. Idiopathic iris inflammatory syndrome or iris pseudo tumor may be considered in the differential diagnosis. Later the optimal plaque-radiotherapy was performed [8]. Patient died. Anytime, when ophthalmologist has a patient with unilateral/bilateral painful, red eye with tumor at the iris, the choroidal metastases must be considered through very detailed team- examination with urologists and radiologists [9]. Patients with eye metastases were found to have widespread metastatic disease elsewhere. This is most like to occur in metastatic scirrhous and solid prostate cancer with regional lymphadenopathy and with severe changed fibrotic stroma [10]. Most of these cases respond well to hormonal therapy and local radiotherapy for the metastases. Chemotherapy and hormonal therapy are usually needed for the primary carcinoma and metastases [11]. Recognizing of metastatic disease and some early treatment are very important to improve quality of life in our patients [11]. The prognosis is very poor, and the mean survival time for patient with prostate cancer was reported to be 1 - 3 years after the diagnosis of eye metastasis and after enucleation or egzenteration [12]. Metastases of prostate cancer to the iris are extremely rare. We presented this case to remind ophthalmologists and radiologists of the diagnosis of metastases prostatic carcinoma to the eye and the usefulness of the hystochemical staining of biopsy material for prostate-specific stain.

CONCLUSION

Every ophthalmologist must remember that eye metastases in men showed need for detailed prostate examination as well as the examination of the whole body. The iris and choroidea can be the only metastatic localization of the prostate carcinoma. Planned diagnostic procedures are the base for the optimal causal therapy of prostate carcinoma as the primary neoplasm [13].

DECLARATION OF INTEREST

Authors declare no conflict or interest.

REFERENCES

[1] Shields CL, Shields JA, Gross NE, Schwartz GP, Lailly SE. Survery of 520 eyes with uveal metastates. Ophthalmology. 1997; 104 (8): 1265-1276.
[2] Jemal A, Siegal R, Ward E, Hao Y, Xu J, Thun MJ. Cancer statistics, 2009. CA Cancer J Clin. 2009; 59: 225-249
[3] Badmus TA, Adesunkanmi AR, Yusuf BM, Oseni GO, Eziyi AK, Bakare TI et al. Burden of prostate cancer in southwestern Nigeria. Urology 2010; 76(2): 412-416
[4] Wolf AMD, Wender RC, Etzioni RB, Thompson IM, D'Amico AV, Volk RJ et al. American cancer society guideline for the early detection of prostate cancer. CA Cancer J Clin 2010; 60: 70-98.
[5] Budendorf L, Schöpfer A, Wagner U, Sauter G, Moch H, Willi N et al. Metastatic patterns of prostate cancer: an autopsy of 1589 patients. Hum Pathol. 2000; 31(5): 578-583.
[6] Long MA, Husband JE. Features of unusual metastases from pros-

tate cancer. Br. J Radiol 1999; 72(862): 933-941.
[7] Shields JA, Shields CL, Brotman HK, Carvalho C, Perez N, Eagle RC Jr. Cancer metastatic to the orbit: the 2000 Robert M. Curts Lecture. Ophthal Plast Reconstr Surg 2001:17(5): 346-354.
[8] Lim JI, Petrovich Z. Radioactive plaque therapy for metastatic choroidal carcinoma. Ophthalmology 2000; 107(10): 1927-1931.
[9] Kosmas C, Malamos NA, Antonopoulos M. Complete regression of choroidal metastases from breast cancer after docetaxel-based systemic therapy. Med Pediatr Oncol. 2000; 34(3): 229-230.
[10] Gittes RF. Carcinoma of the prostate. N Engl J Med 1991; 324: 236-245.
[11] Seat WW, Menon M, Walsh PC. Hormonal therapy of prostatic cancer. Cancer 1980; 45(7): 1929-1936.
[12] Nelson CC, Hertzberg BS, Klintworth GK. A histopathologic study of 716 unselected eyes in patients with cancer at the time of death. Am J Ophthalmol 1983; 95: 728-733.
[13] Hiros M, Spahović H, Selimović M, Sadović S. Incidental prostate cancer in patients undergoing radical cystoprostatectomy for bladder cancer. Bosn J Basic Med Sci 2008; 8(2):147-151

Letters to editor

Researching chemicals in human milk can be conducted without discouraging breastfeeding

José G. Dórea[1], Suzanne E. Fenton[2], Judy S. LaKind[3,4,5], Cheston M. Berlin, Jr.[5]

[1] Faculty of Health Sciences, Universidade de Brasília, 70919-970 Brasília, DF, BRAZIL. [2] Division of the National Toxicology Program, National Institute of Environmental Health Sciences, NIH, Research Triangle Park, NC, USA. [3] LaKind Associates, LLC, Catonsville, MD, USA [4] Department of Epidemiology and Public Health, University of Maryland School of Medicine, Baltimore, MD, USA. [5] Department of Pediatrics, Pennsylvania State University College of Medicine, Milton S. Hershey Medical Center, Hershey, PA USA

Continued monitoring of environmental chemicals is important for understanding human exposure and potentially related health risk(s). Cinar et al. [1] contribute to our knowledge on infant exposures to environmental chemicals in breast milk. However, the messages implicit both in the title and in the paper itself are unnecessarily alarming and are likely to be interpreted by mothers and health professionals as indicating that breast feeding is generally unsafe in certain regions of Turkey. For example, the conclusion that "*Rural area also may not be safe for breastfeed babies*" is based on an evaluation of 90 women, without regard to differences in their potential exposure patterns; lifestyle, smoking status, occupation, body mass index, or residential history. It is unclear whether these women are in any way representative of rural areas in Turkey, or rural areas in general. Further, the authors do not provide reference values with which to compare the levels of metals that they report, and the values that they report for several metals are 10-1000 times higher than the levels reported in other studies (although it is unclear whether they have reported the levels with correct units; the authors note that the mothers' levels were lower than recommended levels of 10 microg/L (Hg) and 30 microg/L (Pb) while describing the mothers' reported levels as being in the low parts per million range [Table 4]). Only under exceptional circumstances including clinical treatment with certain pharmaceuticals or in cases of accidental poisonings have the occurrence of chemicals in breast milk resulted in a recommendation to avoid breastfeeding. Otherwise, studies have shown that breastfeeding can counter subtle adverse effects associated with in utero maternal exposure to hazardous substances [2]. Numerous studies demonstrate the superiority of breastfeeding in lowering risk of adverse health outcomes when compared to formula-fed infants. Thus, the World Health Organization recommends six months of exclusive breastfeeding. Cinar et al. [1] recognized that human milk provides all of the vitamins and essential minerals and trace elements (micronutrients) that are required for the normal development of infants as well as many brain-protective substances. They do not describe the exposures associated with formula-feeding in the regions under study and so the reader has no basis for understanding whether infant exposures to metals would be higher or lower based on the choice of formula over breastfeeding. Further, there is no evidence that formula feeding would attenuate any effects that may occur from fetal exposures [3]. Scientists conducting biomonitoring research using human milk have an obligation to understand the sensitivity of this issue and the impact their information and/or message may have on health professionals and breastfeeding mothers. Indeed, Geraghty et al. [4] highlighted the potential harm from poor reporting methods in breast milk monitoring of environmental chemicals; American women responded that they would immediately wean if told that phthalates were in their milk. It is incumbent on us to strive to contextualize human milk biomonitoring data, constructing a message that puts into perspective both risks of environmental hazards and benefits of breastfeeding. Formula-feeding should never be implied (implicitly or explicitly) as a means to attenuate maternal-infant exposure to environmental chemicals, especially without data to support such a message (5). The otherwise interesting paper of Cinar et al. [1] gives the false impression that milk of Turkish mothers is unsafe and that if the infant is not breastfed, chemical exposures will not occur.

* Corresponding author: Prof. José G. Dórea
C.P. 04322
Universidade de Brasilia
70919-970 Brasilia, BRAZIL
FAX: 55-61-3368-5853
e-mail: dorea@rudah.com.br

Disclaimer: The commentary in this article has been reviewed by the NIEHS and approved for publication. Approval does not signify that the contents necessarily reflect the views and policies of the institute. The opinions in this report are those of the authors.

Key words: metals; pollutants; breastfeeding; human milk, biomonitoring

REFERENCES

[1] Cinar N, Ozdemir S, Yucel O, Ucar F. In which regions is breastfeeding safer from the impact of toxic elements from the environment? Bosn J Basic Med Sci 2011;11:234-239.
[2] Dórea JG. Maternal smoking and infant feeding: breastfeeding is better and safer. Matern Child Health J 2007;11:287-291.
[3] Dórea JG, Donangelo CM. Early (in uterus and infant) exposure to mercury and lead. Clin Nutr 2006;25:369-376.
[4] Geraghty SR, Khoury JC, Morrow AL, Lanphear BP Reporting individual test results of environmental chemicals in breastmilk: potential for premature weaning. Breastfeed Med 2008;3:207-213.
[5] LaKind JS, Birnbach N, Borgert CJ, Sonawane BR, Tully MR, Friedman, L. Human milk surveillance and research of environmental chemicals: Concepts for consideration in interpreting and presenting study results. J Toxicol Environ Health A 2002;65:1909-1928.